FATIGUE BEHAVIOR OF ULTRA HIGH STRENGTH STRUCTURAL MATERIALS

by

Amilcar Quispitupa Yupa

A thesis submitted in partial fulfillment of the requirements for the degree of

DOCTOR OF PHILOSOPHY
in
CIVIL ENGINEERING

UNIVERSITY OF PUERTO RICO
MAYAGÜEZ CAMPUS
2007

Approved by:

_____   _____
Luis E. Suárez, Ph.D   Date
Member, Graduate Committee

_____   _____
Luis A. Godoy, PhD   Date
Member, Graduate Committee

_____   _____
Ricardo R. López, PhD   Date
Member , Graduate Committee

_____   _____
A. Basir Shafiq, PhD   Date
President, Graduate Committee

_____   _____
O. Marcelo Suárez, PhD   Date
Member , Graduate Committee

_____   _____
Genock Portela Gauthier, PhD   Date
Representative of Graduate Studies

_____   _____
Ismael Pagán Trinidad, Prof.   Date
Chairperson of the Department

ABSTRACT

Ultra high strength structural AF1410 steel is commonly used in critical aircraft structural components in aerospace and marine application, because it possesses high toughness and outstanding mechanical properties. However, there exists a lack of knowledge of its corrosion-fatigue properties and hydrogen embrittlement. This study attempts to undertake an accurate simulation of actual service conditions mimicking a realistic environment and to characterize the hold time-fatigue interaction on aircraft structural members. AF1410 steel was evaluated in marine environment and electrolytic hydrogen charged conditions. A decrease in lifetime of AF1410 was observed as a function of increasing severity of the simulated environment and reducing test frequency. The crack growth rate of hydrogen charged specimens and under simulated marine environment was higher than specimens evaluated without hydrogen (air), when evaluated using sinusoidal and trapezoidal loading forms. Furthermore, hydrogen charged specimens at one and two lateral surfaces exhibited a drastic reduction in the lifetime caused by simultaneous effect of hydrogen and fatigue loading. Our results show that hold time effect under environmental hydrogen embrittlement conditions was detrimental on fatigue lifetime of AF1410 steel which is frequently ignored under environmental temperatures. Additionally, the hydrogen charged specimens underwent a change in the fracture modes from ductile to brittle. Since, hydrogen has not permeated the entire specimens; the experiments provided a more realistic approach to the study of large aircraft components

during service. In addition, a phenomenological mathematical model for lifetime prediction was developed to account for the effect of hydrogen on the fatigue crack growth rate for AF1410 steel.   Finally, the phenomenological model developed shows an excellent agreement between the experimental and predicted results.

RESUMEN

El acero AF1410 es comúnmente usado en componentes estructurales críticos en aplicaciones aeroespaciales y marinas, ya que posee una alta tenacidad y propiedades mecánicas excepcionales. Sin embargo, existe una falta de conocimiento de las propiedades de corrosión-fatiga de este acero de ultra alta resistencia. Este estudio intenta iniciar una simulación adecuada de las condiciones actuales de servicio de componentes estructurales imitando un ambiente real y también caracterizar términos de tiempo cortos de carga sostenida combinado con fatiga. AF1410 fue evaluado en ambiente marino y condiciones de cargado electrolítico de hidrógeno. Se observó una disminución en el tiempo de vida del AF1410 como función de incrementar la severidad del medio ambiente y reduciendo la frecuencia. La velocidad de crecimiento de especimenes cargados con hidrógeno fue más alta que especimenes evaluados sin hidrógeno. El tiempo de vida para especimenes expuestos a ambiente corrosivo e hidrógeno disminuyó bajo formas de cargas sinusoidales y trapezoidales. Además, especimenes cargados con hidrógeno en ambas caras laterales exhibieron una drástica reducción en el tiempo de vida por una acción simultánea de hidrógeno y tiempo de carga sostenida. Nuestros resultados mostraron que el tiempo de carga sostenida fue crítico sobre el tiempo de vida del AF1410, el cual es frecuentemente ignorado bajo temperaturas ambientales. Adicionalmente, especimenes cargados con hidrógeno experimentaron un cambio en el modo de fractura de dúctil a frágil. Debido a que el hidrógeno no permea los especimenes

enteros, los experimentos proveen una aproximación real al estudio de estructuras aéreas grandes en servicio. En adición, un modelo fenomenológico para predecir la vida del material fue desarbolado para tomar en cuenta el efecto del hidrógeno sobre el crecimiento de grieta en fatiga para el AF1410. Finalmente, el modelo fenomenológico desarrollado mostró un excelente acuerdo entre los resultados predichos y experimentales.

To my parents and wife for their unconditional support and love

ACKNOWLEDGEMENTS

During the development of my graduate studies in the University of Puerto Rico-Mayagüez Campus several persons and institutions collaborated directly and indirectly with my research. Without their support it would be impossible for me to finish my work. That is why I wish to dedicate this section to recognizing their support.

I want to start by a sincere acknowledgement to my advisor, Dr. A. Basir Shafiq, because he gave me the opportunity to research under his guidance and supervision. I received motivation, encouragement, and support from him during all my studies. With him, I have learned to write papers for conferences and share my ideas with the public. I also want to thank Dr. O. Marcelo Suárez for the motivation, and support I received from him, as well as for his friendly support and assistance. I owe special thanks Dr. Oswald N. C. Uwakweh for the opportunity of researching under his guidance, his support, inspiration and transmitted knowledge for the completion of my work.

I want to extend my sincere gratitude to my friends Norberto, Jhon Jairo, Samuel and Gustavo.

The Grant from NAVY & Office of Naval Research provided the funding and the resources for the development of this research. And last, but most importantly I would like to thank my family, for their unconditional support, inspiration and love.

Table of Contents

ix

List of Tables

List of Figures

List of Symbols and Abbreviations

AE   Acoustic Emission

AFM   Atomic Force Microscope

CGR   Crack Growth Rate

CFCG   Corrosion Fatigue Crack Growth

COD   Crack Opening Displacement

CT   Compact Tension

C_H Hydrogen Concentration

D   Diffusion Coefficient of the Metal

E   Young modulus of the Material (MPa)

FCGR   Fatigue Crack Growth Rate

FHD   Free Hydrogen Desorption

H   Hydrogen

IG   Intergranular Fracture

HE   Hydrogen Embrittlement

HELP   Hydrogen Enhanced Local Plasticity

LDT   Load Decrement Testing

N   Number of Cycles

QC   Quasi-Cleavage

R   Load Ratio

Ra	Roughness Average (ISO-4287/1)
Rq	Roughness Average (DIN 4768)
SEM	Scanning Electron Microscope
UHSS	Ultra High Strength Steels
t_{eff}	Effective Thickness (mm)
t	Specimen Thickness (mm)
t_{ch}	Time of Charging (hours)
t_{HP}	Hydrogen Penetration Depth (mm)
TG	Transgranular Fracture
σ_{ys}	Yield Strength of the Material (MPa)
σ_u	Ultimate Tensile Strength (MPa)
υ	Poisson ratio
K_{IC}	Plane Strain Fracture Toughness
ΔK_{th}	Threshold Stress Intensity Factor
K_{max}	Maximum Stress Intensity Factor
K_{min}	Minimum Stress Intensity Factor
ΔK	Stress Intensity Range

1   INTRODUCTION

Since World War II many fracture theories have been developed, starting with Irwin in the mid-1950s [1]. Fatigue and fracture theories have become an important tool in order to explain structural failures under cyclic loads. The characterization of fatigue lifetime is complex as it depends on various electrochemical / micromechanical processes simultaneously occurring at the crack tip, such as, metal dissolution , hydrogen embrittlement , crack tip microcracking, frequency of loading and ionic concentration, etc. [2-6]. Crack propagation by metal dissolution involves ionic diffusion (of aggressive anions like Cl^-) down the crack length, the rupture of the protective oxide film, followed by dissolution of the bare metal surface (especially under stress) due to localized metal loss. Metal dissolution has been found to be significant in enhancing crack growth rate (CGR) of high strength alloys [6,7]. Furthermore, hydrogen entering to the material is generated as a partial reaction in the electrochemical process, simultaneously gets dissolved into the metal surface especially at region of high stresses to embrittle the material [2-6]. Therefore, the hydrogen plays a significant role in changing the fracture modes from ductile to brittle (transgranular, intergranular, quasi-cleavage to pure cleavage fracture) [6, 7-10].

Much research has indicated that corrosion fatigue of structural materials causes a significant reduction in fatigue lifetime as a function of increasing salt content, and decreasing pH and frequency [7,9]. However, literature on the environmental fatigue properties of AF1410 steel is extremely scarce and somewhat contradictory [5,11]. Significant reduction in fatigue lifetime of AF1410 has been reported at frequencies up to

10Hz and under saline solution of 1% NaCl [5]. However, recent studies of AF1410 steel have shown a moderate reduction in lifetime only when the NaCl level was increased to 3.5% and frequency lowered to 0.5Hz [12]. Both studies agree that the synergistic combination of fatigue stresses and environmental service conditions (especially the environmental hydrogen) acting together is more detrimental than either mechanism alone [5, 11].

Currently the literature shows that the effects of short term hold time and/or high strain rate fatigue at room temperature can be neglected, as creep (longer hold time in hours or years) usually takes place at temperatures greater than approximately 0.4 of the absolute melting temperature $T=0.4T_m$ [11]. At high temperatures, fatigue-hold time behavior has been found to be detrimental as a function of creep time causing changes in modes of failure and subsequent fracture surface morphology [11-14]. However, these assertions need to be verified when the material is subjected to environmental effects. To accurately simulate the arresting shank and landing gear scenarios, high strain rate fatigue short-term hold time tests were performed in this research.

As a requisite to understand the mechanisms of fatigue processes in materials, the atomic force microscope (AFM), and scanning electron microscopy (SEM) have been extensively utilized to study fracture surface morphology. The AFM has been widely used in the study of micro-crack nucleation and growth, striation shapes, slip bands and to extract general quantitative fracture features of a variety of materials. The SEM offers a clear grain size measurement and is excellent for fracture modes identification. These microscopic techniques are complementary to each other to perform a complete fracture surface analysis of failed structural members in order to determine the causes of failure [12,13,15].

Quantitative fatigue lifetime prediction modeling for aircraft structures is generally difficult due to the complexity of electrochemical and micromechanical mechanisms involved at the tip of the growing crack, such as stress field, material properties, environmental conditions, corrosion current density, hydrogen generation, absorption and concentration, and microcracking [6-9,16-18]. All this leads to enormous uncertainty in fatigue lifetime prediction and therefore, no existing model can adequately address the Navy's concerns about structural integrity [2-6].

It is known that the deleterious effects of environment in high strength steels under stress mainly stem from the hydrogen that is electrochemically produced as a result of partial reaction between the metal surface and the environment [2-6]. However, quantifying the rate of production, diffusion and retention of environmental hydrogen into the metal surface (i.e. crack tip) is a challenging task [4]. In order to avoid this problem, hydrogen has been introduced into the alloy through a laboratory controlled electrochemical charging process which can offer a critical insight into the fundamental aspects of environmental hydrogen assisted fatigue crack growth mechanisms [13].

The hydrogen assisted fatigue crack growth models can be divided into two categories: i) analytical, that depend on the fundamental ideas, such as hydrogen diffusion, concentration and crack tip electrochemistry and ii) empirical, based primarily on curve fitting of the experimental data.

Models based on hydrogen diffusion concepts seek to establish a functional relationship between rates of diffusion and accompanying electrochemical parameters in the form of a system of partial differential equations along with complex boundary conditions, as

explained in detail by Turnbull [6]. On the other hand, empirical (Paris type) relationships cannot truly be qualified as a predictive tool as they are all essentially based on curve fitting, and thus fit the data well as long as the constants are properly adjusted. As a result, analytical and empirical approaches have enjoyed a very limited success in predicting fatigue lifetime of materials. However, various modified forms of semi-empirical relationships that seek to establish a phenomenological connection between physical parameters, material and cracking behavior have proven to be more robust in their practical use than the purely analytical or purely empirical predictive models [14]. One such model is developed and proposed in this research. As a final stage of this research, a nondestructive acoustic emission (AE) technique was used to monitor the fatigue crack initiation and growth, hydrogen embrittlement issues and corrosion of materials.

The current test program takes scarcely studied ultra-high strength AF1410 alloy (strength ~ 1.8GPa and toughness ~ 130 MPa-m$^{1/2}$) as a model material that has been used in the Navy's F-18E arresting shanks [3,7]. Experiments performed in this thesis attempts to undertake an accurate simulation of actual service conditions of aircraft structural components mimicking a realistic environment. This work is significant as a large inventory of aging Navy's carrier based aircraft fleet operates under extremely high flight loads with frequent landings and takeoffs.

1.1 Research Objective

The objectives of this research were to characterize and model the fatigue lifetime behavior of ultra high strength structural AF1410 steel in the presence of simulated marine

and permeated hydrogen environment. Additionally, corrosion fatigue behavior of aircraft structural AA7075-T6 was investigated.

1.1.1 Specific Tasks

1. To design a load-decrementing testing (LDT), time and material efficient fatigue life assessment program using compact tension (CT) specimens.

   i. To conduct LDT (strain controlled tests) experiments on AF1410 and AA7075-T6 metal alloys in the presence of simulated marine environment.

   ii. To perform LDT to understand the role of atomic hydrogen on the lifetime reduction of AF1410 as a function of hydrogen penetration depth due to charging process.

2. To design and carry out a load control fatigue short-term hold time testing on compact tension AF1410 steel specimens in the presence of simulated marine and hydrogen charged environment in order to simulate arresting shank and landing gear scenarios.

3. To understand the fatigue behavior of flat un-notched and notched specimens tested in fully reversed fatigue in the presence of simulated marine and quantifiable hydrogen environment.

4. In order to accurately identify the microstructural basis for the observed lifetime behavior, extensive use of fracture surface characterization techniques, such as, optical, SEM and AFM will be completed.

5. Develop a semi-empirical fatigue lifetime model to predict crack growth rates.

6. Finally, use the nondestructive AE technique to monitor the fatigue crack initiation and growth processes of structural materials.

2   LITERATURE REVIEW

2.1 Corrosion Fatigue

The corrosion fatigue mechanism involves the synergistic combination of material, cyclic mechanical loading, and environment. Those factors can cause the initiation and propagation of cracks leading to catastrophic failures in structures if not properly taken into account. Corrosion fatigue also can be explained by several theories, such as anodic reaction (metal dissolution) and the occurrence of hydrogen evolution, both at the crack tip [2,6,15]. Some ductile materials can behave in a brittle manner due to environmental hydrogen effect which also causes changes in the fracture mode.

Metal dissolution can be defined as a process of loss of metal mass. In addition, the hydrogen absorbed by metal is the most dangerous environmental effect on ultra high strength steels such as AF1410, Aermet 100, AISI4340, 300M [2,6,12,13]. These materials become weak to hydrogen embrittlement due to its microstructure and high tensile strength [3, 15, 16].

Several mechanisms have been proposed to understand the corrosion fatigue behavior in metals. These mechanisms include metal dissolution, anodic reaction induced cleavage, surface mobility and hydrogen embrittlement.

Metal Dissolution mechanism is based on the mass loss during the rupture events and the frequency of them, as a series of discrete steps. The process starts when the metal or an alloy (susceptible to corrosion) is exposed to a corrosive environment. During corrosion, some of the dissolved metal ions tend to form oxides and hydroxides that

8

precipitate on the surface, forming a thin protective film. Under conditions of localized straining sufficient to rupture protective or partially protective film, oxidation of bared surface will occur and the crack will advance because of the localized metal loss. At the same time, a repassivation of the bared surface begins occurring cyclically as in the case of corrosion fatigue. The film rupture mechanisms contains the rupture-dissolution-repassivation sequence, that must be followed in order to maintain the process of crack growth [6,16]. Figure 2.1 shows the process of metal dissolution under aqueous media.

Solution at
3.5% NaCl

BULK
MATERIAL

Cl^-

Passive Film
(cathode)

CRACK
TIP

Weak   Hydrochloric
base   Acid

$$Fe^{++} + 2Cl^- + 2H_2O \rightarrow Fe(OH)_2 + 2Cl^- + 2H^+$$

Grain

Cathode

CRACK
TIP

H^+

H^+

H^+

Transport

Cl^-

Fe^{++}

e^-

Hydrogen
Embrittlement
Zone

e^-

H^+

H^+

H^+

Bare Metal
(Anode)

Grain

Figure 2.1 Schematic view of metal dissolution and hydrogen evolution
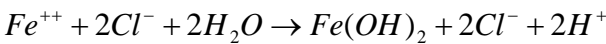
The anodic reaction mechanism suggests that high rates of transgranular crack growth are induced by environmental cleavage, which is frequently associated with embrittlement caused by hydrogen atoms absorbed by metal. This mechanism is commonly used for many systems such as high strength steels and cathodically polarized metals. However, its applicability is limited to ductile alloys under free corrosion conditions [6].

The basic premise of the model was the crack initiated in ductile thin films formed by anodic reaction at the crack tip which can propagate in a cleavage mode. An important factor in this model, in addition to film thickness, is the lattice parameter of the film. If the lattice parameter is less than that of substrate then cleavage can occurs but if the opposite is true then dislocation emissions occur at the film-substrate interface and crack blunting and arrest take place. The extent of crack advance depends on the rate of dislocation emission from the propagating tip [6,18].

Cleavage models explain several features of the transgranular stress corrosion cracking problems. However, an enormous electrochemical, micromechanical and micro-fractography analysis must be carried out in order to discern cleavage-like cracking. Many factors have been considered as the causes of crack arrest such as: a) restraining effects of unbroken ligaments, b) arrest at pre-existing or deformation generated defects, c) crack bifurcation, d) exhaustion.

A model for film-induced cleavage was proposed in the literature [2,6,18] in a very simple way by expressing the crack growth rate as follows (Eq. 1)

$$\frac{da}{dt} = \left(\frac{M}{zFp} Q_f + j \right) \frac{\dot{\varepsilon}_{ct}}{\varepsilon_f}$$

$$\frac{da}{dt} = \left(\frac{M}{zFp} \frac{Q_f}{\tau} \right) \tag{1}$$

where M, F, z, ρ, Q_f, ε_{ct}, ε_f, j, τ are atomic weight, faraday's constant, number of electrons involved in overall reaction of the metal atoms, density of the metal, oxidation charge density, strain rate at the crack tip, strain to fracture, jump distance, interval between the cleavage events. However, the lack of consideration of strain rate effects might appear to arise because the film-induced cleavage model emphasizes a critical film thickness rather than a strain increment, presumably because the film is considered to be inherently brittle. Cleavage cracking is caused by combination of environmental and mechanical loading conditions, therefore, the applicability of the cleavage concept remains limited for practical applications.

The Surface Mobility model [6,18] is based on crack propagation, which results from the capture of vacancies by stressed lattice at the tip of the metal [6]. The model is claimed to be applicable to liquid metal embrittlement and non-hydride forming metals, such as ultra high strength steels.

The proposed crack growth rate model based on anodic reaction-surface mobility processes is given by Eq. 2

$$\frac{da}{dt} = \frac{Ds}{L} \left[\exp\left(\frac{\sigma a^3}{kT} \right) - 1 \right] \tag{2}$$

where Ds, L, a, σ, k and T refer to coefficient of surface self-diffusion on the metal,

12

diffusion path (typically 10^{-8}m), atomic diameter, maximum stress at the crack tip, Boltzman constant and absolute temperature respectively. Furthermore, the direction of vacancy diffusion in the stress field is reflected in the surface concentration and the gradient of vacancies from the surface diffusion process. The literature suggests that the difference in vacancy concentration between the stressed field and the stress-free region is caused by the variation of the concentration along the surface. The vacancy flow is given by the following Eqs. 3 respectively [6]

$$C - C_0 = C_0 \left[\exp\left(\frac{\sigma a^3}{kT} \right) - 1 \right]$$

$$\frac{dC}{dx} = \frac{C_0}{L} \left[\exp\left(\frac{\sigma a^3}{kT} \right) - 1 \right]$$

$$Jv = Dv \frac{dC}{dx} \tag{3}$$

However, there are some controversial assumptions that lead to unsatisfactory crack growth rate predictions.

2.2 Ultra High Strength Steels

Research on the development of new high-strength, high-toughness, corrosion-resistant steels with outstanding fracture toughness and tensile strength combination for landing gear materials has been a subject of intense recent interest. Improved Ni-Co, low-carbon steels (most notably Aermet100 and AF1410), have excellent combinations of properties and are developed to the point where they are now being specified as

replacements for the standard landing gear steels 300M and 4340 [19].

These improved steels are used for landing gear on carrier-based aircraft because they exhibit excellent damage tolerance and environmental resistance. The steels can also find application as attach fittings, horizontal stabilizer spindles, arresting-hook shanks, and catapult hooks. Other aerospace applications under consideration include rotorcraft actuators and masts, gas turbine engine shafts, and rocket motor casings. Non-aerospace applications include ordnance, armor, high-strength fasteners, pump splines, and automotive drive shafts [1,19].

The improved combination of strength, damage tolerance, and stress corrosion cracking resistance provides significant benefits for applications under severe service conditions, such as the naval aircraft environment. An additional benefit includes fatigue strength superior to 300M steel. These materials have good weldability because of low carbon content. Testing has shown that UHSS can be welded, without preheat, with joint efficiencies approaching 100 percent.

It appears that the strength of these new steels cannot increase to higher levels without corresponding decreases in ductility and toughness. However, increased strength can be achieved while keeping toughness at levels acceptable for many applications. Such a balance of properties may be acceptable for landing gear for civil aircraft.

It is well known that, as strength increases, toughness decreases, therefore toughness of ultra high strength steel is an important consideration. These super alloys meet these requirements offering excellent fracture toughness and strength. The ultra high strength of this steel is attributed to the presence and distribution of the fine second phase

particles such as $(MoCr)_2C$, $(MoFe)_xC$, $(Fe,Ni,Co)_3C$ [19]. Furthermore, heat treatment, grain size, precipitates, dislocation structures size-shape and distribution of inclusions and compositions of matrix can generate variations on material properties. All of these parameters are very important in order to enhance the toughness of steel. Large second phase particles (carbides) and less distance between them can produce detrimental effect in toughness and tensile strength of the material. These microstructural characteristics can enhance the crack tip blunting and improve the resistance to fatigue crack growth [19].

2.3 Hydrogen Embrittlement Mechanisms

The hydrogen embrittlement mechanisms in steels have been studied for many years. The hydrogen atoms have the ability to diffuse through metals due to its smaller atomic radius in comparison with other elements. The hydrogen diffusion is affected by materials' microstructure, imperfections and the presence of dislocations, which can enhance the hydrogen embrittlement. However, there are many uncertainties that need to be studied, especially for ultra high strength steels.

The HE occurs by increasing the hydrogen concentration to critical level, which depends on the materials' properties and microstructure. The hydrogen embrittlement phenomena becomes a dangerous matter for steels, especially for ultra high strength steels due to its high tensile strength (> 700MPa) [12, 13, 20]. Several studies were performed in order to evaluate the internal and external hydrogen assisted cracking in UHSS (AISI 4340, Aermet 100 and 300M) and the results revealed degradation on the mechanical and crack growth rate properties [1- 6,20,21].

15

Source of hydrogen, hydrogen can be introduced into the material through the metal processing and fabrication, electroplating, solidification, forging and welding, and due to environmental exposure. The hydrogen absorption may occur in specific offshore conditions, such as corrosion and cathodic protection. Generally, hydrogen travels throughout the material by transport mechanism (diffusion) which commonly occurs by adsorption (in the metal surface), absorption and eventually transport to the material bulk. In corrosion fatigue; anodic and cathodic reactions are occurring simultaneously. Metal dissolution and reduction of oxygen occurs at the anodic part and hydrogen evolution at the cathodic part. Both reactions (Eqs. 4-5) can occur in acidic or alkaline solutions depending on the pH of the medium [12, 21].

Oxygen Reduction:

$$\frac{1}{2}O_2 + 2H_2O^+ + 2e^- \Rightarrow 3H_2O \qquad \text{For Acid Solution}$$

$$\frac{1}{2}O_2 + H_2O^+ + 2e^- \Rightarrow 2OH^- \qquad \text{For Neutral or Alkaline Solution}$$

$$\text{(4)}$$

Hydrogen Uptake

$$H_3O + e^- \Rightarrow \frac{1}{2}H_2 + H_2O \qquad \text{For Acid Solution}$$

$$H_3O + e^- \Rightarrow \frac{1}{2}H_2 + OH^- \qquad \text{For Neutral or Alkaline Solution}$$

$$\text{(5)}$$
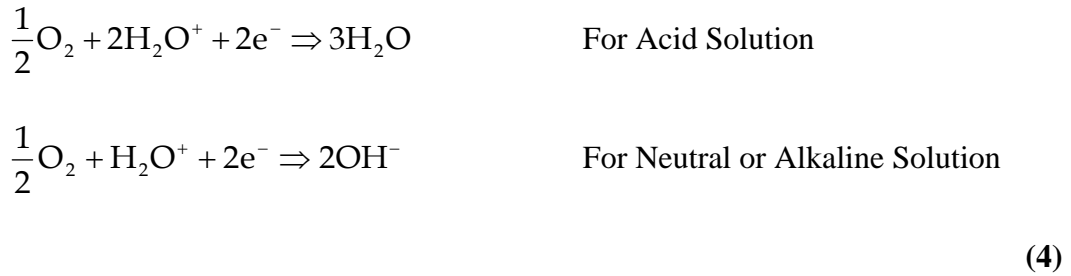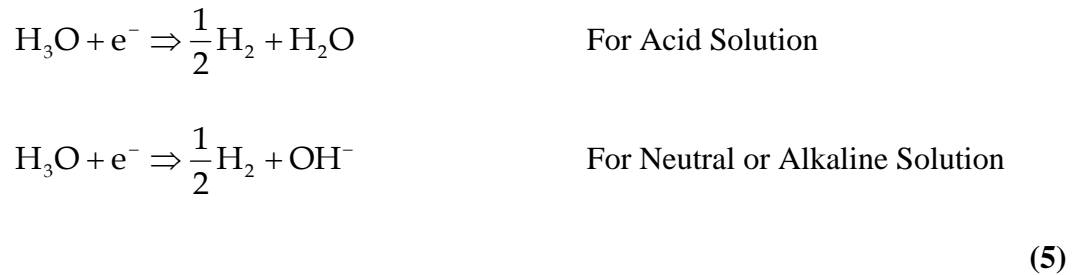
The basic reactions for hydrogen evolution are presented by Eq. 6 [6]:

$$H^+ + e^- \Rightarrow H$$

$$H_2O + e^- \Rightarrow H + OH^-$$ **(6)**
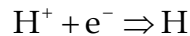
Figure 2.2 shows the distinct steps associated with the entry process of hydrogen into the metal. First hydrated atoms are transported to the double layer (surface), a separation of hydrogen proton and water by adsorption, electro donation with the charge of electrons of material thereby producing a discharge. The process of hydrogen combination can occur by two ways: atom-atom or ion-atom or both. The final stage can be eventually by desorption and entering into the material, with accompanying hydrogen evolution reaction culminating in the formation and hydrogen diffusion [22,23].
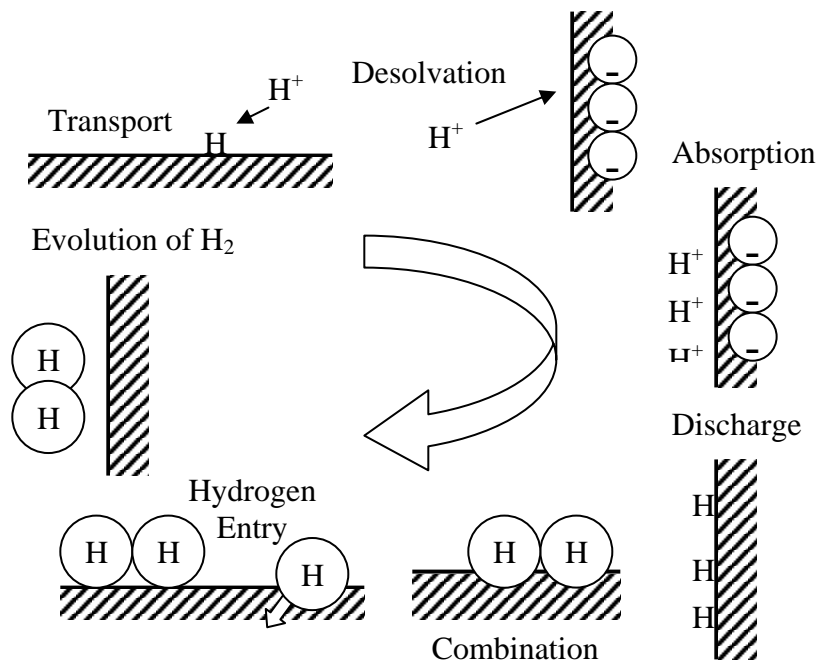
Figure 2.2 Schematic of hydrogen generation

Hydride Induced Cracking as HE mechanism was proposed based on the assumption that HE of any metal could be accounted based on localized formation, whose mechanical properties differ from those of the matrix due to hydrogen enrichment [24,25]. A metal hydride might form ahead of a crack tip, in a region of high triaxial stress. Crack growth could occur due to cracking of brittle hydride phase. No evidence of the presence of hydrides were not detected after mechanical failure in iron and steel, which could lie in the subsequent decomposition of the hydride when the crack begins to open up and its stress field is removed [24].

It is important to note that in terms of microstructure, a material is more vulnerable to hydrogen in the following increasing order: (a) lower bainite, (b) quenched and tempered martensite, (c) pearlite or spheroidized structures and (d) martensite. Fine grain and carbide sizes, along with low carbon content, are beneficial to avoid this phenomenon. However, for the current case, high strength AF1410 steels, this phase change mechanism (hydride formation) does not occur due to the material composition and properties [20,26].

Hydrogen Enhanced Local Plasticity (HELP) was proposed based on the idea that hydrogen enhances the mobility of dislocations, resulting in extreme localization of plastic deformation sufficient to enable sub-critical crack growth that is macroscopically brittle (very small macroscopic deformation) [3,19,25]. This phenomenon caused a reduction in the ductility of the material and a brittle appearance of the fractured surface at low magnifications [10,27]. The HELP mechanism proposes that dislocation mobility is enhanced due to hydrogen accumulation, causing a reduction in the elastic energy on

18

moving dislocations with obstacles (carbides) [3,6,25]. Since hydrogen reduces interaction energy, the stress required for dislocation motion is decreased and localized plasticity is enhanced.

In situ high voltage electron microscopy was used to evaluate thinned specimens subjected to plastic deformation during exposure to either vacuum or hydrogen gas. Such observations revealed a trend to increase the number of dislocations pileups, as well as, initiation of dislocation motion due to hydrogen gas introduction into the scanning electron microscope [19].

The HELP as embrittlement mechanism can be revealed by a dimpled fracture surface appearance as revealed by SEM fracture surface image for AF1410 steel, as shown in Figure 2.3.
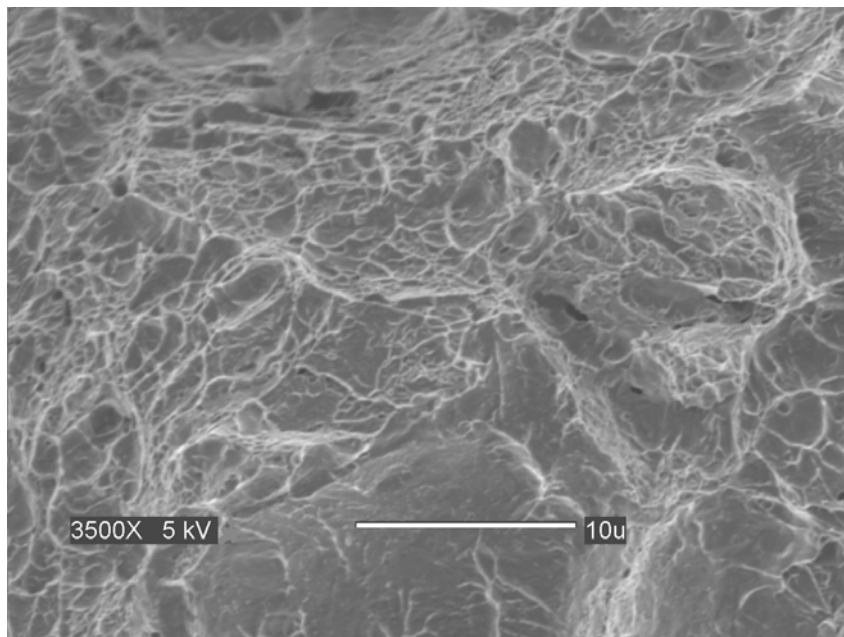
Figure 2.3 SEM fracture surface images showing HELP mechanism in AF1410 steel with dimpled fracture appearance.

High Pressure Theory (H_2) assumes that the high hydrogen pressure is formed into the voids or other microstructural defects that causes the HE. Embrittlement is attributed to high hydrogen concentration localized in voids which start to grow due to the high internal pressure (high H_2 molecules accumulation), increasing the number of microvoids or microcracks in the material. The manifestation of this kind of H-damage mechanism is noticeable as blisters, especially at the sample surface where the H-concentration becomes higher. Furthermore, the presence of blisters can cause the initiation and crack growth in the absence of external applied stresses [28]. This mechanism of HE can be enhanced if the specimen or structural component is subjected to continuous hydrogen supply or high hydrogen fugacities environments observed in marine and hydrogen atmosphere conditions [29]. However, for the case of the UHSS the occurrence of blisters is unlikely to occur due to its high tensile yield strength [10].

Lattice Decohesion Theory was primarily proposed by Troiano and is based on the premise that hydrogen reduces the cohesive strength of steel [30]. Troiano indicated that hydrogen dissolved in steel can concentrate at high triaxial stress regions, causing a weakening of the cohesive force between metal atoms and also enhance the microcrack nucleation [30,31]. When the local hydrogen concentration reaches a critical level, caused by the stress field, then it produces localized embrittlement and crack advances out of hydrogen segregation region, where it is blunted due to plastic deformation at the crack tip. The whole process is reiterated and the crack propagation is discontinuous and controlled by hydrogen diffusion near the crack tip, as further crack growth must await diffusion of hydrogen to the region of high stress state (Figure 2.4).

20
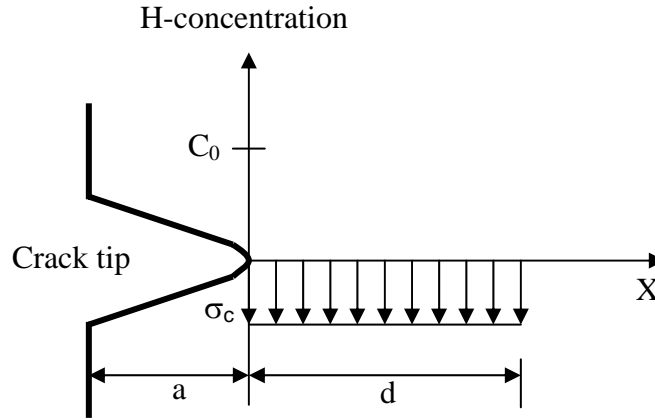
Figure 2.4 Decohesion model for hydrogen embrittlement proposed.

2.4 Hydrogen Assisted Cracking

2.4.1 Internal Hydrogen Assisted Cracking

Several mechanisms serve as a source to introduce the atomic hydrogen into the material's microstructure, which includes manufacturing operations and environmental service conditions. Metals affected by hydrogen suffer a redistribution of dissolved hydrogen from the surrounding microstructure to the fracture process zone due to external loading, which enhances the embrittlement at these localized regions (crack tip). Environmental hydrogen production at the crack tip during stressing is significant since the loading environment is typically aggressive, however, hydrogen evolution takes place also without external stresses [1-3,6,12].

On the other hand, internal hydrogen assisting cracking is highly dependent on hydrogen concentration into the material and the time of exposure under corrosive

environments. Internal hydrogen assisted cracking can be evidenced by microscopic fracture surface of specimens after failure and the causes of failure can be determined. Figure 2.5 shows the internal and external hydrogen embrittlement mechanisms.
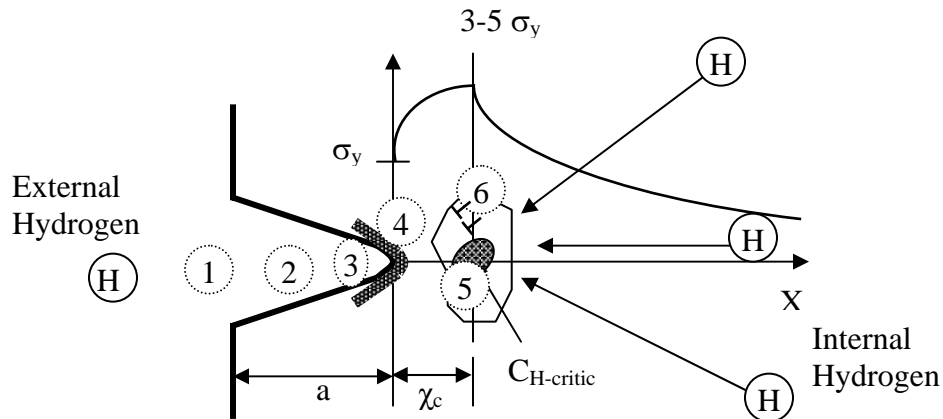
1- Molecular Transport

2- Hydrogen Absorption H_2

3- H_2 Migration, Dissociation to atomic H. Chemical Adsorption

4- Solution to Lattice (into the metal)

5- Bulk Diffusion to Fracture Process Zone

6- Enhanced Fatigue Damage (dislocations)

Figure 2.5 The sequence of elemental process that supply damaging hydrogen to the crack tip fracture process during the hydrogen assisted cracking at different environments and for pre-charged samples.

Figure 2.6 shows the process of internal hydrogen embrittlement, where the surrounding microstructural trapped hydrogen tend to be attracted to regions of high stresses, i.e. crack tip
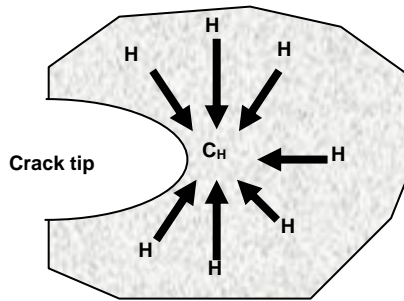
Figure 2.6 Schematic view of internal hydrogen assisted cracking

where C_{H0} is the bulk hydrogen concentration and C_H is hydrogen concentration ahead of the crack tip, where hydrogen concentration at the crack tip becomes higher than C_{H0} due to stress field.

2.4.2 External Hydrogen Assisted Cracking

This mechanism is also called as environmental hydrogen embrittlement assisted cracking. The external embrittlement mechanism is produced by synergistic metal-environmental hydrogen interaction and cyclic or static mechanical loading. Atomic hydrogen is produced predominantly by electrochemical reactions on clean crack surfaces localized close to the tip, followed by hydrogen uptake into the crack tip fracture process zone and subsequent material's embrittlement as shown Figure 2.5 and 2.7. Mass transport mechanisms between the surrounding environment elements are unique to the occluded crack volume and supplies crack tip surface-electrochemical reactions due to marine environment exposure. Hydrogen is produced by dissociative chemical adsorption

for H_2, by chemical reactions for gases such as water vapor or H_2S, or by electrochemical cathodic reactions for acidic or alkaline electrolytes [17]. Once the atomic hydrogen is produced it H diffuses ahead of the crack tip into the fracture process zone causing embrittlement. In addition, metal dissolution and passive film formation can occur at the crack tip, concurrent with H production, which affect crack growth. The extent to which hydrogen dominates the damage in metals remains controversial, but the hydrogen embrittlement assisted cracking mechanism for stress corrosion cracking is accepted broadly for high strength structural metals.

The hydrogen embrittlement mechanism described above is improved by the external loading, which raises the stress concentration at the crack tip. Furthermore, the hydrostatic stress conditions developed ahead of the crack tip caused by external loading attract the atomic hydrogen at this region enhancing the H-concentration that worsens the embrittlement of the material. A schematic view of external hydrogen embrittlement is presented in Figure 2.7.
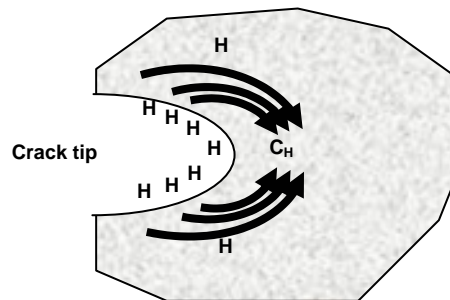
Figure 2.7 External or environmental hydrogen assisted cracking

2.5 Trapping of Hydrogen in Steels

Hydrogen can be trapped by the microstructure of the material depending on the degree of internal defects, presence of second phase particles, precipitates, vacancies, dislocation cores, grain boundaries, inclusions, etc. All of these factors can generate the retention of hydrogen in different stages. Hydrogen trapped can be irreversible and reversible depending on the required activation energy to move through the material [10].

2.5.1 Reversible Trapped Hydrogen

Reversible or some times called diffusible hydrogen has limited resident time into the material because of its relative low activation energy [10,17]. This reversible hydrogen trapped is susceptible to move through dislocation and create new dislocations, especially in UHSS because of its microstructure posses high dislocated lath martensite. Due to external fatigue loading, the reversible trapped hydrogen moves easily and redistributes into the material microstructure, particularly at regions with higher stress concentration such as crack tips, grain boundaries or internal defects. This trapped hydrogen can increase the embrittlement of the material at these localized regions worsening the cracking rates.

2.5.2 Irreversible Trapped Hydrogen

The irreversible trapped hydrogen has permanent resident time into the material at specific temperatures like ambient conditions (~25 ^{o}C). However, at high temperatures its resident time remains contentious. The required activation energy is high and its mobility

very limited. Therefore, it is believed that irreversible trapped hydrogen does not contribute significantly to embrittlement of the material thus not a contributing factor in the fatigue crack growth rates [13,17].

2.6 Mechanical Evaluation

2.6.1 Fatigue Testing

In fracture mechanics, fatigue is defined as the progressive, localized, and permanent structural damage, as a function of time. Fatigue occurs when the material is subjected to cyclic loading at nominal stresses which have maximum values less than the static yield strength of the material. If the resulting fatigue stresses are below ultimate tensile stress, or even the yield stress of the material, this can cause catastrophic failures. Fatigue lifetime is a function of time, material properties, heat treatments, environmental service conditions, etc.

A crack in a structural component can be subjected to three different types of fatigue loading, which involve displacements of the crack surface. There three testing modes are mode I (opening), mode II (sliding), mode III (tearing) and a combination of them. Figure 2.8 shows these three loading modes, which are according to the American Society for Testing Materials (ASTM) [1].
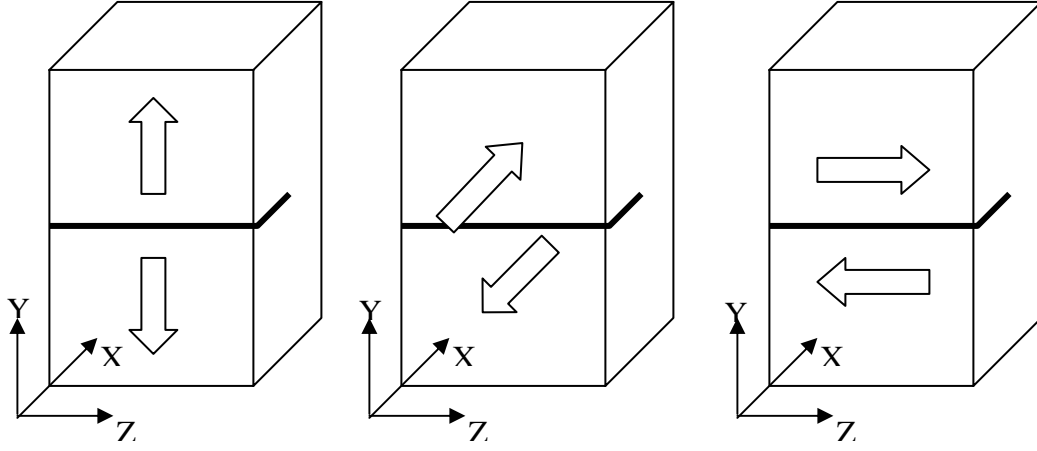
$$K_I = \lim_{r \to 0}\left(\sigma_{yy}\sqrt{2\pi r}\right) \Rightarrow \sigma_{yy} = \sigma_{yy}(r, \theta = 0) \mapsto ModeI$$

$$K_{II} = \lim_{r \to 0}\left(\tau_{xy}\sqrt{2\pi r}\right) \Rightarrow \tau_{xy} = \tau_{xy}(r, \theta = 0) \mapsto ModeII$$

$$K_{III} = \lim_{r \to 0}\left(\tau_{yz}\sqrt{2\pi r}\right) \Rightarrow \tau_{yz} = \tau_{yz}(r, \theta = 0) \mapsto ModeIII$$

Figure 2.8 Testing modes

The stress intensity factor referred for these modes of loading, as K_I (mode I), K_{II} (mode II) and K_{III} (mode III) are shown in Figure 2.8. In addition, the stress intensity factor needs to be calculated and used to determine the crack growth behavior as a function of crack length, loading type, characteristics of aggressive environment, etc.

2.6.2 Effect of Crack Tip Geometry

The effect of the geometry in the crack growth can be caused by the occurrence of blunting during crack incubation period and the presence of branching.

Crack tip blunting takes place in real service conditions, especially for ductile material. Blunting is affected by environment, fatigue crack growth rates, and complex loading conditions. Crack tip blunting is important because it can retard the crack growth by increasing the number of microvoids before to coalescence and therefore require high external stresses to create a new crack surface (Figure 2.9) [32].
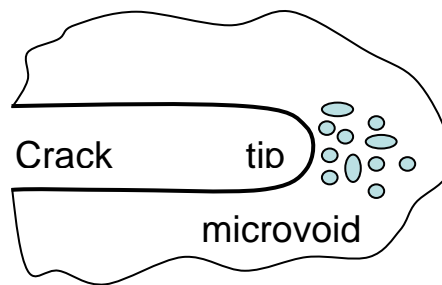
Figure 2.9 Crack tip blunting

Crack branching and kinking serve as an energy dissipation mechanism and lower the stress intensities factors (mode I) at the crack tip. Likewise, both mechanisms can increase the fracture toughness, thresholds for fatigue crack growth rate, and also decrease the fatigue crack growth rate [32]. In metals, the crack branching can be disregarded, because the metal is considered a homogeneous material (Figure 2.10). However, branching can be considered an important factor in crack growth behavior of composite materials.
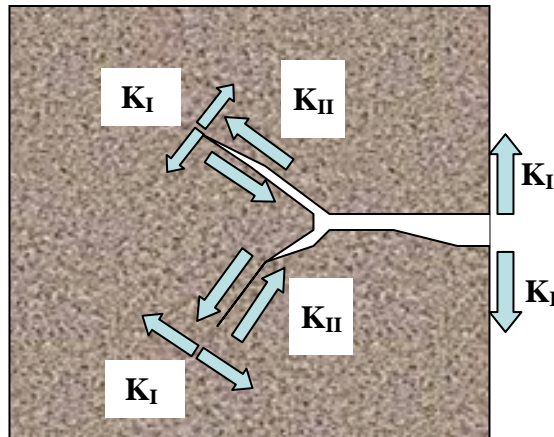
Figure 2.10 Crack branching

2.6.3 Crack Growth Stages

Fatigue crack growth can be divided in three stages, crack initiation (stage I), stable crack growth (stage II), and the onset of the catastrophic failure (stage III).

Stage I is one of the most complicated problems to be studied due to uncertainty in defining the crack size before it grows [1,32,33]. The crack initiation in fatigue depends principally on the material microstructure and environment. Generally dislocation plays an important role in determining the crack nucleation, which generates slip bands at the metal surface. The microcrack initiates at regions with high stress concentrations or with microstructural defects. Furthermore, a corrosive environment has a detrimental effect in the time for crack initiation [32].

Stage II governs the fatigue lifetime of the material following the Paris law regime [1,32-34]. At this stage, several characteristics can be observed on the specimen fracture surface, such as striations and beach marks, which are observed using SEM. These features are typically representative of stage II crack growth but not in all materials

[32-34]. However, parameters such as, material microstructure, mean stress, environment, and specimen geometry does not show significant effect on stable fatigue crack growth rate [34].

Stage III is characterized by larger cracking rates and represents the onset for catastrophic failure. This stage is affected substantially by material microstructure, mean stress, thickness of the sample, and a little influence of environment [34]. Likewise, the fracture surface at this stage is distinguished by dimpled fracture surface appearance, especially for ductile materials. However, the lifetime corresponding to stage III is neglected by designers because it does not contribute to lifetime of the structure.

Figure 2.11 summarizes the three stages of fatigue crack propagation as a function of stress intensity factor.
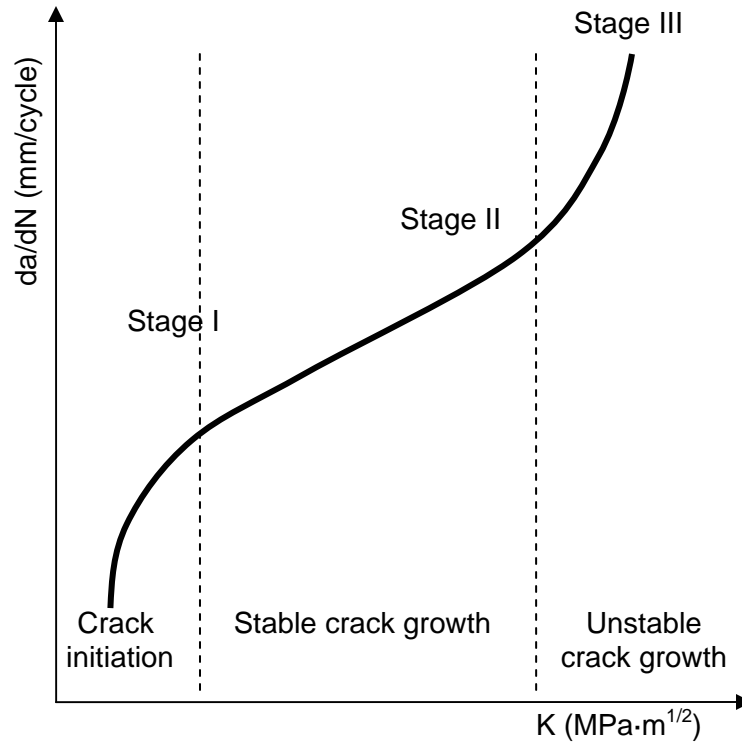
Figure 2.11 Crack growth stages in fatigue

2.6.4 Fracture Surface Analysis

The fracture surface appearance of failed specimens is used to determine the causes of failure [12,35,36]. Fracture modes, striations, beach marks, chevron marks, etc can be observed on the fracture surface. These features can be correlated to some particular aspect occurred during the fatigue testing or in service, for example, some overloads, changes on modes of failure, crack growth rates, material's embrittlement, and others.

Microscopic tools, such as SEM, light microscopes, and AFM were used due to their crucial importance in performing post failure analysis.

2.7 Mathematical Models for Life Prediction

2.7.1 Parameters Identification

It is important to identify the controlling fatigue crack growth parameters in order to predict the total or remaining lifetime of structural components. These parameters can be divided into two principal classes: intrinsic and extrinsic parameters [14].

Intrinsic or material parameters which are inherent to the material and are the following: E, G, σ_{ys}, σ_u, υ, K_{IC}, ΔK_{th}, strain hardening exponent (n), cyclic strain hardening exponent (n'), true fracture strain (ε_f), and material microstructure characteristics.

Extrinsic or external parameters which are referred to the conditions to which the material is subjected and are the following: frequency, temperature, type of environment (liquid, gaseous, etc), loading condition, crack length, hydrogen concentration, specimen geometry (dimensions), loading ratio, maximum stress intensity factor, minimum stress intensity factor, applied stress (σ), mean stress (σ_m), stress intensity range, overload ratio, and others.

Careful and systematic experimental and analytical studies need to be performed in order to determine which parameters affect the fatigue crack growth behavior.

2.7.2 Types of Models

The effects of hydrogen on steels have been extensively studied, however most of the research has been limited to static loading scenarios [2]. The existing hydrogen assisted fatigue crack growth models have been divided into two categories, i) analytical

which depends on the fundamental ideas, such as hydrogen diffusion, hydrogen concentration and crack tip electrochemistry and ii) empirical, based primarily on curve fitting of the experimental data.

Models based on hydrogen diffusion concepts seek to establish a functional relationship between rate of diffusion and accompanying electrochemical parameters in the form of a system of partial differential equations along with complex boundary conditions, as it shown in Eqs. 7 [6],

$$\frac{\partial C}{\partial t} = D\nabla^2 C + \nabla\left(-\frac{DC}{RT}V_H\nabla\sigma_{kk}\right) - \frac{\partial C_r}{\partial t} - \frac{\partial C_i}{\partial t}$$

$$J = -D\cdot\nabla C - \frac{DV_H}{RT}C\nabla\sigma_{kk} \tag{7}$$

where D, C, V_H, σ_{kk}, R, T, C_r and C_i, refers to diffusion coefficient, hydrogen concentration, partial molar volume of hydrogen atoms, hydrostatic stress, gas constant, absolute temperature, reversible trapped hydrogen concentration and irreversible trapped hydrogen concentration, respectively. Analytical elasto-plastic solutions have also been attempted that seek to relate the extent of hydrogen diffusion and crack growth mechanisms, as shown in Eq. 8 [6],

$$\frac{2(1+\upsilon)K_\rho}{3\sigma_{ys}(2\pi)^{1/2}} = \chi_{cr}^{1/2}\left[\ln\left(1+\frac{\chi_{cr}}{\rho}\right)+\frac{1}{2}\right] \tag{8}$$

where K_ρ, ρ, υ and σ_{ys} refer to stress intensity factor, notch-root radius, poisson ratio

and yield strength, respectively. χ_{cr} signifies the critical distance ahead of the crack tip where hydrostatic stresses achieve a maximum value and hydrogen concentration is assumed to become critical. A rigorous and cumbersome analytical/numerical solution (of Eqs. 7 and 8) generally yields the rate of crack growth as a function of stress intensity factor and hydrogen content [6, 17]. However, in spite of the closed and deterministic form of the analytical solutions, the results seldom match actual service lifetime of the steel components due to various crack tip microstructural (e.g., phase transformations) and electrochemical (i.e., rate of hydrogen production, diffusion and retention) errors. Therefore, the applicability of most analytical models as a quantitative basis for life-assessment becomes contentious and limited. On the other hand, empirical (Paris type) relationships as shown in Eq. 9 can not truly be qualified as a predictive tool, as they are all essentially based on curve fitting, and thus fit the data well as long as the constants are properly adjusted.

$$\frac{da}{dN} = C(\Delta K)^m \qquad (9)$$

As a result, both analytical and empirical approaches have enjoyed a very limited success in predicting fatigue lifetime of materials. However, various modified forms of semi-empirical relationships that seek to establish a phenomenological relationship between physical parameters, material, and cracking behavior have proven to be more robust in their practical use than the purely analytical or empirical predictive models [17].

2.8 Acoustic Emission Technique

The non-destructive AE technique has been found to be a useful alternative that may help in conducting in-situ monitoring of critical aircraft components, such as, arresting shanks and landing gears suffering from environmental hydrogen and corrosion [13]. AE signals are emitted by the material when internal damage occurs causing a localized stress field leading to subsequent wave propagation and detection.   However, discerning AE signals can be a complex and challenging process as the output is a mixture of multiple signals emanating from various cracking processes, background noise and friction, etc. [37-39]. Furthermore, the variations in the resulting AE signals in high strength aluminum and steel alloys are generally minute, erratic and the energy levels are too low for proper classification of failure events especially during the crack initiation stages [37].   Therefore, the successful implementation of AE technique requires substantial preliminary calibration, parameters adjustment, and threshold setups in order to filter out the undesirable signals and retain the meaningful AE data [38].

One of the major limitations for the AE technique is the unwanted mechanical or electronic noise present in structures. Precautions against interfering noise are an integral part of AE technology. Noise problems can be addressed in many ways. First, it may be possible to stop the noise at the source. Second, it may be possible to eliminate an acoustic source by applying impedance-mismatch barriers or damping materials at strategic points on the structure. Electrical noise problems are often the result of poor grounding and shielding practices, it can be eliminated by using differential sensors or sensors with built-in preamplifiers [38].

AE technique can also be utilized for processes such as in-process weld monitoring, detecting tool touch and tool wear during automatic machining, detecting wear and loss of lubrication in rotating equipment and tribological studies, detecting loose parts and loose particles, detecting and monitoring leaks, cavitations, and flow, monitoring chemical reaction, including corrosion processes, liquid-solid transformation, and phase transformations, etc [38-39].

3   EXPERIMENTAL PROCEDURE

All testing was conducted at room temperature on compact tension and flat-tension-compression. Specimens with dimensions 5cm x 4cm x 0.32cm and 12cm x 2.8cm x 0.15cm were subjected to fatigue loading at different loading ratios. Furthermore, all CT specimens were pre-cracked according to the ASTM E399-95 standard to perform fatigue crack growth studies. However, tension-compression and aluminum CT samples were not pre-cracked with the purpose of studying the crack imitation process. Quasi-static tests performed at various rates of loading between 8N/s to 15,000N/s indicated virtually the same average ultimate static strength of about 38-kN for CT AF1410 steel. Furthermore, for tension-compression quasi-static tests, 65KN and 30KN of ultimate static strength in tension and compression were found respectively. Flat central holed steel specimens for tension-compression fatigue testing were used to evaluate the crack initiation process due to the presence of the hole as a stress concentrator. On the other hand, acoustic emission technique was used to monitor the fatigue crack initiation process in aluminum and tension-compression specimens. SEM has been widely used in the study of microcrack nucleation and growth, striation shapes, slip bands, and to extract general failure features of a variety of materials. It was utilized in this case for fracture surface analysis in order to corroborate and further understand failure mechanisms and shifts in the modes of failure [2,13]. Crack length was measured using compliance technique that has been proven reliable in crack growth studies of AF1410 steel [40,41]. Periodic visual inspection was also performed to verify compliance based crack length calculations.

3.1 Materials

A promising AF1410 steel with an outstanding combination of high fracture toughness (~130 MPa-m$^{1/2}$) and strength (~1.8 GPa) is high on the list of materials that the U.S Navy is interested in using more widely. AF1410 is currently used in some F-18 arresting shanks. However, before its wider use commences, the interaction between structural loading and marine environmental effects must be carefully examined.

On the other hand, high strength aluminum AA7075-T6 (strength ~537 MPa and toughness ~ 27MPa-m$^{1/2}$) has been widely used in aircraft structural components (fuselage, wing, etc) and therefore, it is important to improve understanding of various agents contributing to the corrosion fatigue characteristics of this material [7].

The chemical composition and material properties for AF1410 steel and AA7075-T6 aluminum alloy were summarized in Table 3.1 and Table 3.2 respectively. The sample geometries used in the current research program are shown in Figures 3.1 (a) and (b) respectively, furthermore, the material microstructure is shown in Figure 3.1 (c).

Table 3.1 Material properties and composition of AF1410 steel

Properties (minimum)	Longitudinal	Transverse
Ultimate Strength MPa (Ksi)	1627.2 (236)	1620 (235)
Yield Strength 0.2% MPa (Ksi)	1482.4 (215)	1469 (213)
Elongation (in 4D, %)	12	12
Reduction in Area (%)	60	55

AF1410 Composition							
C	Ni	Co	Cr	Mo	Mn	P	S
0.14	10.55	13.69	2.06	1.08	0.14	0.01	0.006
Si	Al	Ti	N	O		V	Fe
0.02	0.035	0.011	0.02	< 0.002		0.01	Balance

Table 3.2 Material properties and composition of AA7075-T6 aluminum alloy

Properties (minimum)	Longitudinal
Ultimate Strength MPa (Ksi)	572 (83)
Yield Strength 0.2% MPa (Ksi)	503 (73)
Elongation (%)	11

AA7075-T6 Composition				
Si	Fe	Mn	Ti	Al
< 0.4	< 0.5	< 0.3	< 0.2	87.1 – 91.4
Cu	Mg	Cr	Zn	
1.2-2	2.1-2.9	0.18-0.28	5.1-6.1	

(a)   (b)

(c)
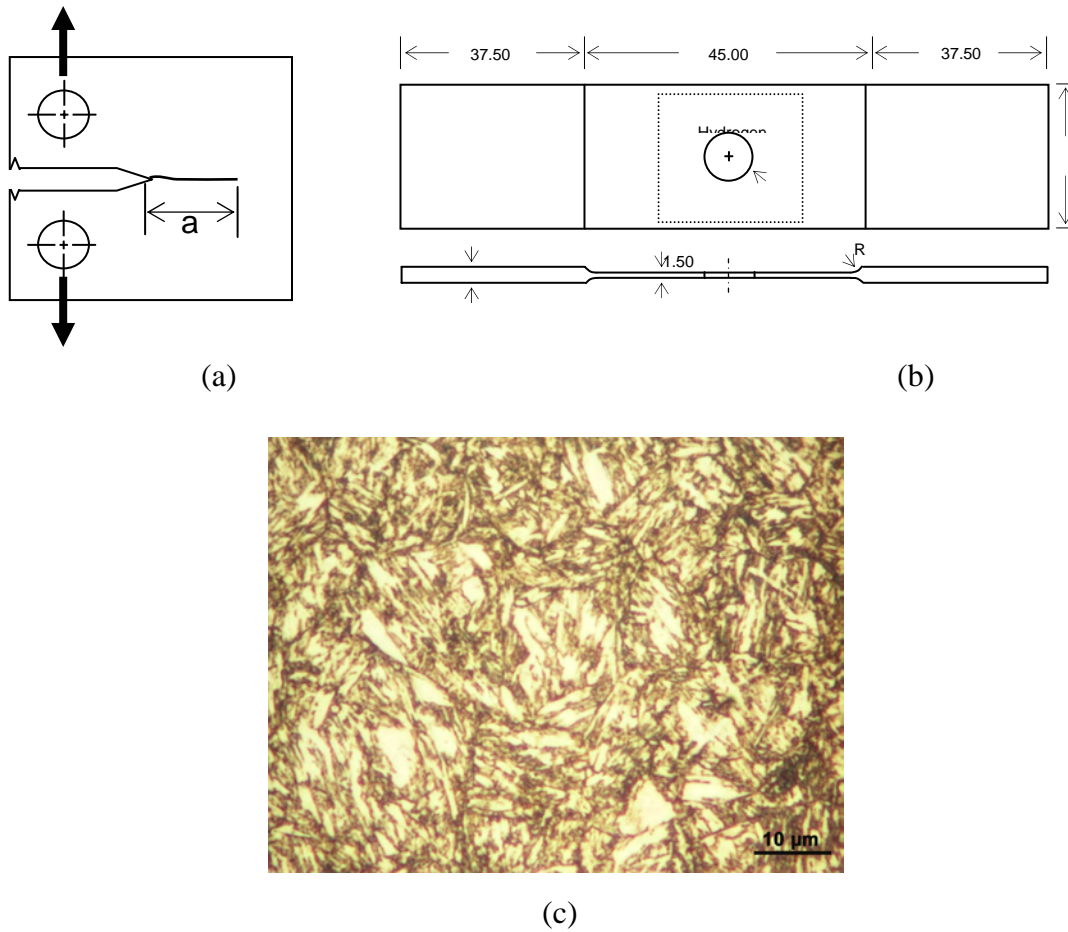
Figure 3.1 (a) AF1410 steel and AA7075-T6 compact tension specimens based on ASTM E-399, (b) tension-compression samples and (d) AF1410 microstructure.

In addition, the microstructure of this multi-phased ultra high strength steel includes lath martensite, some retained austenite, bainite, and carbides, as shown in Figure 3.1 (c).

3.1.1 Material Polishing

Special care must be taken in polishing the steel and aluminum samples in order

to avoid any stress concentration onto sample surface which could affect the crack initiation and growth behavior, which can induce variations in period for crack initiation or in the fatigue crack growth rates calculations. The polishing process was carried out in successive steps with the following grid papers; 60, 120, 240, 320, 400, 600, 800 and 1200 respectively. The final polishing (mirror-like surface) stage was made with 0.05μ alumina suspensions using Buehler Chemomet cloths.

3.2 Mechanical Testing

3.2.1 Crack Length Measurements

Special care was taken in measuring crack length, which is prone to error depending on the method used. Testing load, COD and specimen geometry were used to calculate the corresponding crack length for each loading cycle. Crack length was, therefore, calculated using the compliance technique based on Eq. 10 [40], stress analysis based on Eq. 11 [41] and via visual inspection by using a traveling microscope with 20X magnification lens.

$$a = W[1.0010 - 4.6695U_X + 18.46U_X^2 - 236.82U_X^3 + 1214.90U_X^4 - 2143.60U_X^5]$$

(10)

where a is the crack length and W is the depth of the specimen, and

$$U_X = \frac{1}{\left(\dfrac{tEV_X}{P}\right)^{0.5} + 1}$$

t, E, V_x and P are the specimen thickness, Young's modulus, COD and load, respectively.

Based on stress analysis, crack length was obtained from the real and positive root of the following Eq. 11,

$$35.6(1 - a/W)^3 + [\frac{V_X Et}{P} - 52.91](1 - a/W)^2 + 30.13(1 - a/W) - 19.75 = 0$$

(11)

Crack lengths from these three techniques have been found to be virtually the same as can be observed in Figure 3.2 for aluminum and steel specimens.
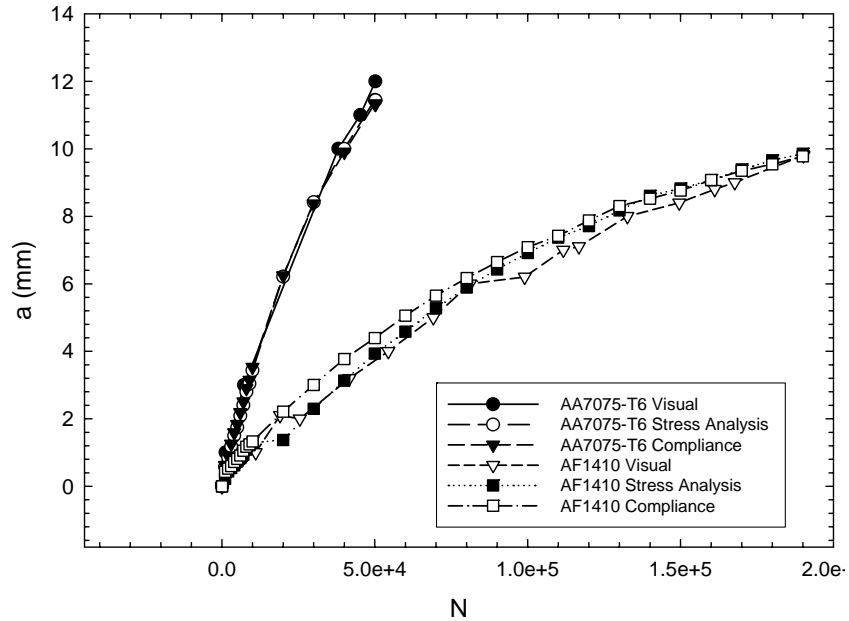

Figure 3.2 Crack length obtained from compliance, stress analysis and visual inspection

3.2.2 Fatigue Evaluation

The fatigue tests were carried out in load and strain control modes by using a servo-hydraulic fatigue testing machine MTS-810 retrofitted by Instron Electronics. The baseline tests were performed in lab air. Fatigue tests for AA7075-T6 and AF1410 alloys

were carried out at load ratio R=0.4 under strain "COD" control mode. In addition, for tension-compression specimens, a load ratio R=-0.5 in load control mode was used. Strain controlled tests are performed under sinusoidal loading form while trapezoidal and triangular loading were used for load control tests. Moreover, fatigue crack initiation studies in compact tension specimens of AA7070-T6 aluminum alloy were evaluated under R=0.3 and using triangular loading form. For strain control mode, a 17% of static yield load was used as maximum cyclic applied load. On the other hand, for load control mode, a 50% of the static yield load was used as maximum cyclic applied load.

The fatigue testing parameters were load range, load amplitude, mean load, load ratio, and load amplitude ratio. These parameters were calculated by using the Eqs. 12:

Load range

$$\Delta P = P_{max} - P_{min}$$

Load amplitude

$$P_a = (P_{max} - P_{min})/2$$

Mean load

$$P_m = (P_{max} + P_{min})/2$$

Load ratio

$$R = \frac{P_{min}}{P_{max}}$$

Load amplitude ratio

$$A = \frac{P_a}{P_m} \tag{12}$$

where P_{max} and P_{min} are maximum and minimum cyclic loads applied to the specimen respectively.

3.2.3 Loading Shape Effects

Different loading forms can be utilized for fatigue lifetime predictions in order to simulate the actual service conditions of structural components. In the current research, loading forms such as sinusoidal, trapezoidal, and triangular were used. Sinusoidal waveform (strain control mode) was used in order to determine the typical crack growth rates for specimens subjected to different environmental conditions such as corrosive (marine) environments, inert environment (air), and with prior electrolytically hydrogen charge. On the other hand, trapezoidal (load control mode) waveform was used to evaluate the short term hold time effect which is generally ignored for many researches at ambient temperatures [42,43]. A triangular waveform (variation of trapezoidal form by using cero seconds of hold time at the peak load) was used to study the effect of fatigue crack initiation in aluminum alloy.

3.2.4 Marine Environment Evaluation

It has been shown that in the presence of chloride ions (sea water) the pH of crack tip can be acidic even when the bulk solution is almost neutral. This occurs due to the hydrolysis of corroding species such as steel and aluminum. Since the pH of the naval (service) environment can vary anywhere between 3 to 5, a mild 1%NaCl and 3.5%NaCl solution of pH ~ 2.5 (simulating crack tip pH) was selected for corrosion fatigue crack

growth studies [1,8,9,12].

3.2.5 Crack Opening Displacement Tests

Fatigue crack nucleation generally occurs from plastic straining in localized regions. As a result, strain "COD" controlled tests can better characterize the fatigue behavior of a material than load controlled tests, especially in the notched specimens where significant localized plastic deformation is frequently present. Load decrementing testing (LDT) is a strain controlled fatigue mechanism in which the COD (maximum and minimum) values are kept constant while the load drops in response to lowering stress intensity at the tip of growing crack. LDT is an excellent technique in conducting comparative FCG studies and it has several advantages over the load controlled fatigue testing. For instance, multiple but complete lifetimes can be obtained from a single specimen, testing time is greatly reduced and stable crack growth (corresponding to region II in the conventional load control testing) can be evaluated satisfactorily [2,12,13]. After sufficient preliminary testing and based on the constraints imposed by the initial K-values used, two complete lifetimes were obtained from each specimen.

The fatigue loading form for COD controlled tests performed by using sinusoidal waveform is depicted in Figure 3.3.
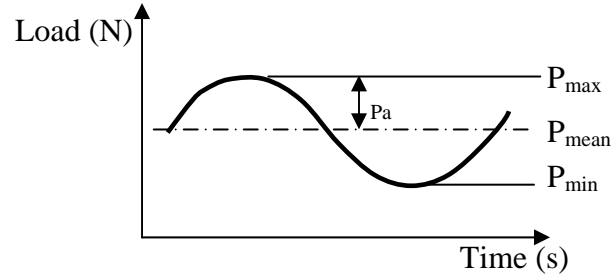
Figure 3.3 Sinusoidal loading form for hydrogen concentration evaluation

3.2.6 Hold Time-Fatigue Interaction

Fatigue in machines/structural components undergoes a loading cycle that depends on the contact time; for example, sustained loads at the peak loads [42,43]. Critical aircraft components, such as arresting shanks or landing gears undergo a sudden rise time followed by a hold time at peak load. Therefore, in order to properly simulate such fatigue scenario, a high rise/descent rate of loading of 100,000-N/s was established, dictated mainly by the equipment limitations, whereas the hold time was varied from 0 to 60 seconds. Hold time testing was conducted under load control trapezoidal waveform. The waveform corresponding to hold time testing is depicted in Figure 3.4. At each hold time, testing was performed on i) specimens in air, ii) specimens in the presence of mild 3.5%NaCl with pH ~ 2.5 (simulating crack tip pH) electrolyte, and iii) on specimens charged with hydrogen for 82 hours.
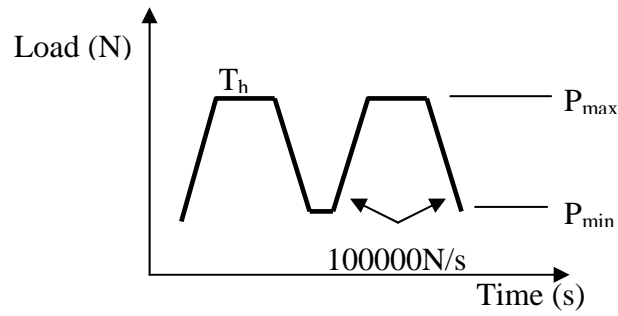
46

Figure 3.4 Hold time loading form.

3.2.7 Tension-Compression Testing

It is well known that tension-compression scenario is more detrimental than either one loading mode separately in the fatigue life of high strength alloys [32]. Furthermore, any realistic aircraft component inevitably undergoes a fully reversed (tension-compression) cycle. To further the understanding of the fatigue crack growth in marine and hydrogen embrittlement conditions, fully reversed cycle was designed and the loading form was triangular as depicted in Figure 3.5. The designed tension-compression fatigue testing simulates the cyclic landings and take offs of landing gears in aircraft structures. Therefore, this part of the research is expected to yield very relevant fatigue lifetime data.
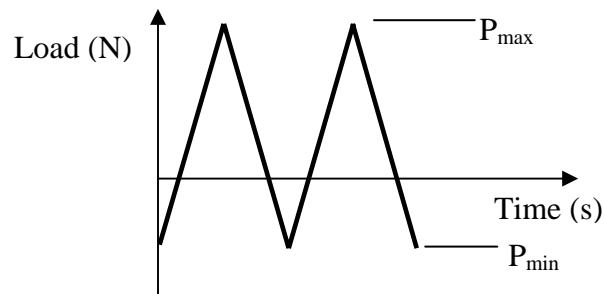

Figure 3.5 Triangular loading form for tension-compression testing

47

3.3 Electrolytic Hydrogen Charging

3.3.1 Hydrogen Permeation

The actual size of these aircraft components, i.e. landing gears or arresting shanks, is larger than laboratory specimens, therefore, aircraft parts in service do not, in general, experience a hydrogen flux through the material thickness. Therefore, small and thin steel specimens were subjected to electrolytic hydrogen charging (Figure 3.6) in order to obtain the diffusion coefficient for the AF1410, resulting $D = 10^{-8}$ cm^2/s which is very low compared to other steels [23,29]. As a consequence, during hydrogen charging process, significant hydrogen concentration remains in the vicinity of the metal surface where it manifests localized embrittlement that leads to subsequent crack initiation and growth under stress.
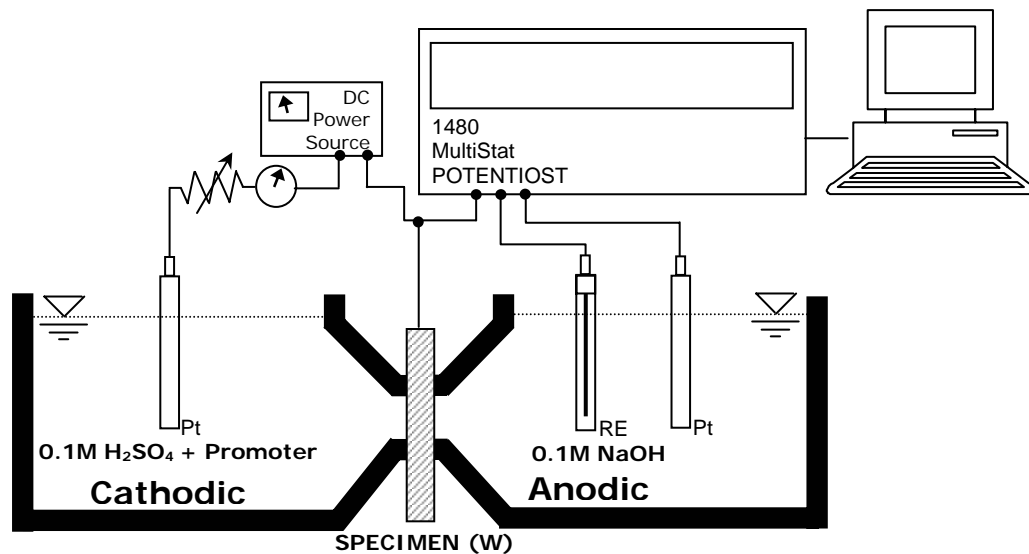

Figure 3.6 Schematic of electrolytic hydrogen charging cell

The electrolytic hydrogen charging procedure for AF1410 compact tension specimens was performed using the following parameters:

- Current density = 0.31-2 mA/cm^2 (low value was used to reduce the pitting corrosion on the lateral side [surface] where hydrogen charging is performed).

- Cathode Area = 6.43 cm^2 (area at the side where the hydrogen evolution/charging is taken place "Input side." Solution at the input side: 0.1M H_2SO_4+1g/l $Na_2HAsO_4 \cdot 7H_2O$).

- Anode Area = 1.89 cm^2 (area where hydrogen leaves the specimen, and it is called "output side." Solution on the hydrogen free side: 0.1M NaOH. It is important to note that hydrogen did not pass through the sample and this side was used to control/measure if hydrogen leaves the material).

- Charging Time = varied from 0 – 84 hours.

- Cell type = cathodic charging – galvanostatic Teflon cell.

For **tension-compression** specimens the procedure was similar to the CT specimens:

- Current density = 2.0 mA/cm^2.

- Cathode Area = 4.84 cm^2.

- Anode Area = 4.84 cm^2

- Charging Time = variable (from 0 to 6 hours)

- Cell type = cathodic charging – galvanostatic Teflon cell.

3.3.2 Hydrogen Concentration Evaluation

The penetration depth of hydrogen upon service can only be in the order of several micrometers which naturally depend on the exposure or service time. In order to obtain a quantitative understanding of the effects of hydrogen on AF1410 steel, fatigue testing was performed on specimens charged with hydrogen at various concentration levels. Figure 3.7 shows the various hydrogen penetration depths as a function of different hydrogen charging times. Hydrogen charging was performed by subjecting one and two surfaces to cathodic polarization simultaneously [23,29]. This ensured that approximately equal amounts of hydrogen were introduced on both surfaces. Specimens were charged in a controlled manner from 0 to (a limiting case of) 84 hours permeating hydrogen to an estimated depth of 0 mm to over 95% penetration on both sides of the specimen as represented in Figures 3.7 and 3.8. The hydrogen concentration scenarios are relevant as hydrogen flux is generally not possible in realistic aircraft components and as a result, significant hydrogen remains only in the vicinity of the metal surface where it manifests localized embrittlement leading to subsequent crack initiation and growth under stress. This part of testing was performed in strain controlled mode under a sinusoidal waveform (as sketched in Figure 3.3) at a frequency of 0.5Hz.
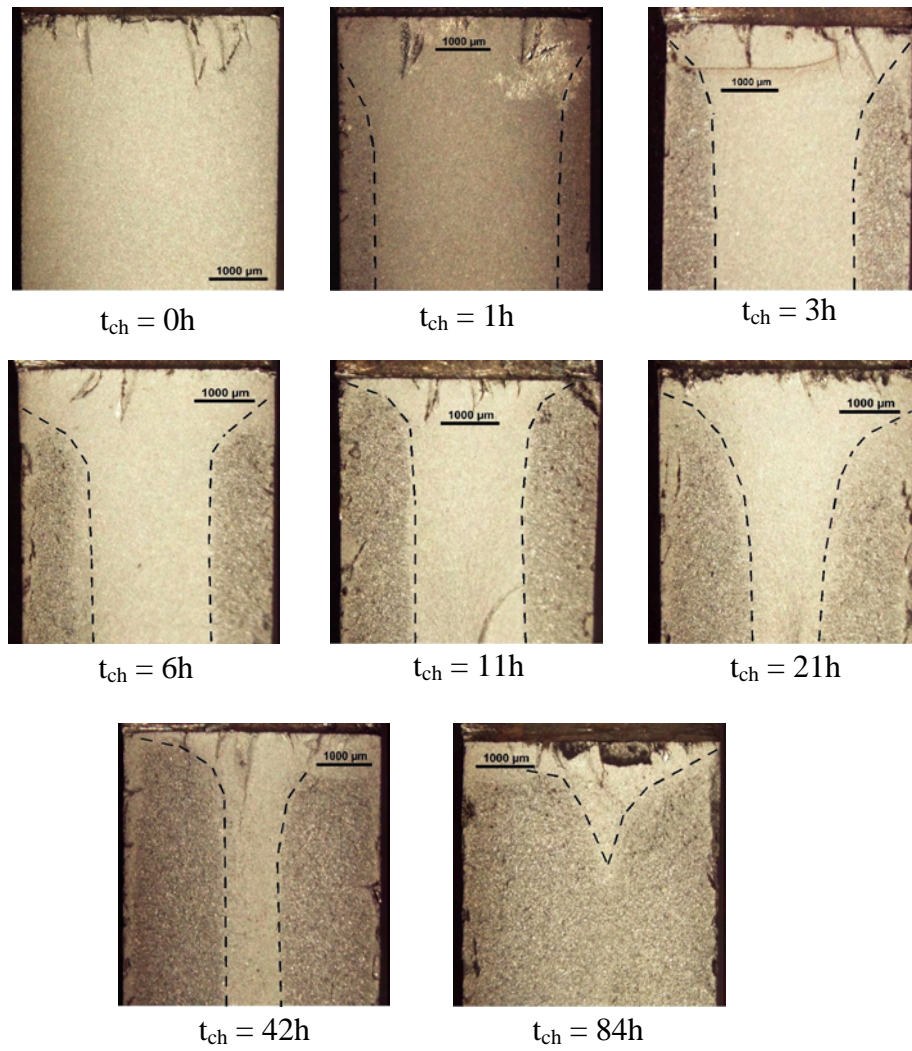
t_ch = 0h   t_ch = 1h   t_ch = 3h

t_ch = 6h   t_ch = 11h   t_ch = 21h

t_ch = 42h   t_ch = 84h

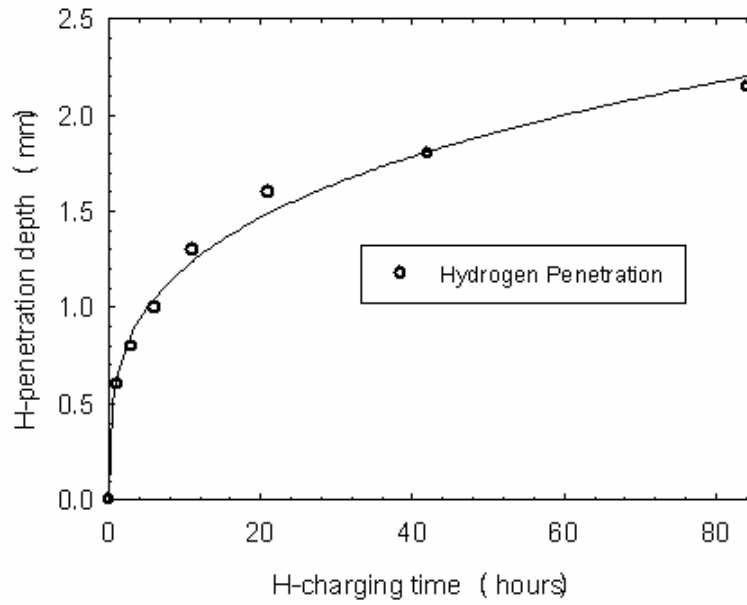**Figure 3.7 Hydrogen penetration depth for AF1410 steel**

Figure 3.8 Penetration depth as a function of hydrogen charging time.

3.4 Fracture Surface Evaluation

3.4.1 SEM and AFM images

Post-failure analysis was performed in fractured specimens by using several microscopic techniques in order to obtain the fractures surface features, which can be used to discern the causes of failure.

A JEOL JSM 6100 SEM was used to obtain the fracture surface images of specimens tested. The SEM (magnifications from 10-10000X) allows us to obtain qualitative information for striation heights, quantifiable grain size measurements, and fracture modes identification. The instrument was operated at 20kV, 20mm working distance and 1mm aperture to enhance the depth of field of the images as recommended for metals [35,36]. Complementary surface analyses were conducted on a NanoSurf

easyScan AFM operated in non-contact mode. The AFM has excellent quantifiable capabilities to obtain complete fracture surface morphological information such as striation widths-heights and cross sectional profile [35,36]. The operating parameters used to obtain fractured surface images was performed adjusting the parameters such as Z-range (varied from 5-30µm), scan-range (varied from 5-100µm), and time-line (varied from 0.1-1 seconds).

Figure 3.9 shows the fracture surface of an aluminum alloy tested in corrosive solution where complete morphological information can be observed and measured [12]. In addition, SEM fracture surface image displayed in Figure 3.10 shows a typical inter-granular fracture of high strength AF1410 steel evaluated under hydrogen assisted cracking condition [13].
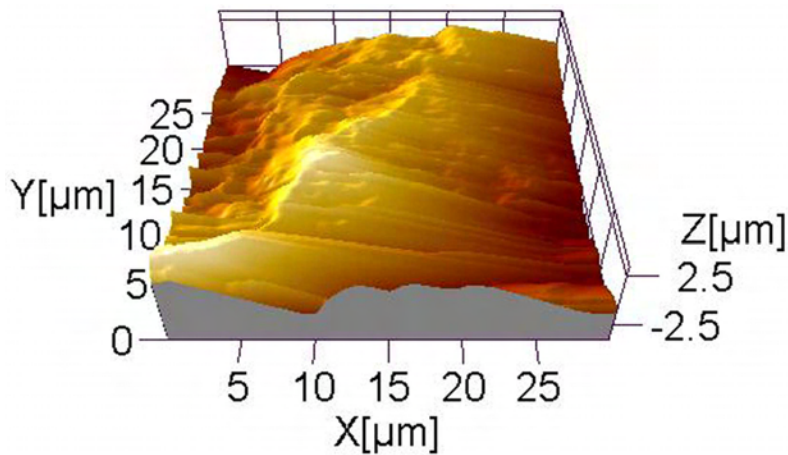

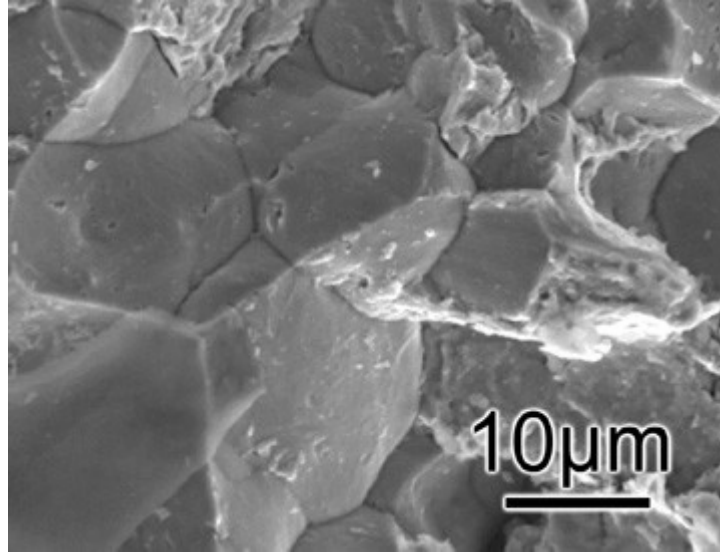**Figure 3.9 AFM fracture surface of AA7075-T6 aluminum alloy.**

Figure 3.10 SEM fracture surface image showing an IG fracture mode for an AF1410.

3.5 Acoustic Emission Setup

An 8-channel AE system manufactured by Physical Acoustics Corporation, Inc. was used to monitor cracking process. The AE system setup and sensors location is shown in Figure 3.11. Two Pico-sensors were used in a linear array on the specimen surface at 30 mm distance from each other. Preliminary testing was performed according to ASTM E976 standard, where the lead breaks of 0.5 mm diameter and 2H of hardness are used to calibrate the AE system and source location parameters with respect to the material used [37-39].

Acoustic emission signals from growing fatigue cracks present difficulties in eliminating extraneous background noise. Therefore, high damping rubber was used around the loading pins in order to minimize frictional noises. After significant preliminary testing and data processing, it was concluded to use 20 dB as a pre-amplifier

parameter. In order to enhance the filtering of background noise a threshold value of 35dB and filtering frequency of 10-1000 kHz were used. These values were selected because most of the background noise has low amplitudes and frequency with long duration times (for example friction). Moreover, very short signals with high frequencies may indicate electrical noise peaks, especially if they arrive at all channels at the same time [39].
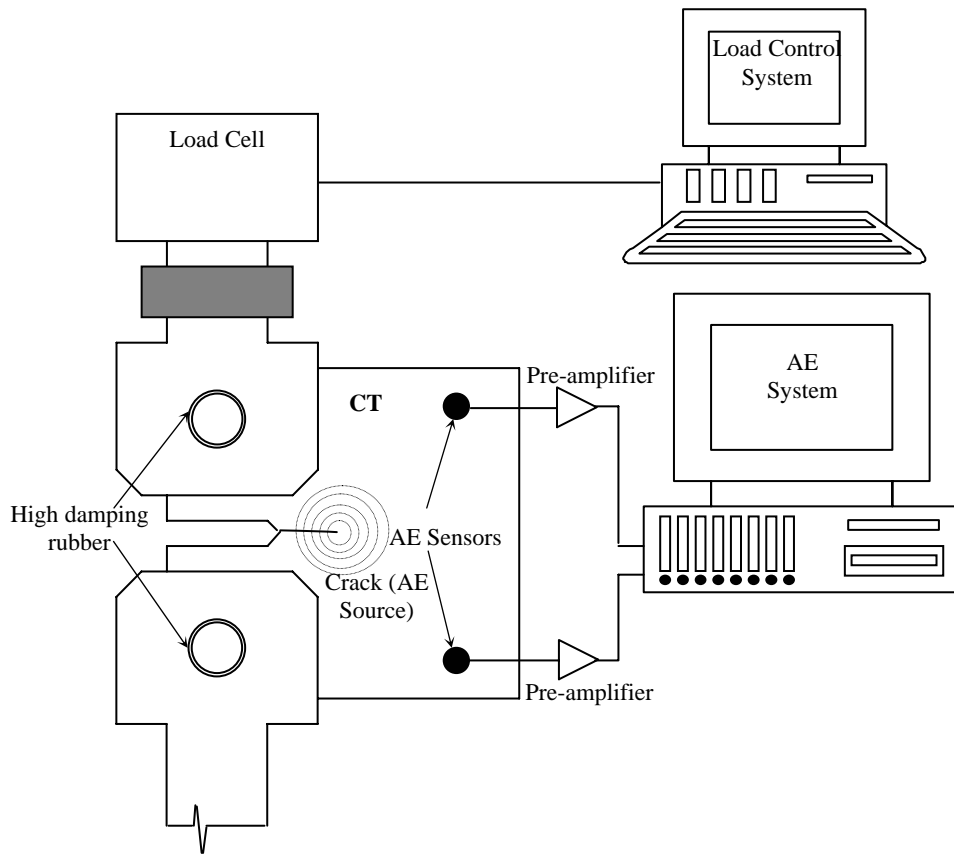

Figure 3.11 AE monitoring setup for a CT sample

4 RESULTS AND DISCUSSION

4.1 Corrosion Fatigue of AA7075-T6 and AF1410 under COD Controlled

Initial tests conducted in the presence of electrolyte indicated that the second lifetime obtained from the same specimen was consistently lower than the first lifetime, as shown for a typical specimen in Figure 4.1. This result suggested that the salt laden electrolyte was being diffused into the corrosion process zone ahead of crack tip even at a relatively high test frequency of 1Hz. Probably, the electrochemical processes were not limited to the crack tip and the crack may be propagating into a region already altered by the corrosion process. Test results indicated that the presence of a mildly aggressive marine environment, even at sub-critical fatigue stresses, can significantly raise CFCG rates and impose its detrimental effects on AA7075-T6 aircraft structural components. Furthermore, Figure 4.2 shows up to two times increase in the CFCG for all AA7075-T6 specimens tested in the presence of electrolyte as compared to those tested in air. The results matched well with published literature [7, 43-46].
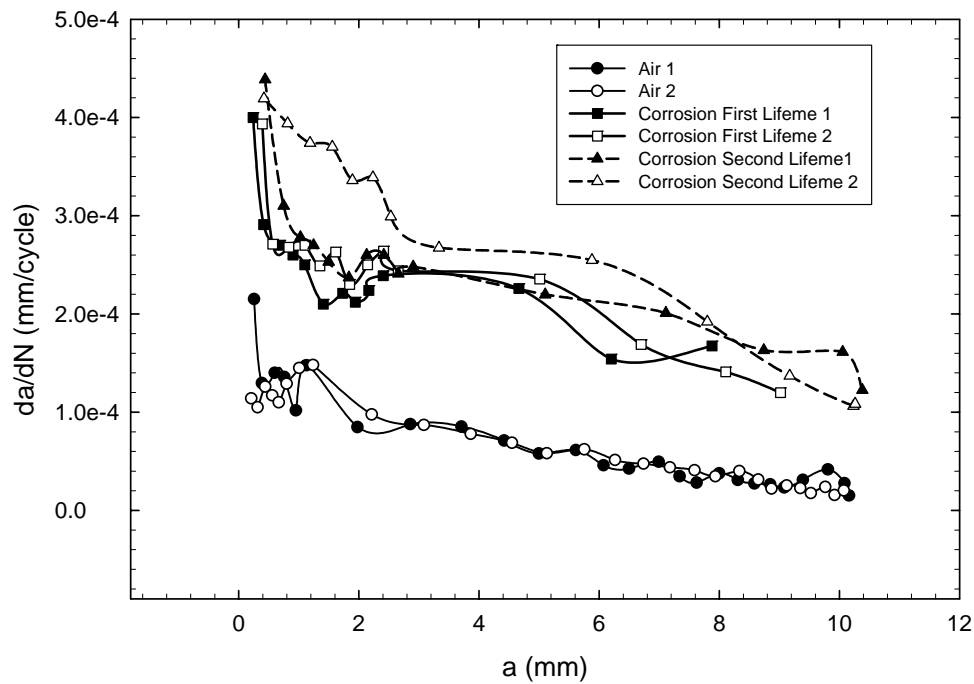
Figure 4.1 Typical results of CFCG lifetime for AA7075-T6 specimens
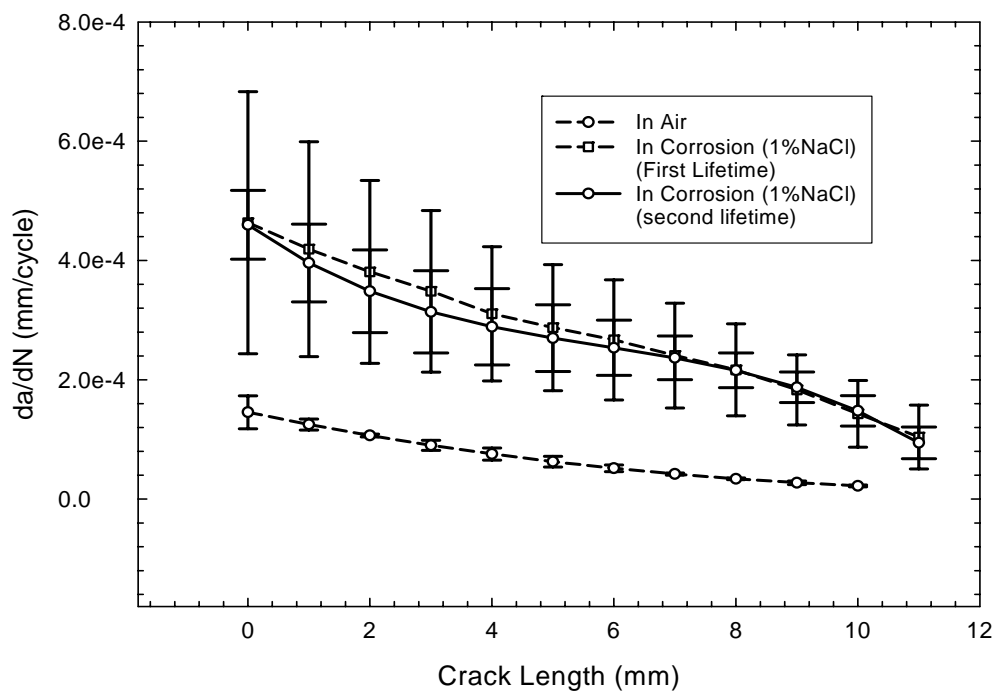

Figure 4.2 Average results of CFCG shown for AA7075-T6 specimens

On the other hand, no significant changes in the CFCG rates of AF1410 specimens subjected to 1% and 3.5%NaCl solution at 1Hz frequency in comparison to the tests conducted in air. However, reducing the frequency to 0.5Hz significantly increased the CFCG at 1% and 3.5%NaCl electrolyte, as shown in Figure 4.3. It is obvious, that the reduction in lifetime at 0.5Hz frequency is greater in 3.5%NaCl solution compared to 1%NaCl. These observations were not in complete agreement with the reported results by Antolovich [2,5].
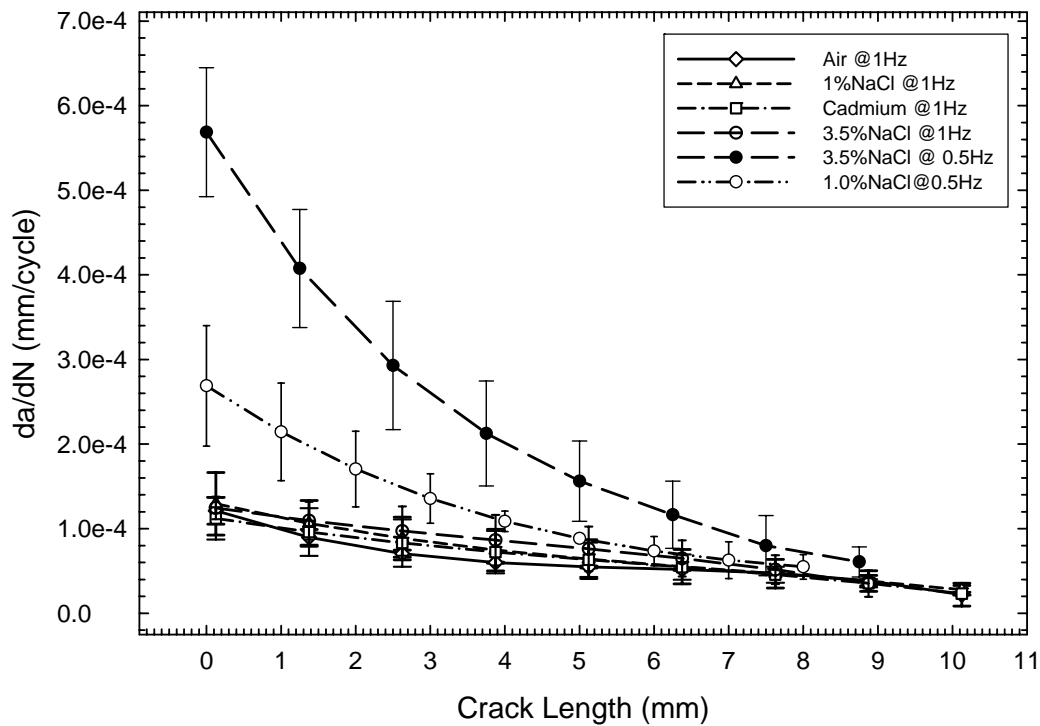

Figure 4.3 Average results of CFCG shown for AF1410 specimens

In fact, the increase in CFCG rate of AA7075-T6 and AF1410 can be explained in terms of various electrochemical / micromechanical processes, which occur

58

simultaneously at the crack tip, such as, metal dissolution, hydrogen embrittlement, crack tip microcracking, frequency of loading and ionic concentration, etc. [5,6,44-46].

However, literature on AF1410 and AA7075-T6 provides a substantial reduction in lifetime at up to 10Hz frequency and as the concentration of NaCl is increased [5,7]. Rate of loading frequency have significant effect on the crack tip chemistry. However, its effect on CGR is not quite clear due to complex interaction of various factors [46]. For example, high frequencies can cause an increase in the pumping effect of corrosive solution, while low frequencies decrease the pumping effect at the crack tip; however, the testing time and pH at the crack tip increases causing **metal dissolution**.

Probably, an increase in the concentration of NaCl leads to higher concentration of chloride ions with antecedent deleterious effects based on electrochemical considerations, presence of Fe^{2+}, OH^-, H^+, Cl^-, with anodic/cathodic reactions. For instance, $Fe^{2+} + 2e^- = Fe$ can be anodic with respect to $Fe^{3+} + e^- = Fe^{2+}$, therefore, presence of chloride ions can lead to the development of multiple and/or parallel sources to enhance CFCG rate due to the multi-valence nature of Fe. In addition, high concentrations of NaCl enhance crack tip current density and subsequently promote metal dissolution ($Fe = Fe^{2+} + 2e^-$) and enhance CFCG rate as shown in Figure 4.3. Therefore, metal dissolution as a function of loading frequency, pH and NaCl content, etc., plays a significant role in the observed experimental results. However, there is considerable controversy associated with known metal dissolution based models primarily due to the fact that as the current flowing at the crack tip cannot be isolated from processes occurring in the area adjoining it, it is nearly impossible to accurately quantify i_a at the tip

of the growing crack [6,9].

On the other hand, changes in lifetime observed in Figures 4.2 and 4.3 can also be explained in terms of **hydrogen effect**. In the presence of aqueous solution, hydrogen embrittlement results from generation of hydrogen on the metal surface as a partial reaction in the corrosion process. Dissolving NaCl in H_2O causes the H^+ and OH^- ions to be "freed" more than otherwise and causes the dissociation of Na^+ and Cl^- ions therefore, overall conduction activity is increased. While Cl^- activity goes on in the metal dissolution process, H^+ simultaneously gets dissolved as well in the material thereby weakening the material through reduction in bond strength. H^+ is much smaller than Cl^-, and therefore diffuses faster than Cl^-. Some of it forms HCl with Cl^- ($H^+ + Cl^- = HCl$) that causes further electrolysis. The H^+ and OH^- produced subsequently react and/or get absorbed into the metal surface to form a brittle oxide film or a hydride phase or capture and move with the vacancies [2,6,19]. Hydrogen diffusion generally tends to regions of high triaxial tensile stress, such as, the crack tip where the material undergoes dilation. This process is particularly conducive with lower loading frequencies as the diffusion time increases. Brittle crack growth occurs as the film is ruptured and/or crack grows into brittle hydride phase by plastic strain. Combination of stress, and electrolytic medium such as aqueous NaCl increases chances of H generation, increased mobility of Cl^-, weakening of atomic bonds (faster at the crack tip), and overall increase in the CFCG.

Our **hold time-fatigue lifetime** results consistently depicted an increase in lifetime as a function of increasing hold time (roughly from 0-5s) followed by a gradual decrease for specimens tested in air or in the presence of 3.5%NaCl solution. In addition,

the samples subjected to hold time-fatigue interaction showed a parabolic trend for the specimens tested in air and in the presence of electrolyte, as shown in Figure 4.4. In addition, Figure 4.5 exhibits the comparative CGR results at typical hold times for specimens tested in air and in the presence of 3.5%NaCl. Furthermore, Figure 4.5 shows no discernable change in the CGR results between specimens tested in air and in the presence of 3.5%NaCl electrolyte. However, this is mainly due to the nature of logarithmic presentation which serves to diminish small variations in the data.
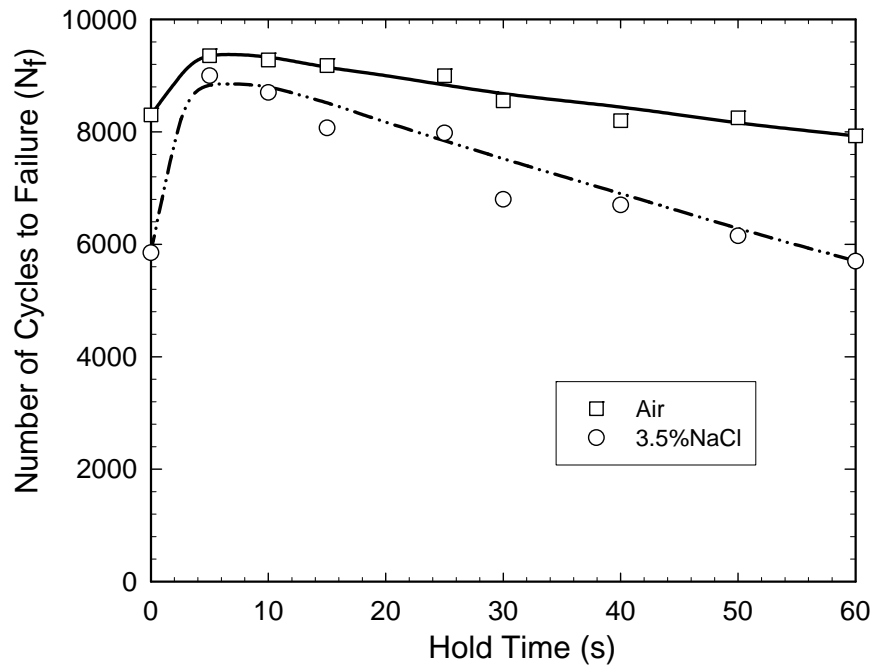

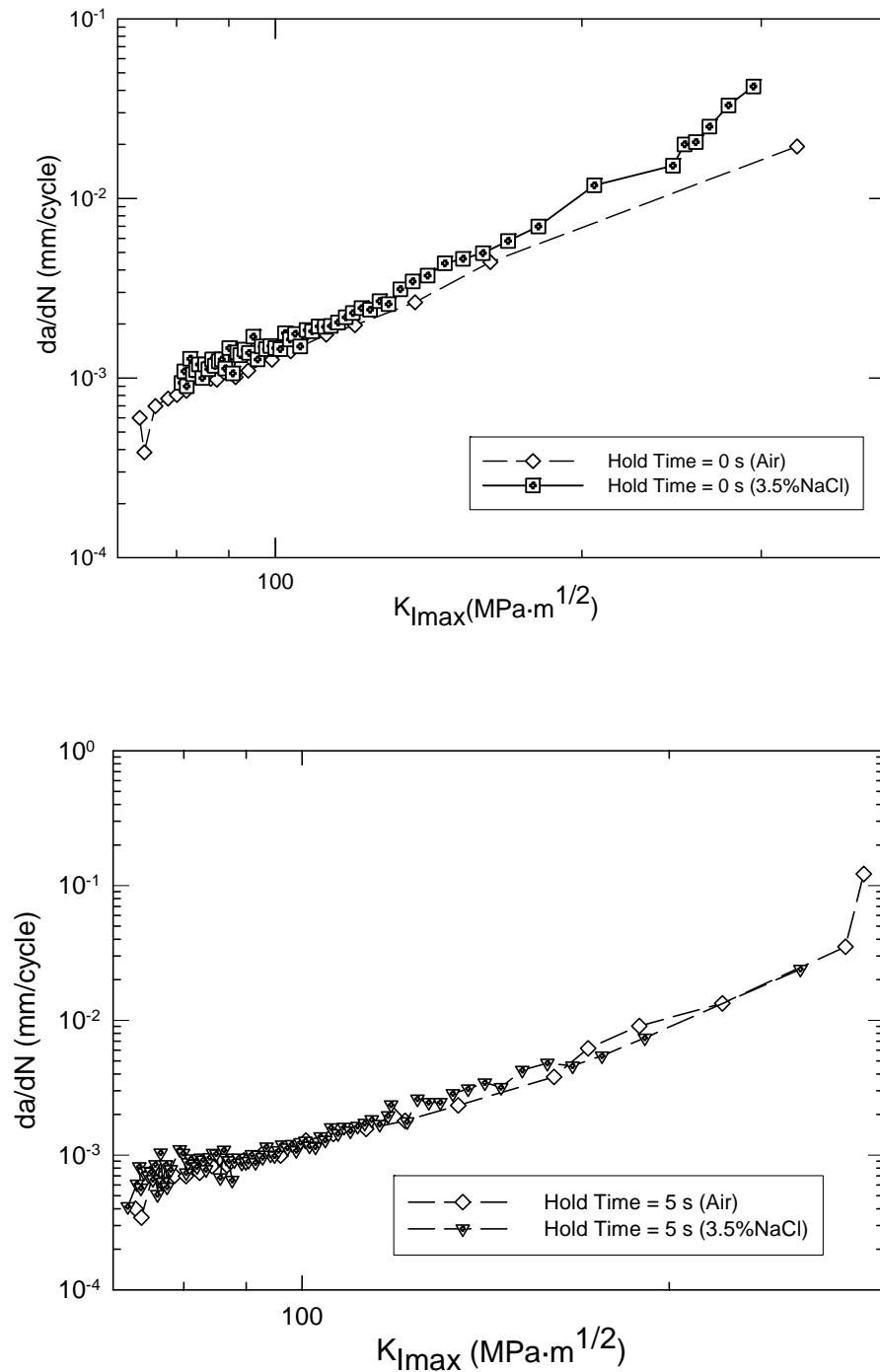**Figure 4.4 Hold time effect for specimens tested in air and 3.5%NaCl solution**

Figure 4.5 Typical CGR as a function of hold time for specimens tested in air and in the presence of 3.5%NaCl solution.

Interestingly, a surprising hold time effect at ambient conditions was found. This result contradicts the literature that suggests materials are only significantly affected by hold time under prolonged creep loading or at higher temperatures [42,43]. The initial increase in strength for specimens tested in air (~5 s hold time), might be associated to austenitic phase transformation into martensite (stable phase) which served as a strengthening mechanism that is strain-induced. For specimens subjected to 3.5% NaCl solution, as explained earlier, the Cl- ions are known to provoke loss of strength due to corrosion and therefore CG rates was enhanced [5,20]. Furthermore, as increasing the hold time (e.g. 60 s) the corrosion effect increased and therefore the fatigue lifetime and CG rates of corroded specimens decreased, as exhibited in Figures 4.4 and 4.5.

4.2 Hydrogen Effects in Fatigue Behavior

The experimental results showed once the metal is subjected to hydrogen charging, the fatigue lifetime was reduced and the crack growth rates become faster compared to specimens without hydrogen. Furthermore, the typical ductile fracture behavior becomes brittle.

4.2.1 AF1410 steel one and two sided hydrogen charged

Fatigue crack growth results for one sided hydrogen charged specimens are presented in Figures 4.6 and 4.7.   Figure 4.6 shows the crack growth rate as a function of the crack length while Figure 4.6 corresponds to the crack extension vs. number of cycles indicating a significant reduction in fatigue lifetime in the hydrogen charged specimen.
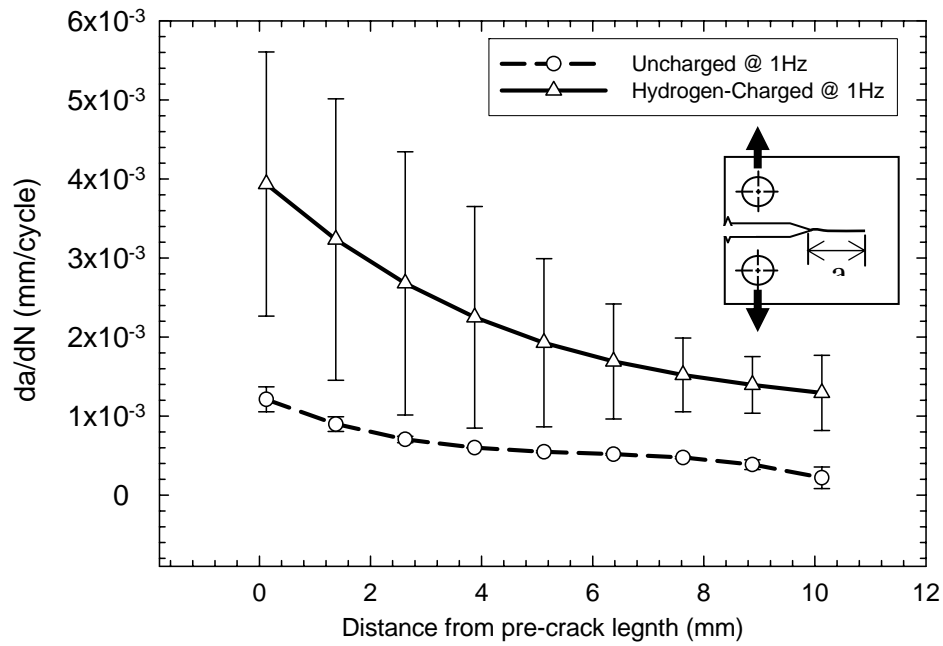
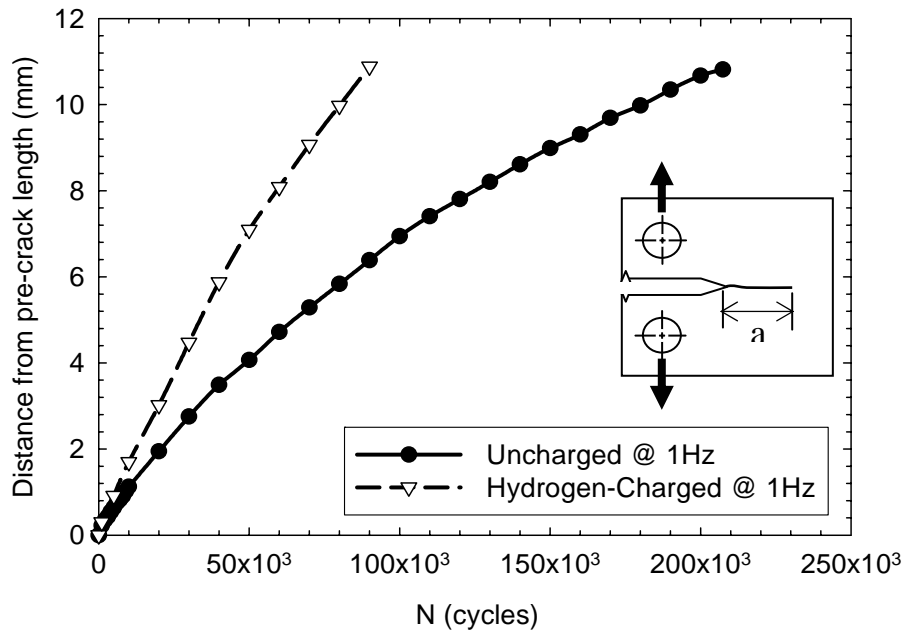**Figure 4.6 Crack length and crack growth rates for AF1410 specimens tested in air and hydrogen charged at one side**

Figure 4.7 Lifetime comparison of both conditions: AF1410 specimens in air and hydrogen charged at one side

64

The morphological variation observed in the cracking pattern (evidenced in Figure 4.4 where charged and uncharged portions of a specimen are shown) suggests that the concepts of reversible and irreversible trapped hydrogen could be used to account for it. Figure 4.8 shows a montage displaying a macroscopic optical image of the one-sided hydrogen charged specimen. The regions affected by hydrogen (input side) and without hydrogen along with the extent of penetration are clearly visible as well as the induced final fracture zone (indicated on the photograph).

Fatigue test results for two sided hydrogen charged indicated a sharp but gradual decrease in the lifetime as a function of increasing hydrogen content (charging time), as shown in Figures 4.9 (a) and (b). An order of magnitude difference in the CGR's can be observed between uncharged and fully charged (at 84 hours of charging time) specimens. The results agreed well with the reported literature [13,47]. In addition, Figures 4.10 (a), (b) and (c) present the lifetime of the steel as function of charging time, crack length vs. lifetime and fatigue crack growth rates vs. crack length as a function of varying hydrogen concentration.
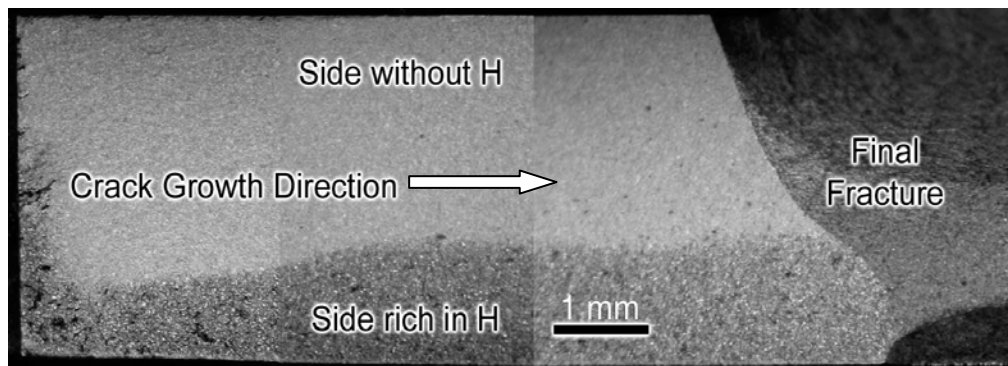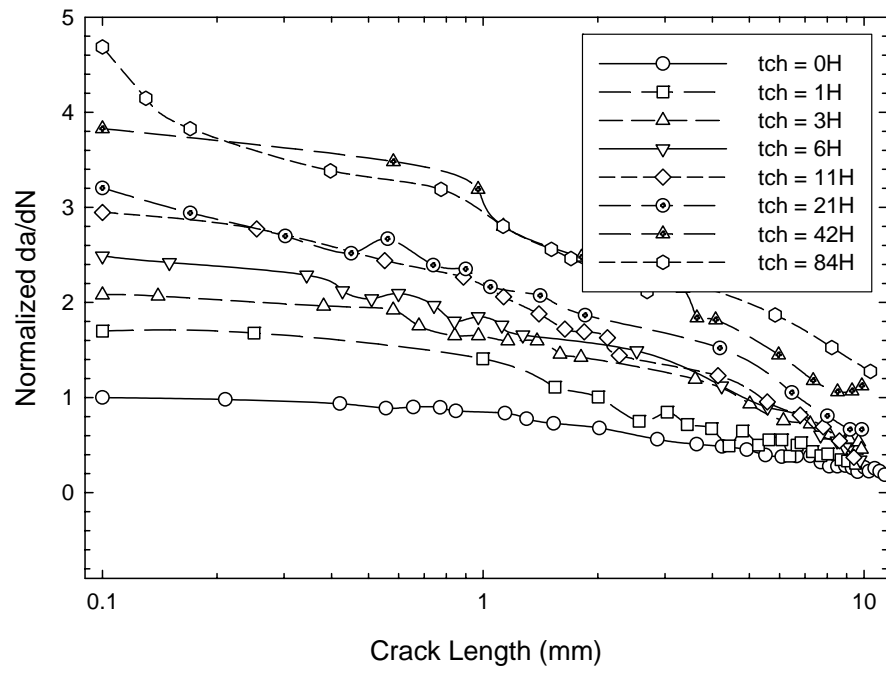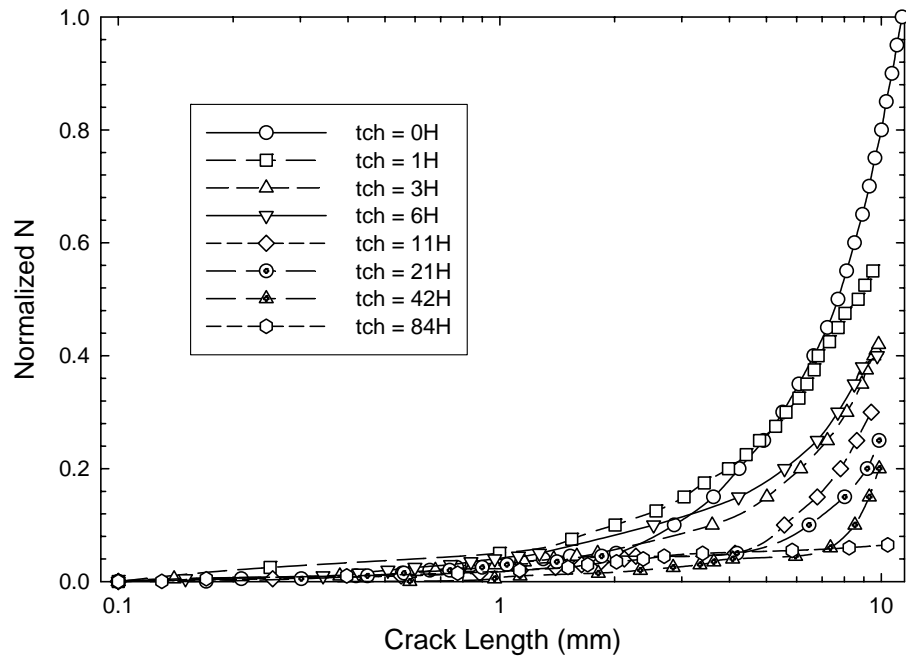

Figure 4.8 Penetration depth of hydrogen charging and crack growth direction

(a)

(b)

Figure 4.9 Experimental results for different hydrogen charging times as a function of: (a) crack length and (b) number of cycles
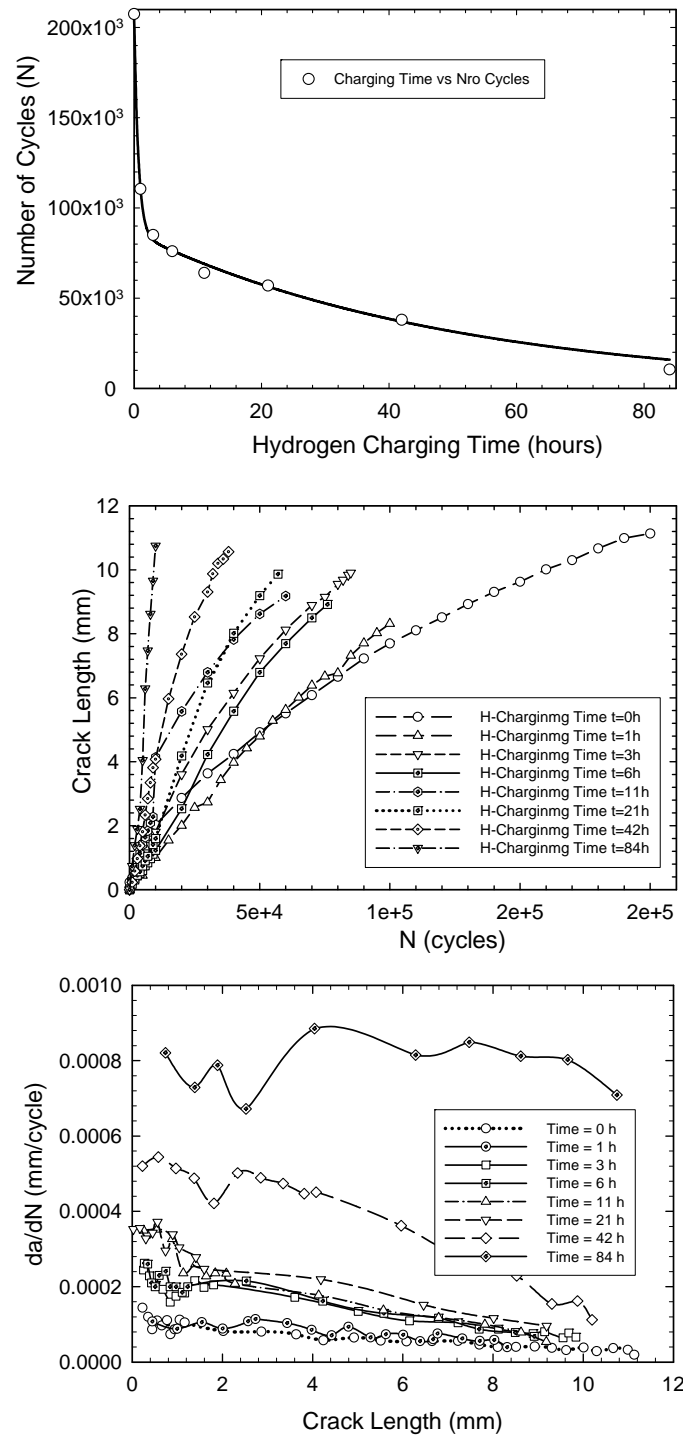
Figure 4.10 (a) Fatigue lifetime as a function of hydrogen charging time depicting (a) charging time vs. # cycles to failure, (b) Crack length vs. # cycles (c) crack growth rate vs. crack length.

67

For one and two sided hydrogen charged specimens, fatigue loading induces hydrogen redistribution into the material microstructure causing concentration build-up especially at the crack tip, which leads to accelerated embrittlement and faster crack growth rates observed in Figures 4.6, 4.7, 4.9 and 4.10.

The type and severity of specific hydrogen degrading effects depend on the steel microstructure which is composed of ferrite structure, lath martensite structure, small volume fraction of retained austenite structure and carbide precipitates (such as $(MoCr)_xC$); with their relative abilities to retain hydrogen (reversible and irreversible). Literature suggests that steels with strength levels below 700 MPa (100Ksi) show no significant embrittlement [48]. This implies that AF1410 steel with a strength level of ~1800 MPa was very susceptible to hydrogen embrittlement fostered by diffusible hydrogen.

Following electrolytic charging, reversible trapped hydrogen (RTH) in localized regions such as vacancies, grain boundaries and other microstructural defects becomes mobile during the fatigue loading. This translates into a reduced or limited RTH residence time of these defects. Conceivably RTH should affect the nucleation of microvoids at the particle-matrix interface thereby leading to the increase in the microvoid density and corresponding decrease in their average size. It is reasonable to expect that trap sites such as interstitial sites, dislocations and grain boundaries will either be directly involved in the cracking process or indirectly as transporting paths or conduits of hydrogen during the application of stress on a material [5,6,19].

With hydrogen charging, hydrogen is expected to migrate to the high strain fields

(such as crack tip) associated with coherent and semi-coherent interfaces of the finely dispersed complex carbide precipitates. During strain application following fatigue test, the hydrogen-carbide atmosphere would change since a break up of the interfaces will occur, which would translate to decrease or loss in strength. Therefore, an increased amount of hydrogen would make crack tip failure (and enhanced CGR) more likely as a result of the increasing loss of coherency [2,49]. In the case of semi-coherent interfaces between the carbides and matrix, it is expected that hydrogen would preferentially lodge around the dislocations in the martensite and banite phase. During stress application, loss of strength can only result if hydrogen enhances particle cutting (incoherency). The chance of this is remote, therefore, hydrogen atmosphere around semi-coherent or incoherent surfaces would not explain the continuous drop or loss of strength observed in the tests.

Furthermore, martensitic phase is generally more stable and as a result austenitic transformation into martensite can lead to strengthening (as may be the case in the uncharged samples) or presence of hydrogen in austenite can prevent this martensitic transformation (as in the case of charged samples). Therefore, in the uncharged samples, increase in strength and its longer lifetime can be explained from the combination of factors, such as toughening due to austenitic to martensitic transformation that is strain-induced. The absence of this in the hydrogen charged samples can be explained from the elimination of this transformation due to prior hydrogen-induced transformation of some of the retained austenite, or the stabilization of the austenitic phase due to solid solution solute interaction with hydrogen. Thus, uncharged samples would not be affected to the

69

same degree as the ones charged with hydrogen via cathodic polarization [17,21].

The ideas of reversible and irreversible trapped hydrogen also play an important role in understanding the effects of hydrogen on the lifetime of AF1410 steel alloy. During the fatigue loading, the reversible trapped hydrogen (limited resident time) can move through dislocations (highly dislocated lath martensite) to localize into microstructural sites, such as, faults, vacancies and grain boundaries or to produce new dislocations [25,49]. As a result the hydrogen concentration at these regions is enhanced. The hypothesis is that upon stressing, hydrogen repartitions from low to moderate strength RTH sites and is attracted to the crack tip stress field. Therefore, an increase in the hydrogen concentration increases the level and mobility of RTH and subsequently to an increase in the crack tip embrittlement and CGR as seen in Figures 4.6, 4.7, 4.9 and 4.10. On the other hand, the irreversible trapped hydrogen (ITH) has permanent resident time into the material under ambient conditions accompanied by high activation energy and as a result its mobility is limited [25]. Therefore, it is believed that ITH does not contribute significantly in the embrittlement process and hence would not be a contributing factor in the observed fatigue lifetime reduction.

4.2.2 Hold Time-Fatigue interaction

An almost complete loss of life was observed as the hold time increased from 0-10s in the hydrogen charged specimens, as shown in Figure 4.11 (a). Figures 4.11(a) and (b) contains also the fatigue lifetime data of specimen tested in air and corrosive solution. These figures serve to observe the detrimental hold time effect for hydrogen charged

samples compared to samples evaluated in air and corrosive solution. Figure 4.12 exhibited the fatigue crack growth rates for hydrogen charged specimens with 0 and 5 seconds of hold time, and Figure 4.13 presents the fatigue crack growth rates as function of various hold times.
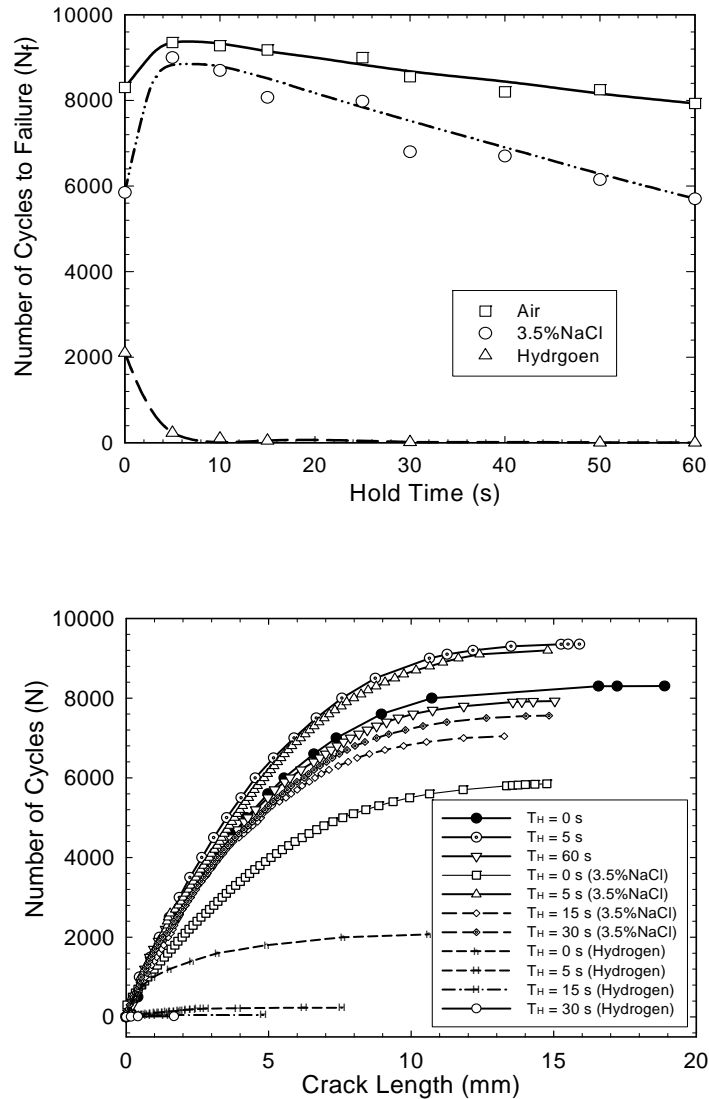

Figure 4.11 Fatigue lifetimes for specimens tested in air, in the presence of 3.5% NaCl electrolyte and electrochemically hydrogen charged depicting (a) number of cycles to failure as a function of hold time "T_H" (b) crack length vs number of cycles for typical hold times used.
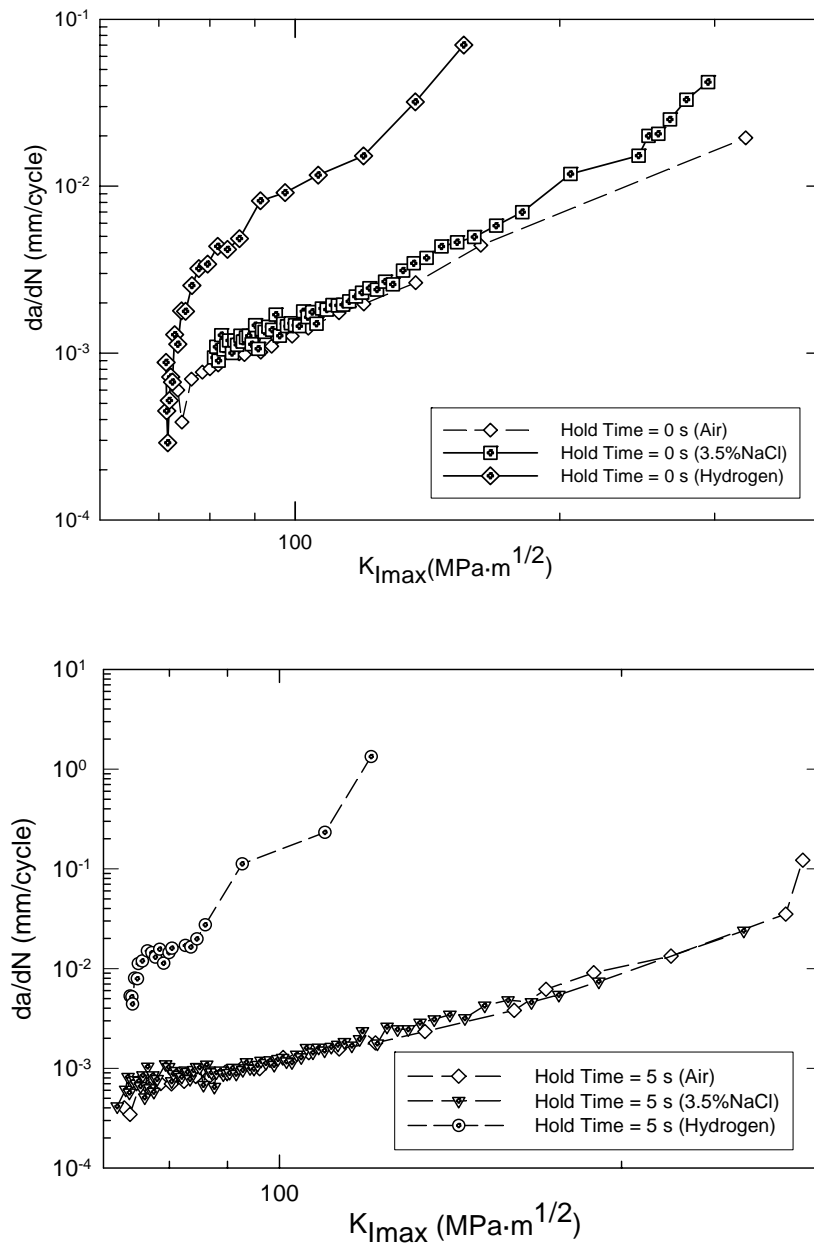
Figure 4.12 Typical CGR as a function of hold time for specimens tested in air, in the presence of 3.5% NaCl and hydrogen charged.
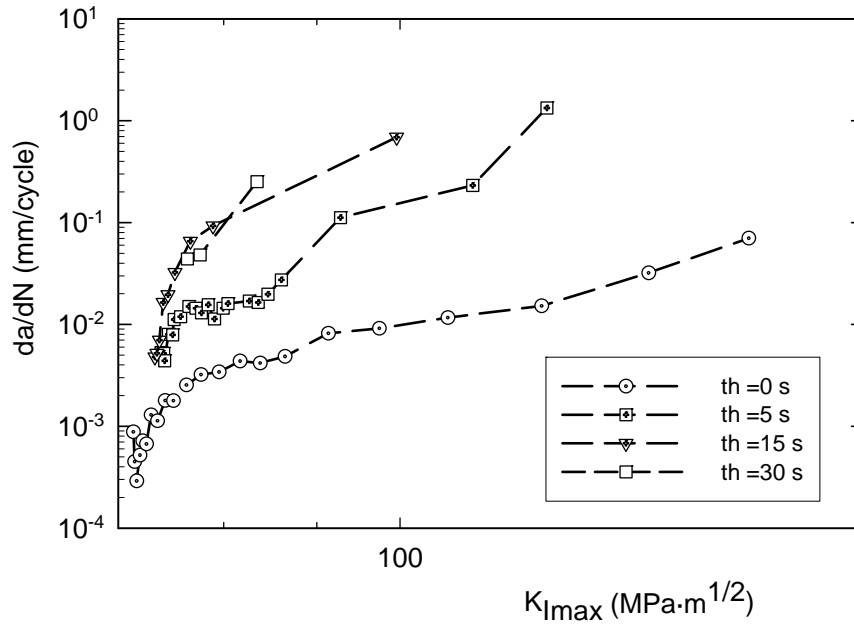
Figure 4.13 Fatigue crack growth rate as a function of various hold times

4.3 SEM and AFM Fracture Surface Analysis

4.3.1 AFM Fracture Surface of Corrosion Fatigue

AFM fracture surface analysis of **AA7075-T6** specimen revealed the presence of metal dissolution as the predominant corrosion process which leads to lifetime reduction in specimens exposed to electrolyte. The specimens tested in lab air showed typical rough surface (Ra = 1.02 μm roughness average) caused by grain pullout and transgranular failure, whereas, the specimens tested in the presence of electrolyte exhibited inter-granular failure reflected by smoother cracked surface (Ra = 0.905 μm) along with pits and crevices, a commonly observed feature of metal dissolution induced corroded surface, as shown in Figure 4.12 for a typical specimen. As it can be shown in

73

AA7075 T6 alloy, roughness average is smaller in the saline solution than in air, this presented more ripples in the fracture surface; it is consistent with Cl- and H+ ions effect mentioned earlier. The fracture in air exhibited finer, feathery river pattern lines. In sodium chloride solution, the river pattern lines were generally coarser and more distinct. The fatigue striations formed in the saline solution had a brittle appearance. Likewise, the reduction in the fatigue life of the specimens tested in the 1% sodium chloride solution is reflected in the fracture appearance. The mechanism responsible for the decrease was hydrogen embrittlement. The embrittlement attack is enhanced by the cyclic mechanical rupture of the passive film and the prevention of repassivation by the presence of the chloride ion.

Figure 4.13 shows AFM images of a typical AF1410 specimen at 30μm resolution of fracture surface morphology of typical specimens tested under various conditions. The analysis indicated an increase in fracture surface roughness at short crack length due to the nature of COD testing mode. The largest roughness values were observed at 2mm from the pre-crack tip on corroded samples except for the specimens tested in air. AFM evidence collected for AF1410 steel reveals features related to the presence of hydrogen embrittlement, such as straight lines (striations and shear bands) [50-52]. Note that the AF14010 steel does not have alloy elements in the Group VB of the periodic table, which are the ones susceptible to form hydrides. Therefore, the brittle nature of the fracture surface can not be attributed to the formation of hydrides. Since the hydrogen produced during corrosion affect only several micrometers ahead of the crack tip, these brittle features were correlated to metal dissolution process.
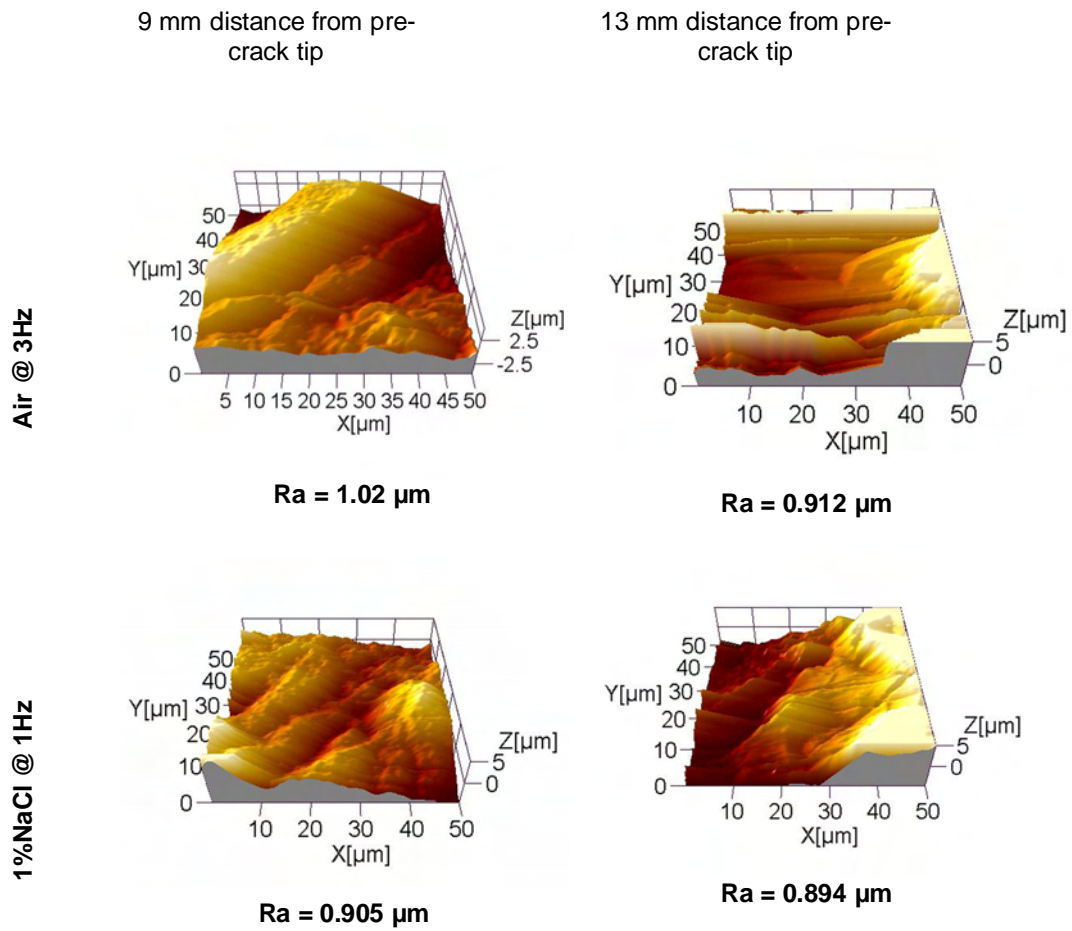
74

9 mm distance from pre-crack tip

13 mm distance from pre-crack tip

Air @ 3Hz

Ra = 1.02 µm

Ra = 0.912 µm

1%NaCl @ 1Hz

Ra = 0.905 µm

Ra = 0.894 µm

Figure 4.14 AFM images of AA7075-T6 fractured surface obtained from specimens tested under conditions as shown above.

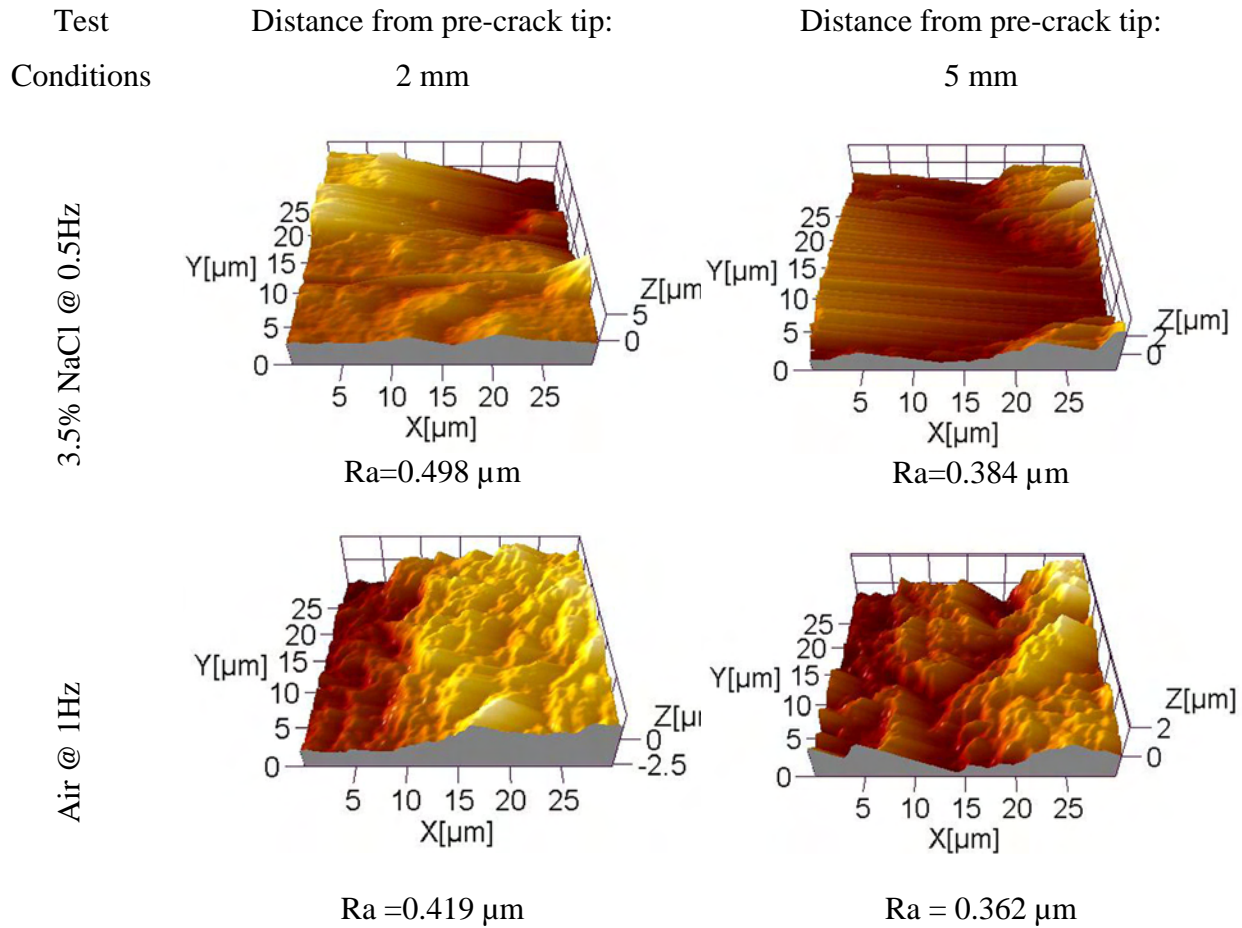| Test Conditions	Distance from pre-crack tip: 2 mm	Distance from pre-crack tip: 5 mm

3.5% NaCl @ 0.5Hz

Ra=0.498 µm

Ra=0.384 µm

Air @ 1Hz

Ra =0.419 µm

Ra = 0.362 µm

Figure 4.15 AFM images of AF1410 fractured surface obtained from specimens tested under different conditions. The reported z-range on the image corresponds to the maximum height mesured at the mapped region on each image.

4.3.2 AFM fracture surface of AF1410 steel one sided hydrogen charged

The AFM images corresponding to the input side and output side are shown in

Figure 4.16. The mean roughness based on AFM measurement was 0.355µm and 0.173

µm for the input and output sides, respectively. Furthermore, AFM fracture surface and cross sectional profile images were presented in order to discern fracture modes in Figure 4.19.

AFM analysis was carried out to reveal fracture surface features. Presence of hydrogen in the steel reduced the macroscopic plastic deformation and the resulting plastic process zone size ahead of the crack tip. Lateral AFM images on the input side and hydrogen free side revealed large differences on surface appearance primarily due to varying hydrogen concentration distribution in the specimen (see Figure 4.8). Figure 4.16 (a) exhibits the superficial damage typical of uniform pitting corrosion of the (input side) specimen when the electrolytic charging was performed. This is accompanied by a roughness increment (measured at = 0.355µm). On the other hand, Figure 4.16 (b) corresponds to the hydrogen-free lateral surface of the specimen, which shows substantially lower mean roughness of approximately 0.173µm. in addition, crack tip plasticity is evident for specimen devoid of hydrogen as shown in Figure 4.17.

A topographic representation of the fracture surface is presented in Figures 4.18. A cross-sectional profile along line A-A (Figure 4.18(a)) for the hydrogen charged specimen on hydrogen free side exhibited a smoother appearance. This is related to a ductile transgranular fracture with Rq = 0.363µm and the Ra = 0.291µm. A similar cross-sectional profile along line B-B (Figure 4.18 (e)) was taken at the side rich in hydrogen resulting in about 2.5 times higher roughness profile with Rq = 0.759µm and Ra = 0.874µm. The large differences between the hydrogen-side and hydrogen-free side are attributed to the IG and TG fracture features. As expected, the IG fracture has larger

roughness values due to the presence of hydrogen especially at relatively low stress intensity factors (<40 MPa•m1/2). The intergranular brittle fracture of the hydrogen-rich side was also confirmed by AFM analysis since SEM fracture surface images revealed an approximate 20µm grain size in the steel.

Additional AFM images demonstrated the decreasing tendency of the fracture surface roughness as a function of increasing crack length for the hydrogen-free side. Furthermore, roughness was found to be proportional to the loading conditions (stress intensity factor and CGRs); these results are in qualitative agreement with data reported in the literature [35].

The AFM image of Figure 4.18(c) indicated a mean roughness R_a = 1.060 µm and R_q = 1.310 µm, revealing a brittle fracture appearance and corroborating results presented in Figure 4.19 (c). On the other hand, Figure 4.18 (c) and (e) showed the intergranular fracture mode (assisted by hydrogen) as revealed by SEM fracture surface images for the side with higher H content. Figure 4.18 (d) evinced the presence of brittle transgranular fracture (induced by the fatigue loading), whereas grain boundaries are delimited by the deeper gaps. From the observations mentioned above, for one-sided hydrogen charged AF1410 steel sample, it is clear that the hydrogen-rich side underwent a brittle fracture and presented higher roughness than the hydrogen-free side in which ductile fracture mode took place.
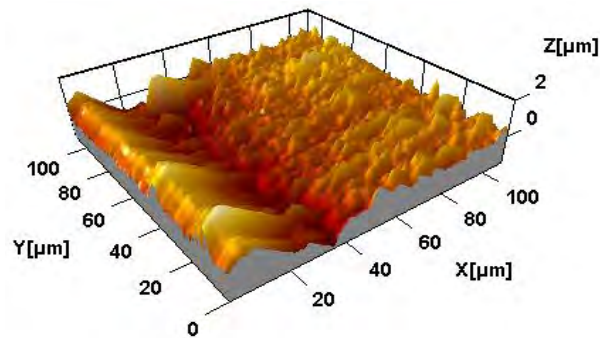
a) Mean Roughness = 0.355um
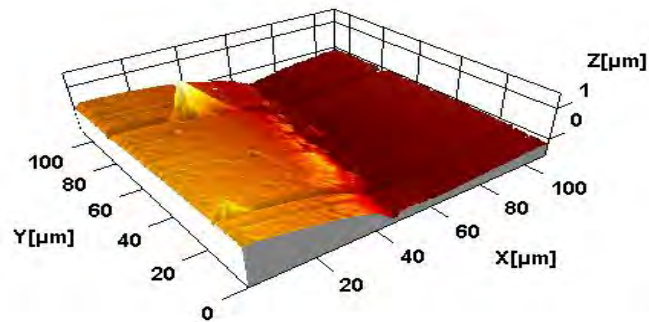
b) Mean Roughness = 0.173µm

Figure 4.16 Lateral surface of AF1410 steel: (a) side exposed to hydrogen (b) side exposed to air and (c) plasticity at the crack tip
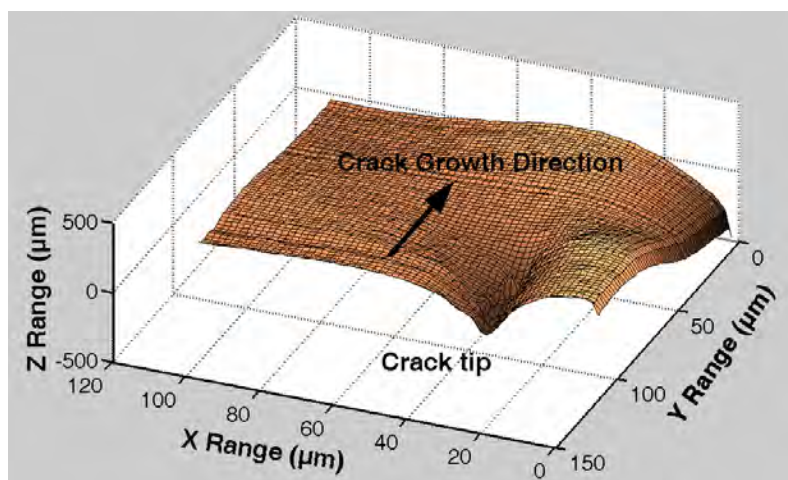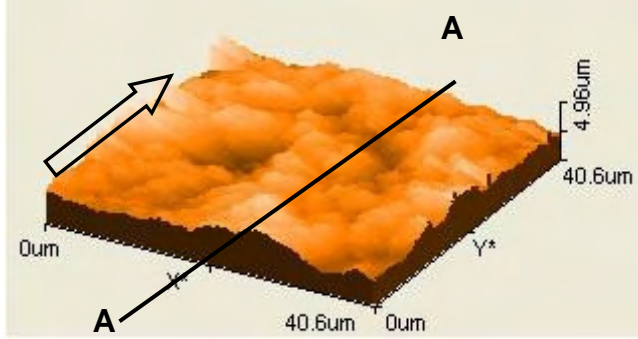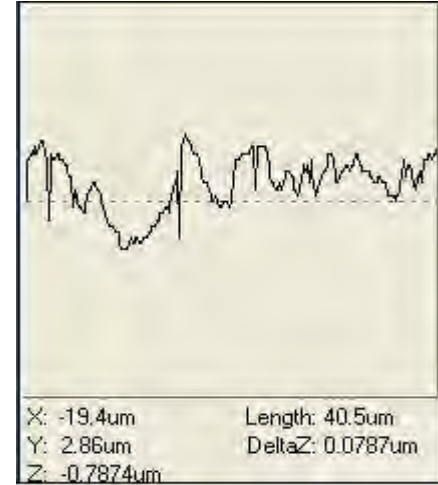

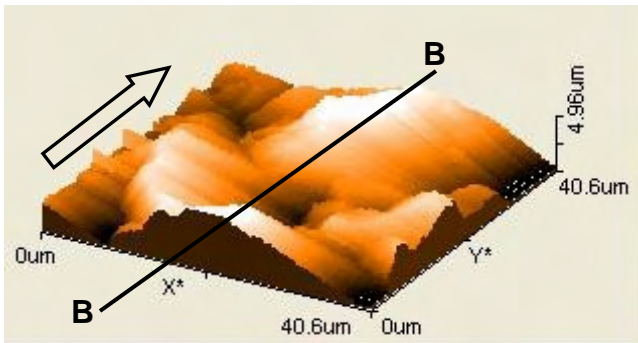**Figure 4.17 AFM showing the plasticity of a growing crack tip**

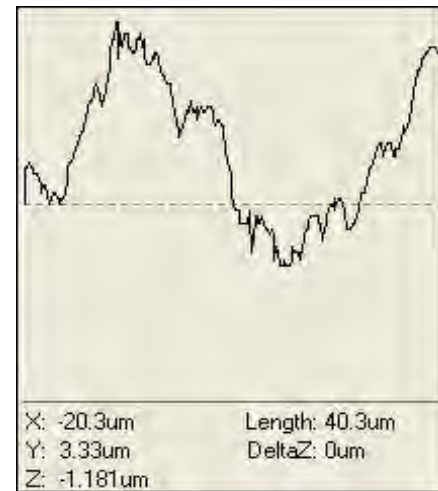a) Morphology at the side without H

c) Morphology at the side with H

d) TG Fracture at the side rich in H

X: -19.4um   Length: 40.5um
Y: 2.86um   DeltaZ: 0.0787um
Z: -0.7874um

Ra=0.291 μm
Rq=0.363 μm

b) Profile A-A:Side without H

X: -20.3um   Length: 40.3um
Y: 3.33um   DeltaZ: 0um
Z: -1.181um

Ra=0.759 μm
Rq=0.874 μm

e) Profile B-B: Side with H
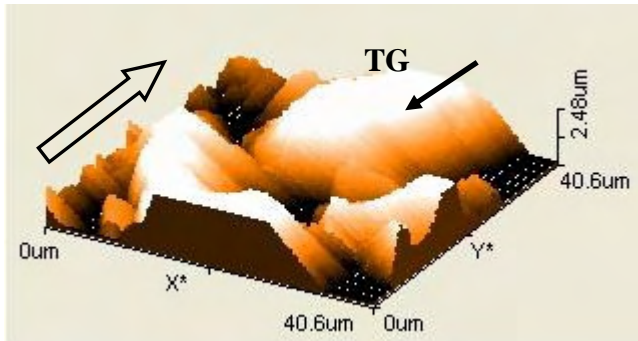
Figure 4.18 AFM images revealing the fracture modes due to hydrogen embrittlement: (a) without hydrogen, (b) profile of side without hydrogen, (c) hydrogen charged side, (d) typical TG fracture mode and (e) profile of hydrogen charged side

4.3.3 SEM fracture surface of AF1410 steel one and two sided hydrogen charged

For one side hydrogen charged specimens, SEM secondary electron images of the fracture surfaces are presented in Figures 4.19 along with their corresponding locations on the studied sample (at crack length = 4mm and da/dN=$3.3 \cdot 10^{-4}$ mm/cycle). Ductile fracture is apparent in the hydrogen free-side (Figure 4.19 (a)) whereas Figure 4.19 (b) shows the transition region with mixed ductile – brittle fracture. Figure 5c displays a combined TG and IG fracture of brittle nature which is as a result of hydrogen assisted cracking (mainly IG).
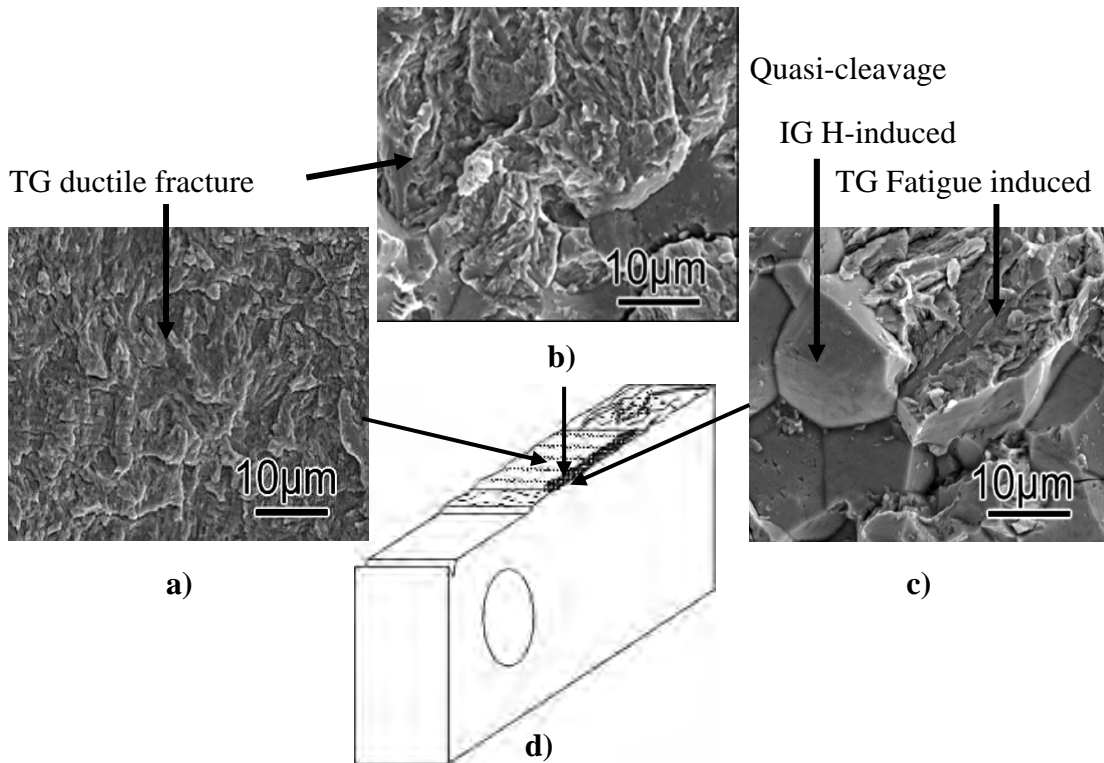

Figure 4.19 SEM fracture surface images for one sided hydrogen charged: (a) side without hydrogen, (b) interface of hydrogen charged side and without hydrogen, (c) IG and TG fracture mode due to HE and (d) half broken CT specimen

IG fracture appeared to be the predominant fracture mode in the hydrogen charged side as shown by the SEM fracture surface images of Figure 4.19 (c). This image also revealed a reduced macroscopic ductility around the crack tip associated with faster CGR for one and two side hydrogen charged specimens. Fracture propagation mode remained ductile in general where hydrogen was absent whereas at the interface between the input and hydrogen-free zones a mixed ductile / brittle QC fracture mode was observed, as shown in Figure 4.19 (b). The cleavage fracture occurred when the grain interface strength was exceeded and the decohesion mechanism took place as a brittle fracture mode. IG cracking (in the hydrogen-rich zones) dominated for conditions that produced threshold stress intensity levels below about 50 MPa·m$^{1/2}$ (Figure 4.19 (c)). Conversely, TG cracking was favoured at lower H contents and higher thresholds, as shown in Figure 4.19 (a) [2,6]. For AF1410 steel, the K_{IC} exceeded 100 MPa·m$^{1/2}$, while hydrogen embrittlement assisted cracking occurred at K_{IC} levels between 15 to 40 MPa·m$^{1/2}$ [48]. Furthermore, the maximum stress intensity (~32 MPa·m$^{1/2}$) factor occurred at short crack lengths which combined with higher hydrogen concentrations at one side of the specimen reduced the macroscopic plasticity (Figure 4.16) at the crack tip (in the hydrogen charged side). Therefore, predominantly IG fracture was observed accompanying brittle TG fracture at the earlier stages of the test.

For two sided hydrogen charged specimens, SEM images shown in Figures 4.20 and 4.21 clearly indicate a shift in the modes of failure for specimens partially charged with hydrogen. On the portion hydrogen charged, predominantly IG (intergranular) or quasi-cleavage (QC) brittle features with TG (transgranular) pockets were observed, as in

the case for one side hydrogen charged. The occurrence of pure brittle IG fracture could be attributed to the ability of grain boundary to act as a hydrogen trapping site and due to synergistic effect of hydrogen and impurities segregated at grain boundaries, which reduce the grain boundary strength [3,17]. Similarly, QC features that were mainly observed in specimens with higher hydrogen concentration (charging time over 3 hours in the current case) can be produced as a result of metal and H atoms interaction causing the alignment of some crystallographic planes/dislocations in the weak direction. Cleavage or QC features in the host metal can also occur as hydrogen degrades cohesive forces by occupying interstitial sites in the metal lattice thus causing an increase in the lattice volume and inducing internal stresses along specific crystallographic planes (cleavage planes) [31,47]. The occurrence of IG or QC features depends on the relative strength of both the grain boundary and the metal lattice, however, the probability of occurrence of QC mode increases as hydrogen concentration increases in the host metal.

Hydrogen diffusion is in general a function of specimen thickness, therefore, the amount of hydrogen decreases almost linearly going from specimen surface to the midplane. As a result, microvoid ductile type of features were observed mostly in the central regions of the specimen, as evidenced by the typical low magnification SEM image shown in Figure 4.22. Whereas, at the interface between the regions affected by hydrogen and devoid of hydrogen, a combination of fracture modes such as brittle IG, TG, QC, and ductile TG, MV features can be observed.

The SEM fracture surface analysis and results were summarized in order to construct Figure 4.23 which can be used to qualitatively predict the expected failure

83

mode for hydrogen charged specimens as a function of applied stress intensity factor. Figure 4.22 indicates that under strain controlled testing the expected fracture mode passes from brittle TG and QC to IG. Notice that TG and QC features predominantly occur at intermediate stress intensity factors, whereas, IG fracture modes occur at low stress intensity factor which also coincides with the threshold level for crack initiation [1,16]. Figure 4.23 serves for both K-rising (load control) and K-decreasing (strain control) testing as indicated by the arrows shown. It can easily be inferred from Figure 4.23 that expected fracture mode under load control will follow a path in reverse of strain controlled testing. Figure 4.23 offers a convenient methodology for failure mode prediction, however, the procedure is found to be somewhat sensitive to testing mode and applied stresses.

An interesting SEM feature was observed when charged and uncharged specimens were subjected to fast fracture by monotonic loading. Uncharged specimens exhibited a dominant dimpled ductile fracture, whereas, hydrogen charged specimens presented a combination of brittle IG, TG, QC and smaller dimples, as indicated in Figure 4.24; the results agree well with the literature [10,17]. Presence of dimples in hydrogen charged specimens is related to hydrogen enhanced localized plasticity, whereas, for uncharged specimen, the dimple phenomena can be attributed to microvoids formation and coalescence due to macroscopic plastic deformation. Absence of dimples under fatigue testing is believed to be due to low stress intensity factor used in the current (strain controlled) testing. At low stress intensity factor, the plastic zone is not large enough to incorporate a large number of microvoid inclusions and as a result dimple

phenomena do not take place [2, 27].

Additionally, from SEM fracture surface analysis, it was determined that the maximum depth from where the reversible hydrogen could leave the sample freely was less than 100 µm. However, this depth could be negligible when compared with the measured hydrogen penetration depth of 1 to 1.8mm as indicated in Figure 4.8. Therefore, it was assumed that the CGR's calculated for hydrogen charged specimen were not affected substantially by the escaping hydrogen.
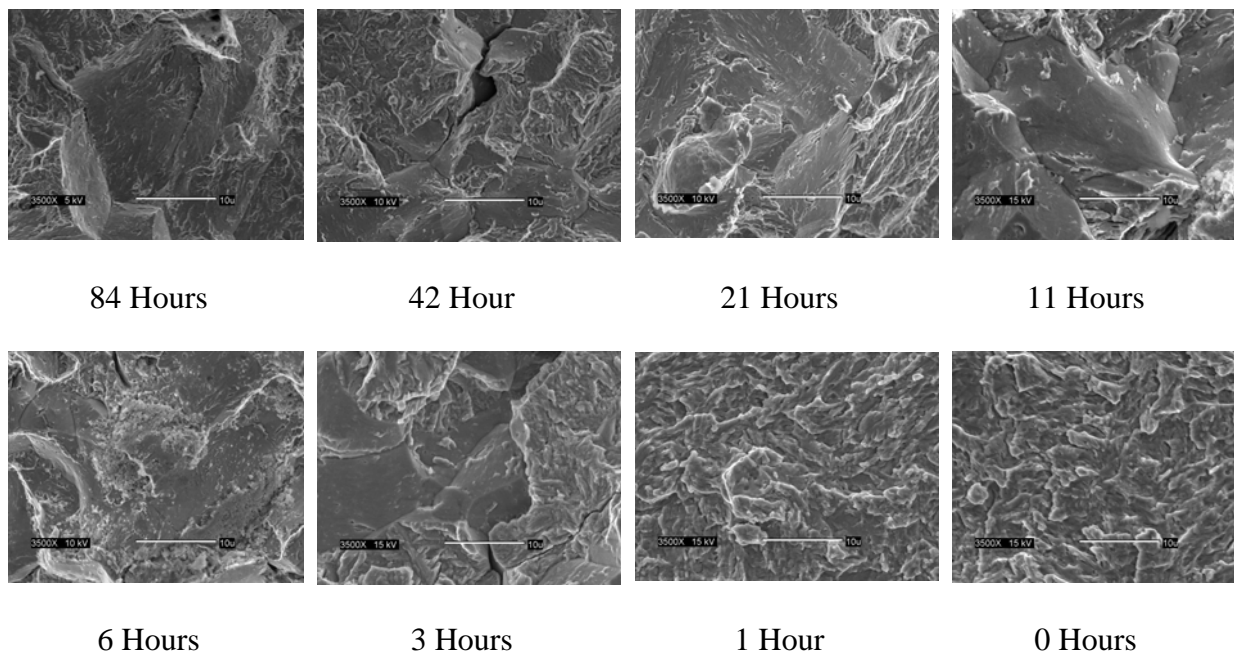

| 84 Hours | 42 Hour | 21 Hours | 11 Hours |

| 6 Hours | 3 Hours | 1 Hour | 0 Hours |

Figure 4.20 SEM fracture surface images (two side hydrogen charged) taken at ~1mm from the pre-crack length (3500X) for various hydrogen charging times (0-84 h) revealing the shifts in fracture mode due to increasing hydrogen content

| 84 Hours | 42 Hour | 21 Hours | 11 Hours |

| 6 Hours | 3 Hours | 1 Hour | 0 Hours |
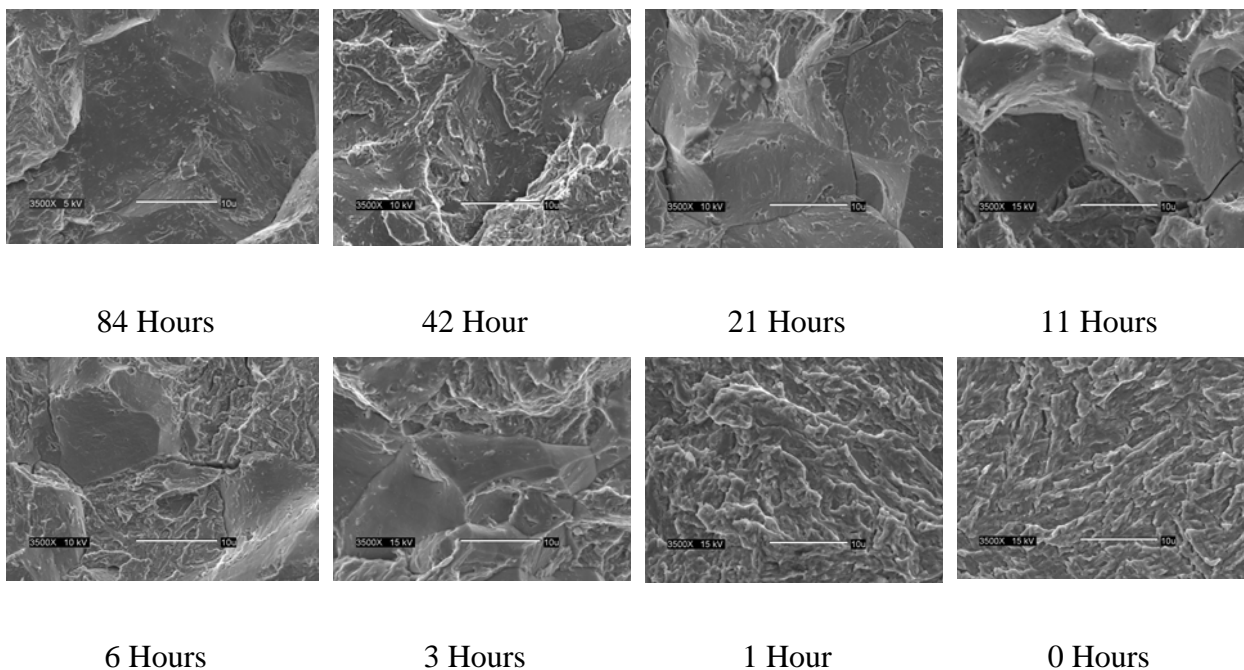
Figure 4.21 SEM fracture surface images (two side hydrogen charged)taken at ~8mm from the pre-crack length (3500X) for various hydrogen charging times (0-84 h) revealing the shifts in fracture mode due to increasing hydrogen content
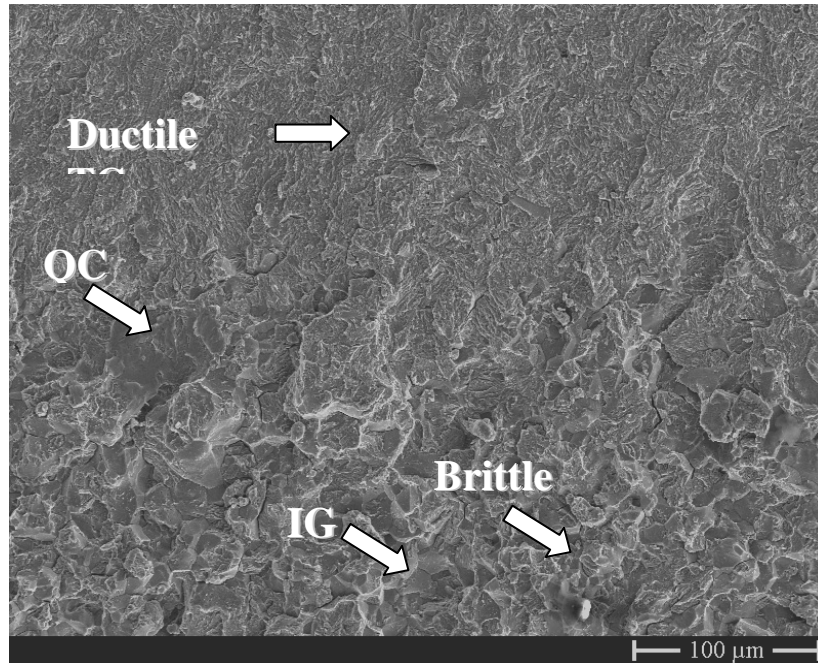
Figure 4.22 SEM fracture appearance at regions affected by hydrogen and devoid of hydrogen. Brittle IG, TG, QC and microvoid ductile fracture modes can be observed
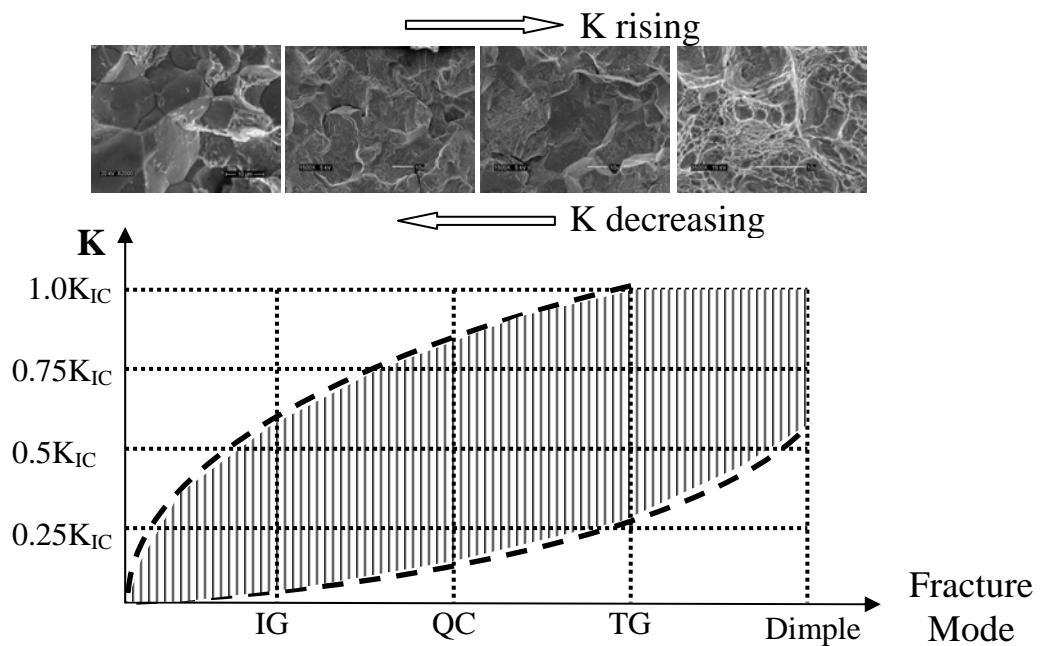

Figure 4.23 Qualitative fracture modes identification for hydrogen charged samples as a function of the applied stress intensity factor (Fatigue testing)
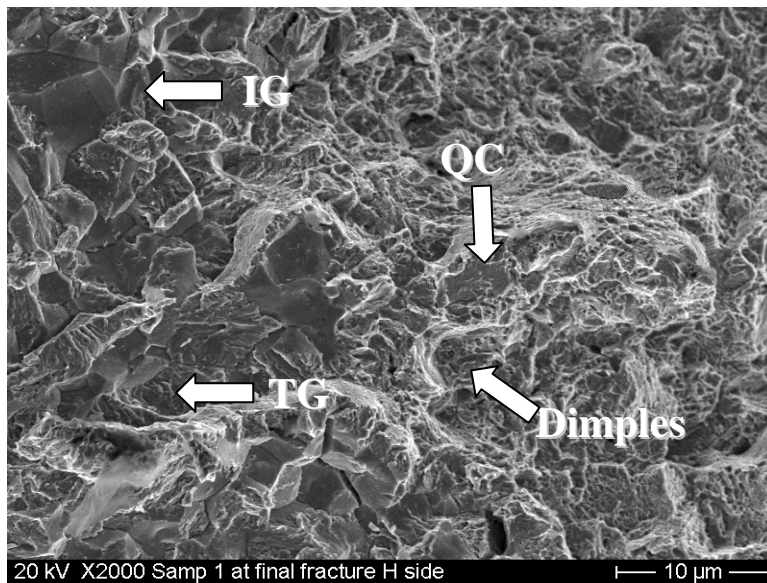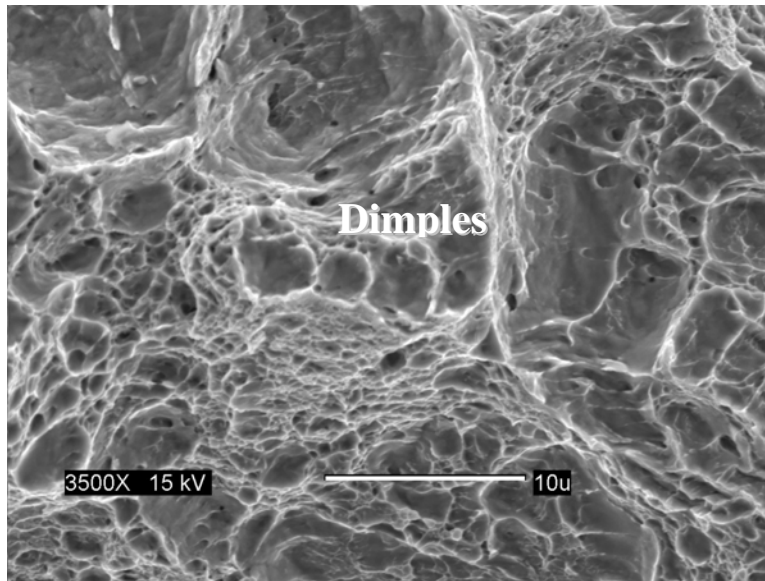
Figure 4.24 SEM fracture surface of specimen subjected to fast fracture under monotonic loading. Uncharged specimen (top) and hydrogen charged specimen (bottom)

4.3.4 SEM fracture surface of AF1410 steel hydrogen charged and hold time effect

The hold time effect on the fracture surface appearance of steel was evidenced by means of SEM images. SEM images taken in the region of stable crack growth revealed a dominant dimpled fracture features. It can be associated to the enhanced local plasticity at the crack tip due to the presence of hydrogen as depicted in Figures 4.25 [2,27]. The sizes of dimples or microvoids are affected by the presence of the second phase particles $((MoCr)_2C, (MoFe)_xC, (Fe,Ni,Co)_3C)$, etc [20,53]) of coherent, semi-coherent and incoherent nature. It is believed that dimpled size increases as hold time increases, however, more statistical analysis would need to be performed and it is out of the scope of the research. The hydrogen permeated into the steel tends to accumulate at the interface of the second phase particles; however, the coherent and semi-coherent locations are preferable for RTH and the incoherent for ITH [25,54]. As a result, RTH appears to affect the nucleation of microvoids at the particle-matrix interface and as a result the microvoid density is increased and the average size decreased.

SEM images shown in Figures 4.26 indicate a shift in the modes of failure for hydrogen charged specimens. The fracture appearance observed in Figure 4.26 were similar to the feature observed in Figures 4.19-4.21. Furthermore, as evidenced earlier, on the portion of the specimen devoid of hydrogen (Figure 4.26 (c)), mainly microvoid ductile features were observed.
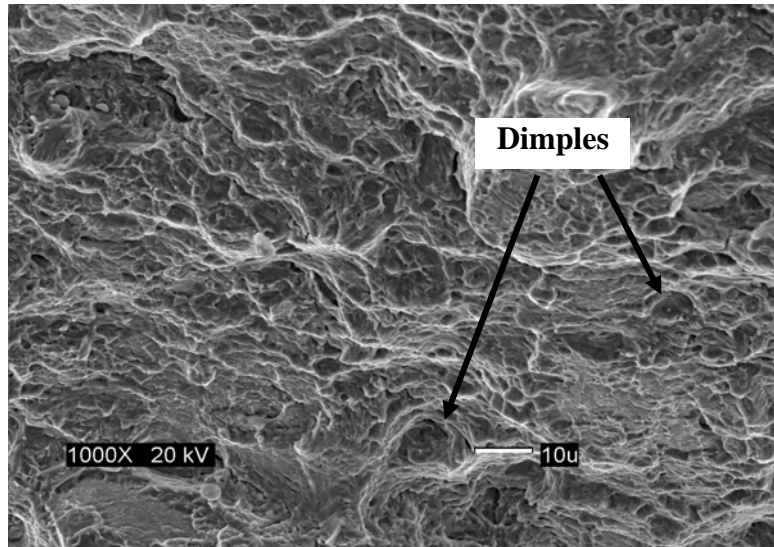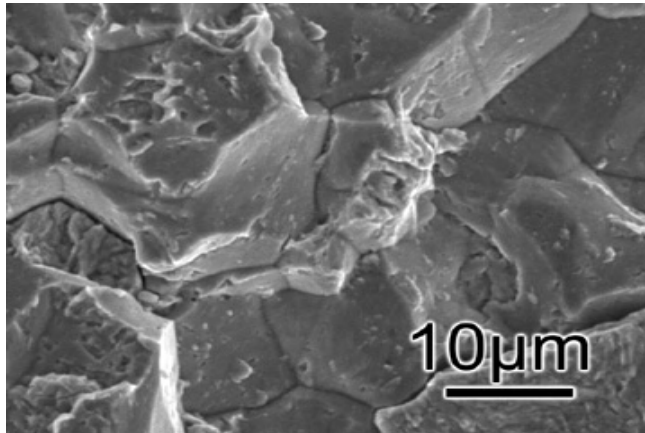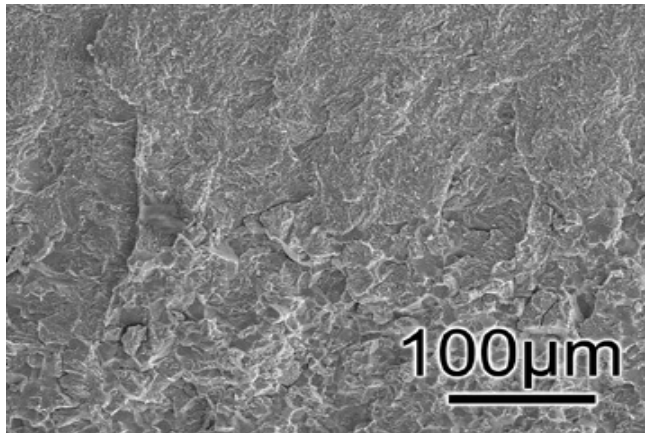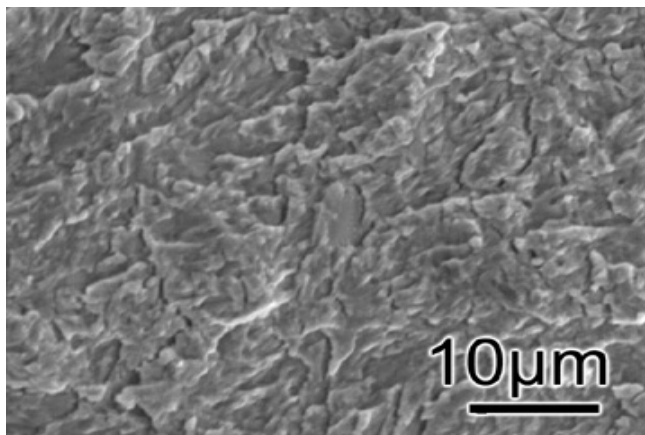
a)
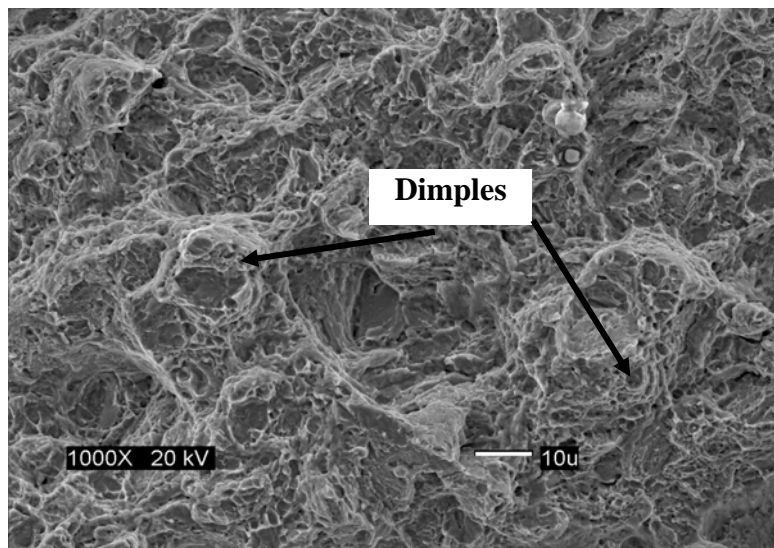
b)

Figure 4.25 SEM images of fracture surface morphology showing the dimpled surface for a hydrogen charged specimen with (a) hold time = 0 s and (b) hold time = 5 s.

a)

b)

c)

Figure 4.26 SEM images of fracture surface morphology showing mainly (a) IG brittle features in the hydrogen charged portion of the specimens, (b) mixed mode ductile-brittle failure at the interface and (c) mainly microvoid ductile features on the side devoid of hydrogen

4.4 Mathematical Model for Life Prediction

Results of hydrogen assisted fatigue lifetime testing indicated a substantial but gradual increment in crack growth rate as a function of increasing hydrogen content. A convenient deterministic model is proposed that seems to reasonably accurately capture the crack growth rate behavior under strain controlled testing conditions.

4.4.1 Mathematical Model and Experimental Validation

A semi-empirical crack growth model was developed in order to account for the environmental hydrogen effect that seeks to avoid the complexities involved in the existing analytical and empirical fatigue lifetime predictive methodologies. The model incorporates several relevant intrinsic (E, σ_{ys}, σ_u, etc.) and extrinsic (frequency, environment, crack length, hydrogen concentration, specimen geometry, etc) parameters in order to enhance its predictive capabilities [5,13].

The model introduces an effective thickness that reflects the hydrogen concentration within the material, as indicated in Eq. 13

$$t_{eff} = t - t_{HP} \tag{13}$$

where t is the specimen thickness and t_{HP} refer to experimentally obtained hydrogen penetration depth and represented as,

$$t_{HP} = C t_{ch}^{n} \tag{14}$$

where t_{ch} is the hydrogen charging time and the constants 'C' and 'n' depend on the hydrogen charging conditions such as aqueous solution, charging current and charging time. For the $0.1MH_2SO_4 + 1$ g/l sodium arsenate electrolyte with charging current of $2mA/cm^2$, $C = 0.6297$ and $n = 0.2823$ were obtained for the current case (see Figure 3.8). Combining Eqs. 13 and 14 yielded the following convenient form for the effective thickness,

$$t_{eff} = t - 0.6297 t_{ch}^{0.2823}$$

(15)

Using effective thickness and various mechanical and environmental intrinsic and extrinsic parameters a fatigue lifetime relationship between number of cycles and crack length was developed, as given in Eq.16,

$$N = \frac{\pi E a^{(\frac{t_{eff}}{t}+1+\upsilon)}}{\sigma_{ys}} + \frac{4\sigma_u a}{\left(\dfrac{t - t_{eff}}{0.6297}\right)^{\upsilon/0.2823} + 1}$$

(16)

where $N, a, E, \sigma_{ys}, \sigma_u$ and υ refers to number of cycles, crack length (mm), Young modulus (MPa), yield strength (MPa), ultimate tensile strength (MPa) and Poisson's ratio, respectively. Finally, taking the derivative of Eq. 16 and reordering the terms, the crack growth rate model is expressed by the following expression

$$\frac{da}{dN} = \left[\pi \cdot E \cdot a^{\left(\frac{t_{eff}}{t} + \upsilon + 1\right)} \cdot \frac{\left(\dfrac{t_{eff}}{t} + \upsilon + 1\right)}{a \cdot \sigma_{ys}} + \frac{4 \cdot \sigma_u}{\left(\dfrac{t - t_{eff}}{0.6297}\right)^{\upsilon/_{0.2823}} + 1} \right]^{-1}$$

(17)

Using Eq.17, crack growth rate for each testing condition (i.e., at various hydrogen charging times) was obtained as shown in normalized Figure 4.27 which presented a good fit (within 5% in most cases) when compared with the experimental results. On the other hand, Figures 4.28 (a) and (b) show the predicted fatigue crack growth rates versus crack length and number of cycles for the all hydrogen charging times from 0 to 84 hours, respectively. It can be easily inferred from Figures 4.28 (a) and (b) that the predicted crack growth rates increased and lifetime decreased as hydrogen charging times increased which confirmed the damaging effects of hydrogen on the fatigue lifetime and the consistency of the model in predicting the crack growth behavior. The small variations observed in Figure 4.27 between the experimental and predicted results can be attributed to the random behavior of the hydrogen into the material due to stress field and the presence of material imperfections/dislocation cores that could accelerate or impede the crack propagation.

The main attraction of this model is that it is physically sound as it incorporates various relevant physical parameters in its development, the experimental curve fitting is kept to a minimum, it avoids the complexities involved in the analytical solution of simultaneous partial differential equations, and yet the model remains very convenient to apply. The model can also be used for the fatigue lifetime assessment of specimens

subjected to corrosive (marine) environments. However, a limiting aspect in such problems is the inaccurate crack tip hydrogen production estimation (resulting from electrochemical reactions) and its subsequent concentration/penetration depth.
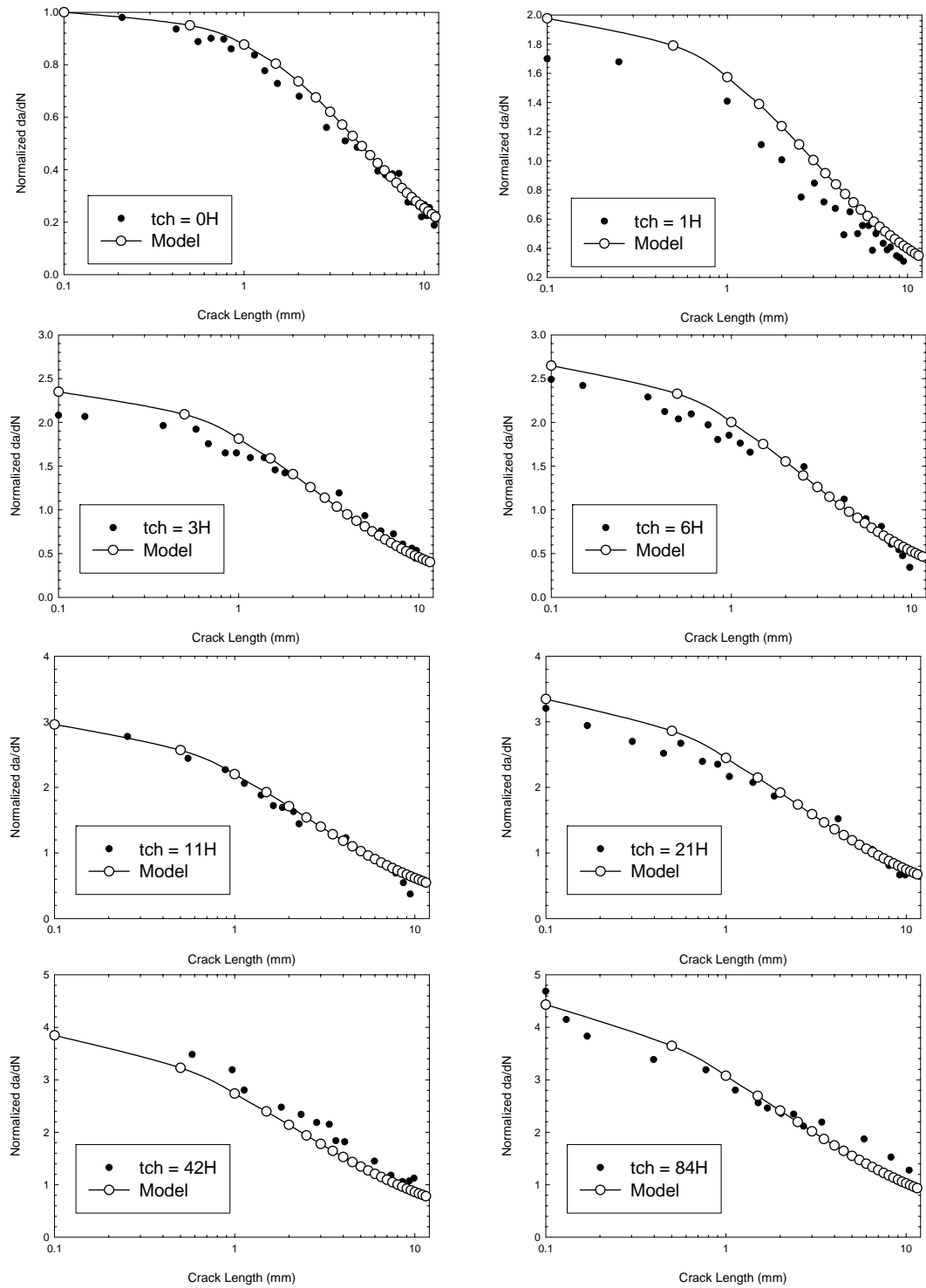
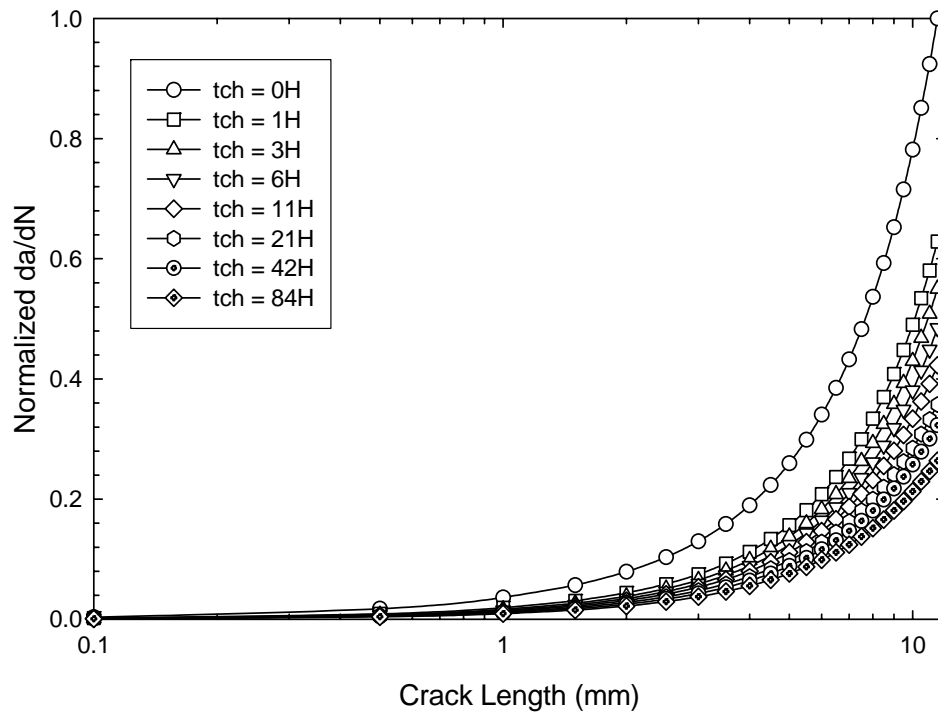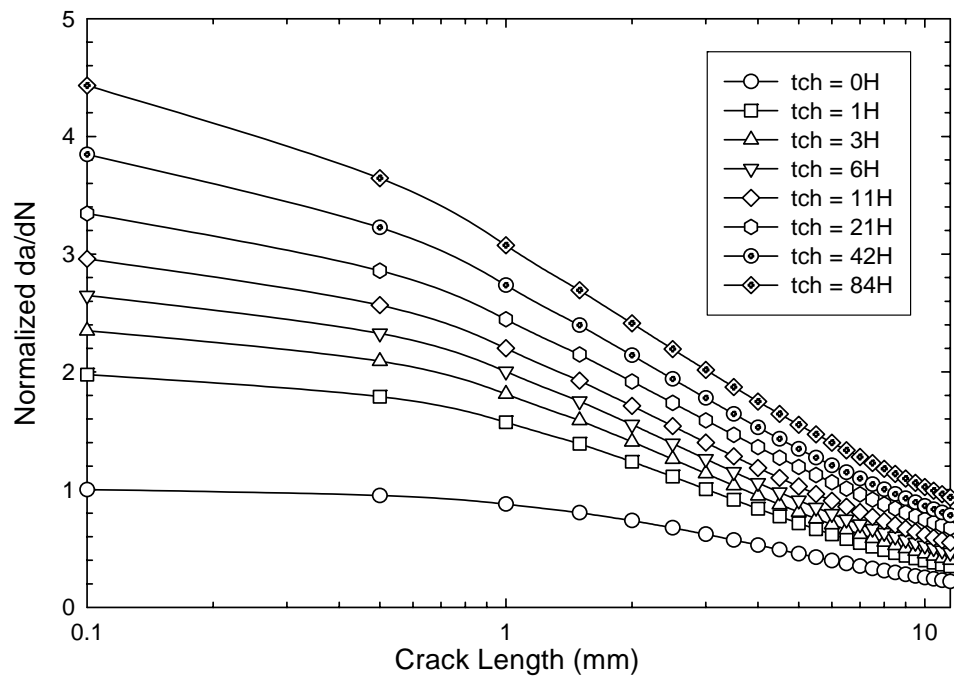**Figure 4.27 Crack lengths vs. CGR at different hydrogen charging times**

96

Figure 4.28 Modeling results for different hydrogen charging times as a function of crack length

4.5 Acoustic Emission Analysis

For AA7075-T6 results presented in Figure 4.29 showed a negligible effect on the threshold stress intensity factor (ΔK_{TH}) for aluminum alloy due to exposure to corrosive solution. However, the corrosion effect increased the crack growth rates especially in stage II (stable crack growth) as compared to tests conducted in air at all stress ratios. Crack initiation time in AA7075-T6 was reduced in 52% while the overall lifetime was found to be reduced in 62% when the specimens were tested in the presence of corrosive marine environment as compared to test conducted in air at R = 0.1. However, at R = 0.4 and 0.7 the lifetime reduction is less severe than R=0.1 as can be observed in Figure 4.30. It can also be observed from Figures 4.29 and 4.30 that both crack initiation and overall lifetime decrease as a function of decreasing stress ratio.

Tension-compression results for AF1410 steel exhibited a drastic reduction in lifetime when specimens were subjected to electrochemically hydrogen charged. However, the effect of marine environment was less severe, as it can be seen in Figure 4.31. Figure 4.31 indicates an increasing fatigue lifetime of steel specimens as a function of increasing the FHD time because the hydrogen concentration diminishes into the material and therefore the embrittlement of AF1410 steel was less severe.
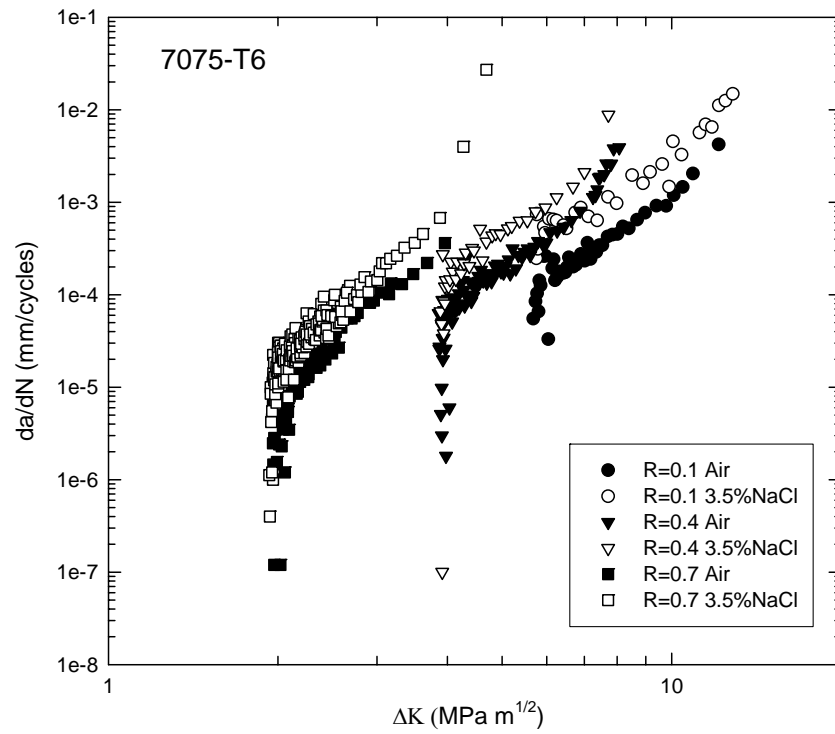
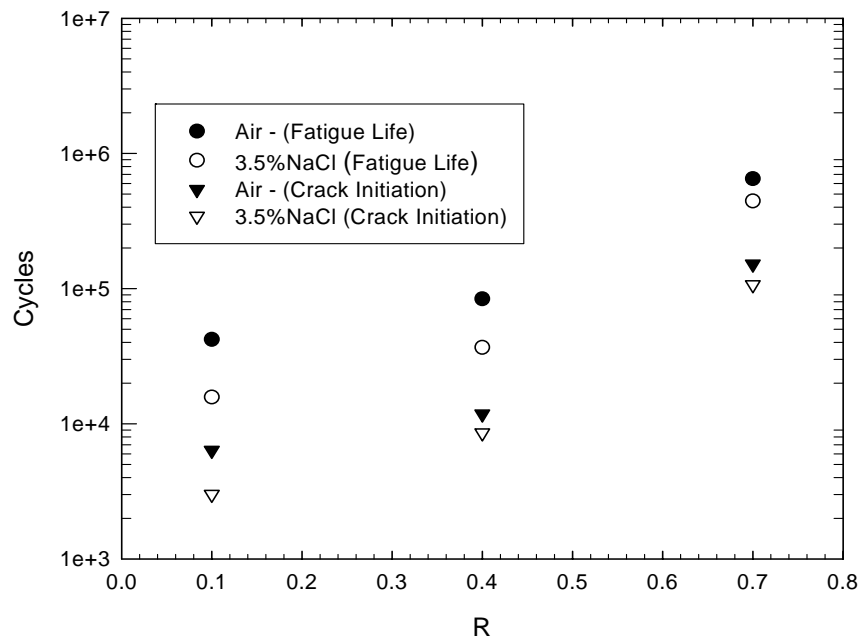**Figure 4.29 CG rate vs. ΔK for AA7075-T6 as a function of load ratio**

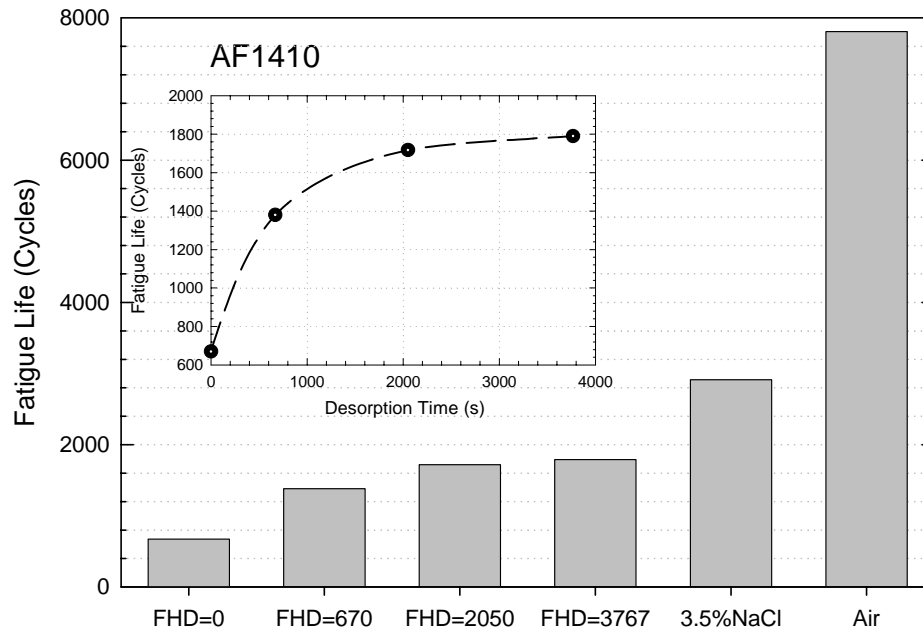**Figure 4.30 Fatigue crack initiation on AA7075-T6 and overall lifetime**

Figure 4.31 Tension-compression fatigue results for AF1410 steel specimens tested in air, 3.5%NaCl and hydrogen charged for 35 minutes.

In Figure 4.32, the AE activity for AF1410 showed an increasing trend as rising the FHD time. However, specimens evaluated under corrosive solution exhibited low AE activity as it can be observed. Figure 4.33 illustrates the AE results for AA7075-T6. For specimen evaluated in air, the AE activity decreased as the stress ratio increases [55]. Furthermore, for specimens tested in 3.5%NaCl solution a trend to increase was observed as a function of increasing the stress ratio.
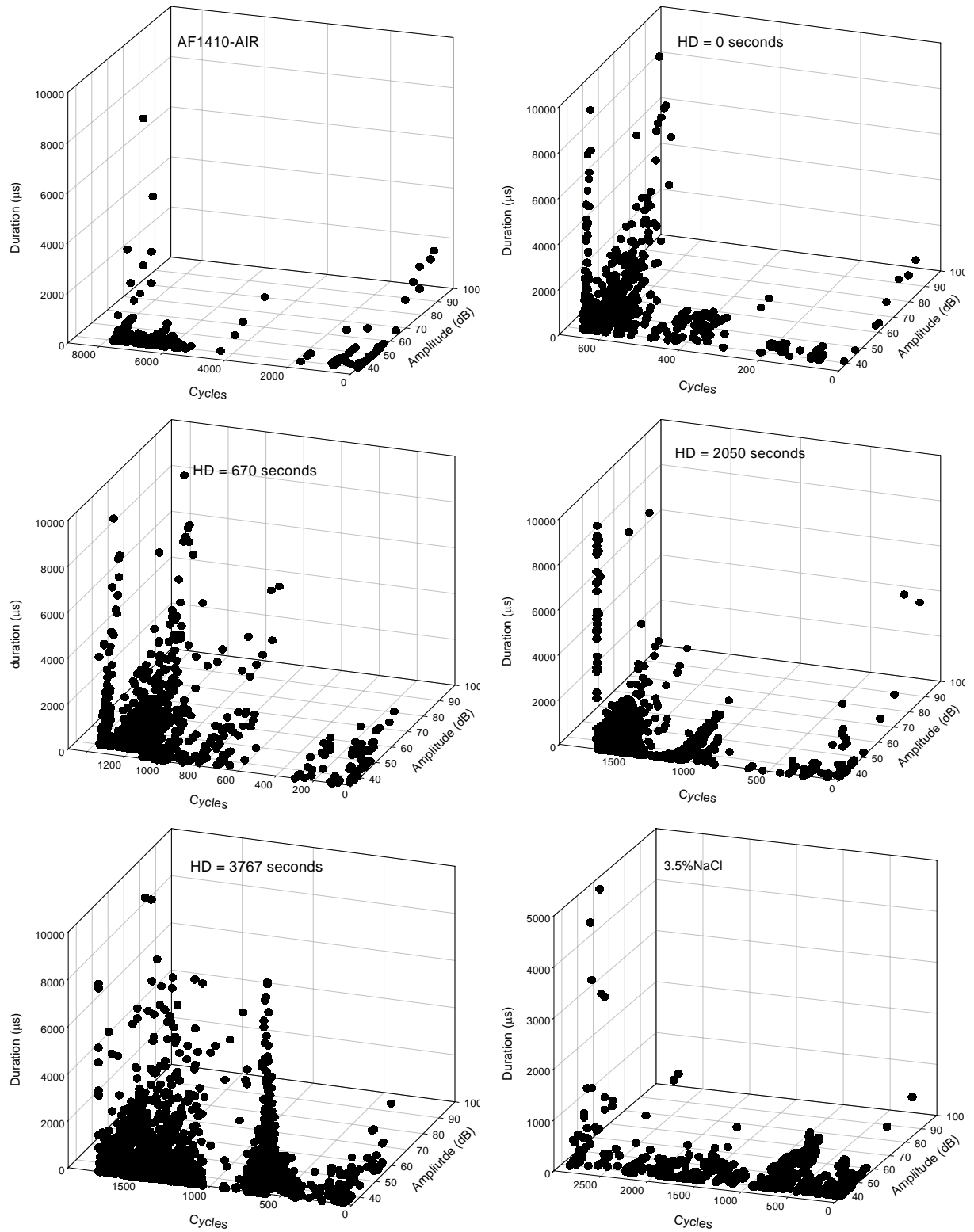
Figure 4.32 AE results for AF1410 steel tension-compression testing
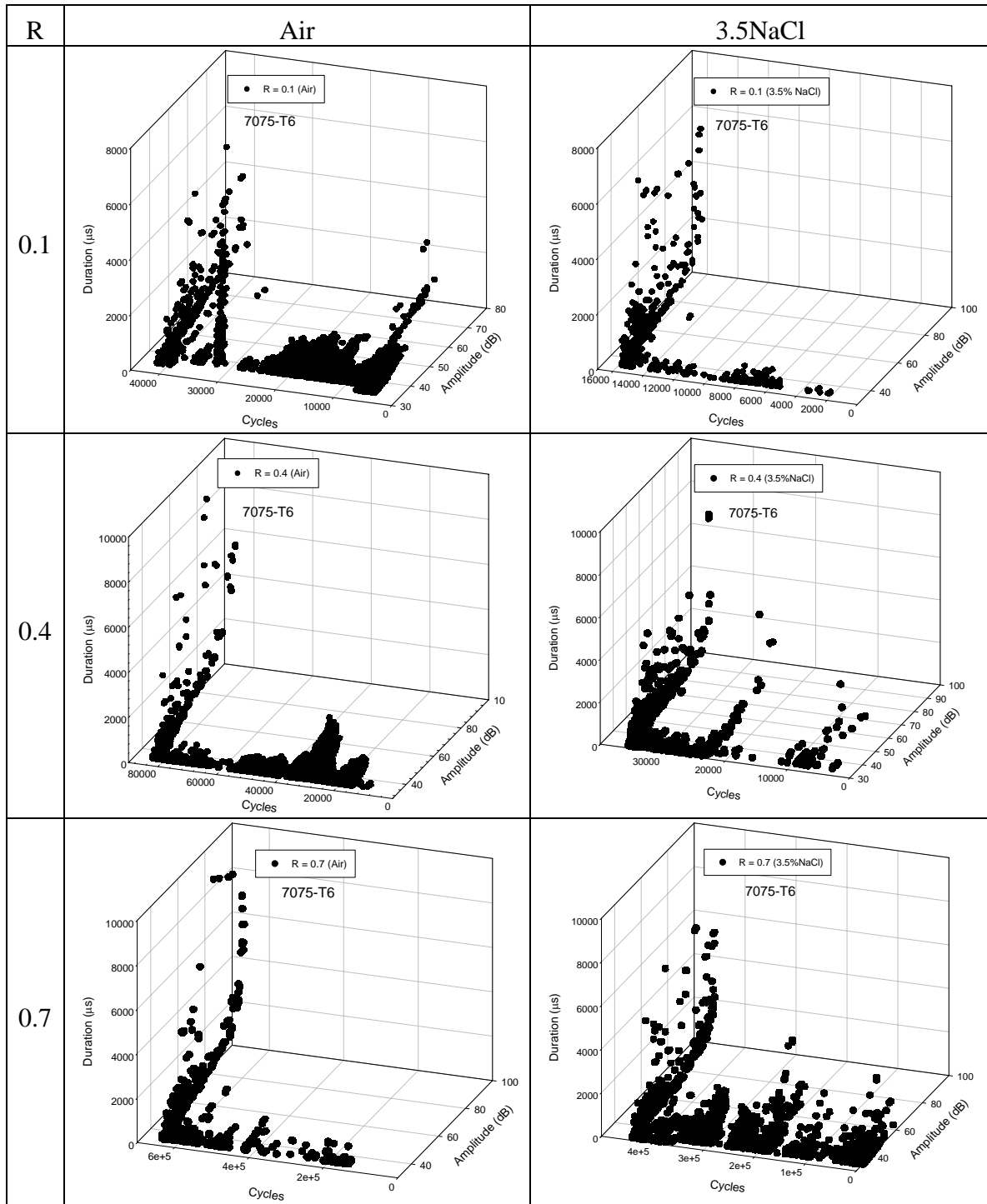
Figure 4.33 AE results for AA7075-T6 under various load ratios

Fatigue crack initiation and growth for AA7075-T6 was observed to suffer a decrease when the specimens were subjected to a corrosive environment, as can also be seen in Figures 4.29 and 4.30. As explained in the corrosion fatigue part (section 4.1), this enhancement in crack growth rate occurs due to an increase in the potential difference that takes place as the zone of high stress concentration (i.e. crack tip) becomes an anode while the material surface behaves like a cathode, thus producing a galvanic cell between the anode and cathode [45-46]. Furthermore, an enhanced cyclic pumping effect of corrosive solution exists specially at low stress ratios (0.1). Therefore, the transport phenomena of corrosion product/species become more active. However, as the stress ratios increase, (0.4 and 0.7) the cyclic pumping effect tends to decrease.

Current results indicate a decrease in crack initiation period and CGR as the stress ratio is increased (as shown in Figures 4.29 and 4.30). The reduction in crack initiation and growth time can be attributed to the load amplitude and its relationship with the microstructural changes [7]. Aluminum alloys have been known to rearrange their microstructure due to mainly to enhanced dislocation mobility especially at the crack tip (zone of higher stress concentration). This effect of repeated microstructural rearrangement is expected to be a major contributing factor in the observed effect of stress ratio.

Since the precise moment of crack initiation is difficult to define, however, stage I primarily included crack initiation and early growth up to 1.5 mm length from the crack tip. Stage I exhibited the highest level of acoustic emission activity. Figure 4.33 show plots of amplitude vs. duration of specimens tested at stress ratios of 0.1, 0.4 and 0.7 in

103

air and in the presence of electrolyte. Crack nucleation shows an AE activity with amplitude and duration below 50dB and 200µs at stress ratio of 0.1, and decreases to 45dB and 100 µs and 40dB and 20 µs at stress ratios of 0.4 and 0.7. A clear downward trend is observed in the amplitudes and duration as a function of increasing stress ratio that are related to lowering plastic deformation at the crack tip and therefore microcracking processes as a result of diminishing energy levels.

SEM fracture surface images in Figure 4.34 exhibited a dominant cleavage features at R=0.7, which is caused principally by the alignment/movement of a set of dislocations in the same weak crystallographic direction and consequently reflected in a low AE amplitude (below of ~50dB). This behavior occurred at the crack nucleation and initial stages. Specimens evaluated with R=0.1 (high CGR) the main fracture mode was transgranular tearing, which produced an increment in the amplitude of signals compared to the cleavage mode as shows in Figures 4.33 and 4.34. In corrosion environment, the fracture mode shift from transgranular in air to be mainly intergranular fracture at all stress ratios. The corrosion processes enhanced the AE activity due to the occurrence of metal dissolution, hydrogen induction and evolution as can be observed in Figure 4.33 for specimens subjected to 3.5% NaCl solution.
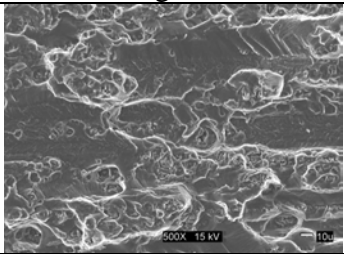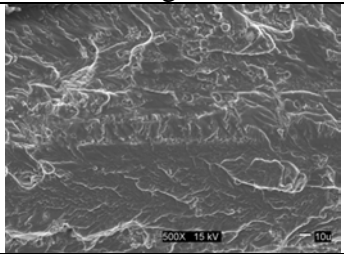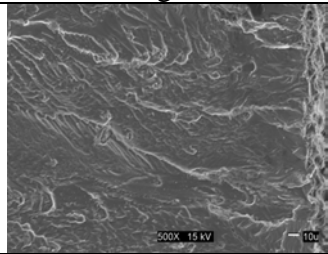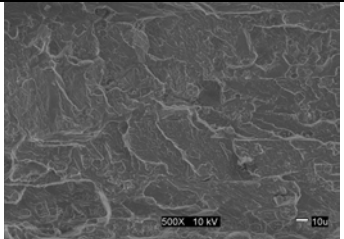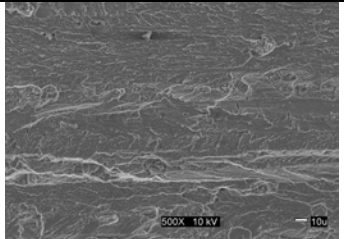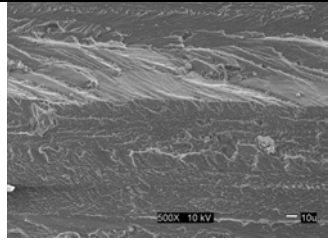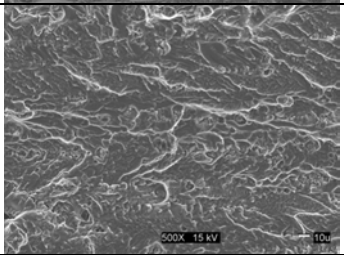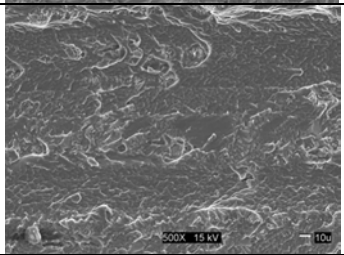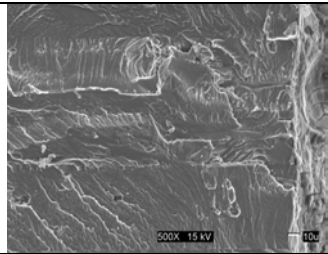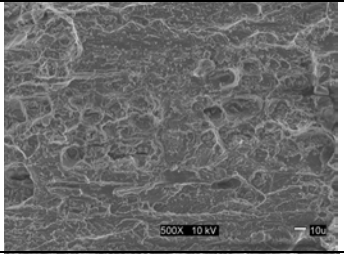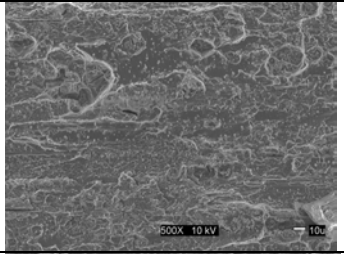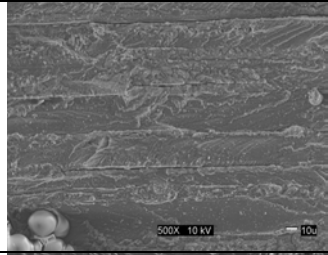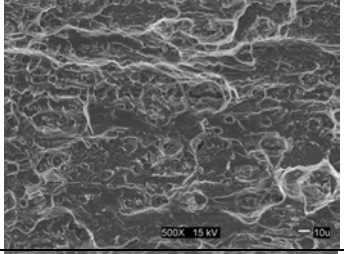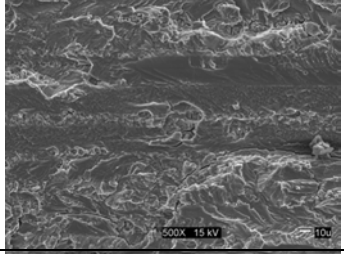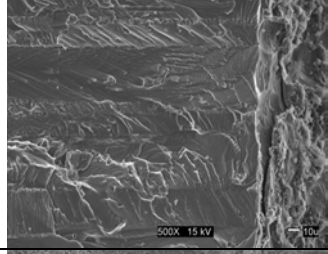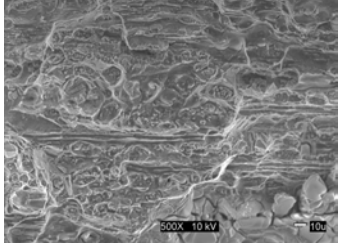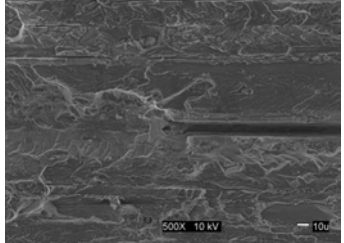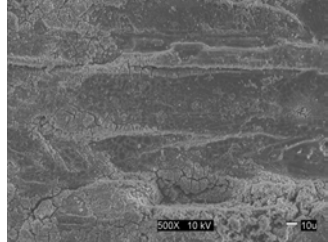
R	Environment	Stage III	Stage II	Stage I
0.1	Air			
	3.5% NaCl			
0.4	Air			
	3.5%NaCl			
0.7	Air			
	3.5%NaCl			

Figure 4.34 SEM images of AA7075-T6 at various load ratios

For AF1410 steel, as described earlier the hydrogen had a detrimental effect on the fatigue lifetime of the material and a shift in the modes of failure for specimens charged with hydrogen was observed [12,13,47]. During tension-compression tests of AF1410 steel, the fracture surface suffered a detrimental effect due to contact (flatten) face to face of the fracture surfaces during the compressive loads at initial stages of the test, revealed in Figure 4.35. For H-charged specimens, the morphological variations observed in the cracking pattern (evidenced in Figure 4.35 (a) where charged and uncharged portions of a specimen are shown) was mainly brittle intergranular fracture at the side rich in hydrogen and ductile transgranular and microvoid ductile fracture features at the side devoid of hydrogen. Fracture features remained ductile in general where hydrogen was absent whereas at the interface between the hydrogen charged side and hydrogen-free zones a mixed ductile / brittle fracture features were observed, as revealed in Figure 4.35 (a). The presence of brittle intergranular fracture is caused by the embrittlement effect of hydrogen and is associated to the concepts of reversible trapped hydrogen as mentioned earlier. Figure 4.35(b) exhibited surface cracks away form the main crack path at the surface rich in hydrogen (H-charged side) that confirmed the severity of hydrogen assisting fatigue cracking also at regions away from the main stress fields [13,29]. In addition, Figure 4.35 (c) displayed a multiple secondary cracks close to the main growing crack which is also associated to severe action of reversible trapped hydrogen worsening the cracking process. Experiments performed in air and 3.5% NaCl presented a lower AE activity (activity and duration). However, samples tested with previous hydrogen charge present a significant increment in the AE activity. As

explained earlier, the AE activity of fractures process are divided in three stages, which present high activity at the crack nucleation and the initial crack propagation, after that decreases significantly. Elsewhere at the final stage the amplitude and duration present a maximum value, which is reflected of the suddenly failure process.

High AE activity during the crack initiation stage was observed and it can be attributed to material accommodation, internal friction and microstructural rearrangement at the region of higher stress concentration (to generate the crack). Furthermore, these H-charged specimens presented secondary cracks and multiple surface cracks (Figure 4.35(b)) at regions away from the main stress field that can also generate additional AE signals increasing the AE activity observed in Figure 4.32. However, at stage II of stable crack propagation the AE activity decreases because the occurrence of surface cracks away from the main crack decreased and mainly secondary cracks (Figure 4.35(c)) around the crack tip were present and therefore the AE signals for this stage was less. At final stage (onset of failure 'stage III'), the CGR and the energy released are higher at high ΔK values and therefore, the AE activity and signal characteristics increased as observed in Figure 4.32.

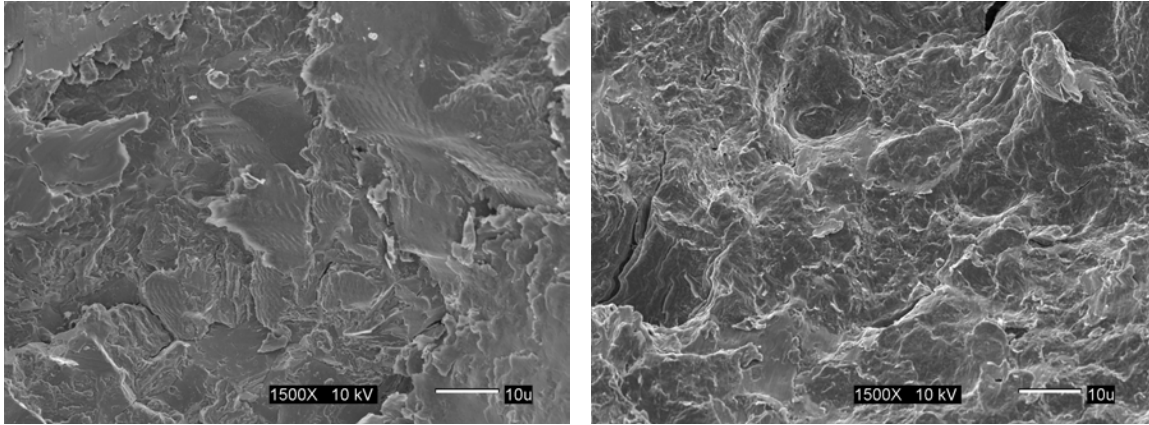**Figure 4.35 SEM Fracture surface image at initial stage and final stage (onset of cracking) of H-charged AF1410 steel**

| (a) | (b) | (c) |
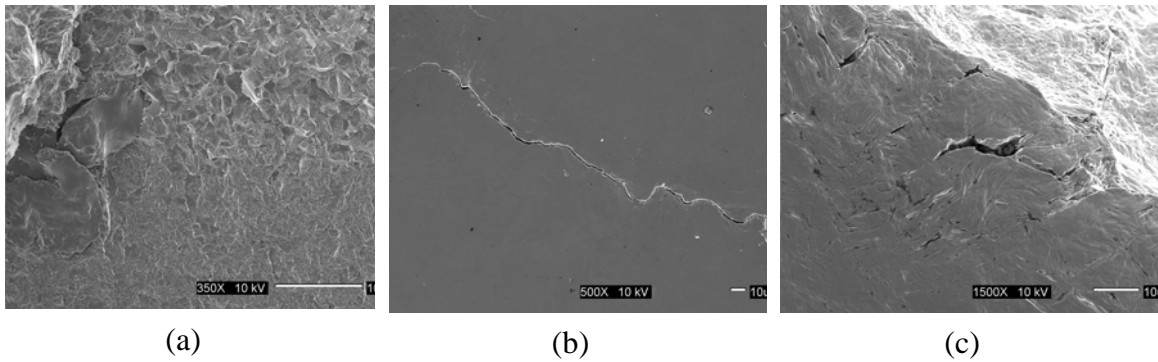
Figure 4.36 (a) Fracture surface at boundary region (high hydrogen content and without hydrogen), (b) surface crack at the hydrogen charge surface and (c) multiple secondary cracks close to main growing crack.

5   CONCLUSIONS

The following conclusions can be drawn from the results of our research:

- Corrosion fatigue testing of AA7075-T6 and AF1410 steel was performed under simulated marine environment. Results indicate an enhancement of CFCG in AA7075-T6 in the presence of 1%NaCl electrolyte, while AF1410 indicated an increase in CFCG at 1% and 3%NaCl only as frequency of loading was decreased.

- Lifetime in AF1410 also reduced as a function of increasing NaCl concentration.

- For corroded AF1410 and AA7075-T6, AFM analysis was used to discern fracture morphology features. From an electrochemical perspective both MD and HE were deemed likely sources of enhanced CFCG as a function of increasing NaCl concentration and decreasing frequency of loading. However, AFM analysis primarily pointed to MD induced features.

- For one side hydrogen charged specimens, the fatigue lifetimes of one-sided hydrogen-charged specimen were significantly lower than the ones tested in air.

- SEM analysis pointed to a shift in the mode of failure from ductile to brittle, and a reduction in plastic deformation. Furthermore, the hydrogen charged side induced mainly intergranular fracture with pockets of transgranular features mixed with quasi-cleavage mode, whereas the uncharged side exhibited predominantly transgranular ductile mode of failure.

- In terms of the fracture surface roughness, AFM analysis indicated an increase in the fracture surface roughness as a consequence of hydrogen embrittlement.

- The lateral hydrogen charged surface was found to suffer broadly from superficial damage by pitting corrosion.

- For two sides hydrogen charged steel specimens, the lifetime performance of the ultra-high strength AF1410 steel was found to be highly dependent upon the level of hydrogen concentration thereby confirming its detrimental effect on the material's cracking behavior.

- Novel short term hold time-fatigue interaction testing performed under ambient conditions indicated a sharp decreasing trend in the number of cycles to failure with increasing hold time for hydrogen charged specimens, while a parabolic trend was observed in the cases of lab air and NaCl environments tested samples.

- Hold time testing results were explained based on the microstructural features of the multiphase AF1410 steel. Possibly, material toughening due to strain induced transformation of some of the retained austenite to martensite in the uncharged samples occurred, while absent or limited in extent with the hydrogen charged ones where softening due to loss of interfacial coherency between phases out weighed the transformation induced strengthening.

- The combined SEM and AFM analyses indicate a shift in modes of failure from ductile to brittle as a function of increasing hydrogen content consistent with the overall results. Rigorous SEM analyses indicated transition from brittle to ductile modes corresponding to hydrogen rich and regions devoid of hydrogen, respectively.

- The fatigue crack growth rate behavior of ultra high strength (AF1410) steel was modeled satisfactorily. The results indicated a significant jump in the CGR as the

110

level of hydrogen concentration increased.

- A semi-empirical model is proposed which is expected to be useful and relevant in the fatigue lifetime prediction due to its robustness and simplicity. The model incorporated various relevant fatigue crack growth parameters in its development and fits the current data within 5% accuracy in most cases.

- Lifetime of AA7075-T6 was found to be sensitive to the varying stress ratio under marine environment.

- Acoustic emission aided in the understanding of crack initiation and growth mechanisms of the materials tested that may have otherwise been missed, however, requiring substantial preliminary testing, thresholds verification and parameter setup. Furthermore, the AE results for these two different material AA7075-T6 and AF1410 steel confirmed that AE activity and its signal characteristics are highly dependent on material properties and specimen geometry.

6   FUTURE WORK

- Further study of hold time-fatigue interaction especially the strain-induced microstructural transformation of austenite into martensite as a toughening mechanism. Furthermore, introduce this factor in the fatigue crack growth and lifetime prediction methodologies for AF1410 steel.

- Develop a technique able to quantify the amount of hydrogen produced as a result of corrosion processes.

- Extend the use of the crack growth rate model developed in the current research to other high strength materials such as Aermet100, AISI 4340, 300M.

- Perform additional experimental and analytical fatigue crack growth studies taking into account the load ratio effect on the fatigue lifetime of an AA7075-T6.

- Improve the applicability of the acoustic emission technique to evaluate the behavior of materials subjected to corrosion-fatigue and hydrogen embrittlement. It is important to improve the filtering techniques to reject the unwanted noise (friction, vibration, etc) that could mask the good acoustic emission signals. Furthermore, the fracture modes observed in AF1410 steel as result of hydrogen effect could be identified and classified by means of acoustic emission parameters such as amplitude, duration, strength and number of events. However, a more detailed and rigorous experimental program needs to be addressed in order to achieve this objective.

REFERENCES

1. S. Rolfe and J. Barsom. 'Fatigue and Fracture Control in Structures: Applications of Fracture Mechanics', Prentice-Hall Inc. 1977.

2. C. Beachem. 'A New Model for Hydrogen-Assisted Cracking (Hydrogen "Embrittlement)', Metallurgical Transactions, Vol. 3, 1972, pp. 437-451.

3. H. K. Birnbaum. 'Hydrogen Related to Failure Mechanisms in Metals', Department of Metallurgy and Mining Eng., University of Illinois at Urbana Champaign, Illinois, 1980.

4. W. A. Thompson. 'Stress Corrosion Cracking and Hydrogen Embrittlement', Carnegie Mellon University, Pittsburgh, Pennsylvania.

5. S. D. Antolovich. 'Fatigue Crack Propagation and Corrosion Fatigue of AF1410 Steel', Department of Material Science and Metallurgical Engineering, University of Cincinnati, Ohio, January 1980.

6. A. Turnbull. 'Modeling of Environment Assisted Cracking', Corrosion Science, Vol. 34, No. 6, 1993, pp. 921-960.

7. B. Shafiq and V. Agarwala. 'Corrosion and Fatigue in High Strength 7075-T6 Aluminum: Life Prediction Issues', Journal of Aircraft, Vol. 41, No. 2, pp.393-398, 2004.

8. J. Boodey and V. Agarwala. 'Hydrogen in Metals: Cadmium Plated Steel, Paper # 224', Corrosion87, San Francisco, California, 1987, pp.224/1-224/11.

9. V. Agarwala. 'What's Eating Us: Corrosion', Naval Research Reviews, Vol. 50,

No. 4, 1998, pp. 14-24.

10. L. S. Richard Thomas, J. R. Scully, and P. R. Gangloff. 'Internal Hydrogen Embrittlement of Ultrahigh Strength Aermet 100 Steel', Metallurgical and Materials Transformation A. Volume 34A, February 2003, pp 327-344.

11. Y. Jun Oh, S. Woo Nam and J. H. Hong. 'A Model for Creep-Fatigue Interaction in Terms of Crack Tip Stress Relaxation', Metallurgical and Material Transactions A, Vol.31A, July 2000, pp 1761-1775.

12. A. Quispitupa, B. Shafiq, O. M. Suarez and O. Uwakweh. 'Corrosion Fatigue of High Strength Aircraft Structural Alloys', Journal of Aircraft, Vol. 43, No. 3, 2006, pp. 787-792.

13. A. Quispitupa, O. M. Suárez, B. Shafiq, S. Charca, O. N. C Uwakweh. 'Fatigue and Hydrogen Embrittlement Evaluation of AF1410 Steel', International Journal of Microstructure and Material Properties, Submitted in February 2006.

14. J. P Bailon and S. D. Antolovich. 'Effect of Microstructure on Fatigue Crack Propagation: A Review of Existing Models and Suggestions for Further Research', Fatigue Mechanisms: Advances in Quantitative Measurement of Physical Damage, ASTM STP 811, J. Lankford, D. L. Davidson, W. L. Morris, and R. P. Wei, Eds., American Society for Testing and Materials, 1983; pp. 313-349.

15. A. W. Thompson and I. M.. Bernstein. 'Stress Corrosion Cracking and Hydrogen Embrittlement', Metallurgical Treatises, J. K. Tien and J. F. Elliott, Eds., TMS-AIME, Warrendale, Pennsylvania, 1981; pp. 589-601.

16. R. Ayer and P. M. Machmeier. 'Microstructural Basis for the Effect of Chromium

on the Strength and Toughness of AF1410-Based High Performance Steel', Metallurgical and Materials Transactions A, Vol. 27A, 1996; pp. 2510-2517.

17. R.P. Gangloff. 'Critical Issues in Hydrogen Assisted Cracking of Structural Alloys', Environment Induced Cracking of Metals (EICM-2), Sergei Shipilov, Eds., Elsevier Science, Oxford , UK . 2005 In press.

18. A. Turnbull. 'Modeling of the Chemistry and Electrochemistry in Cracks – A Review', Corrosion, Vol.57, No 2, 2001; pp. 175-189.

19. J. Tien, A. Thompson, Bernstein and I. R. Richards 'Hydrogen Transport By Dislocations', Metallurgical Transactions A, Vol. 7A, 1976, pp. 821-829.

20. P. R., L. Jemian. 'Characterization of Steels by Anomalous Small-Angle X-Ray Scattering', Ph. D. Dissertation, Northwestern University, Evanston Illinois, June 1990; pp. 5-8.

21. J. J. DeLucia. 'Electrochemical Aspects of Hydrogen in Metals', Hydrogen Embrittlement: Prevention and Control, STM STP 962, L. Raymond, Ed., American Society for Testing and Materials, Philadelphia, 1988; pp. 17-34.

22. R.D. McCright, 'Effects of environmental species and metallurgical structure on the hydrogen entry into steel'. Stress corrosion cracking and hydrogen embrittlement of iron based alloys. R.W. Staehle, J. Hochmann, R.D. McCright and J.E. Slater Editors, Conference Proceedings, France, 12-16 June 1973, NACE – 5, 1977; pp. 306–325.

23. S. Charca. 'Study of Hydrogen Diffusion and Permeation in Steels', M. Sc. Thesis, University of Puerto Rico at Mayagüez, Mechanical Engineering Department,

2005.

24. D.G. Westlake, 'A generalized model for hydrogen embrittlement', Transactions ASM, Vol. 62, No.4, 1969; pp. 1000–1006.

25. H. K. Birnbaum, 'Mechanisms of hydrogen related fracture of metals'. Hydrogen effects on material behavior, N.R. Moody and A.W. Thompson Editors, 1990; pp. 639–660.

26. Eun U. Lee and Jeffrey Waldman. 'Corrosion of Aircraft Landing Gear Steels', Naval Engineers Journal, November 1994; pp. 77-83.

27. A. Quispitupa, B. Shafiq, O. N. C Uwakweh, S. Charca, O. M. Suárez. 'Effect of Hydrogen and Hold Time on the Fatigue Lifetime of AF1410 Aircraft Structural Steel', Accepted for publication in Journal of Aircraft, 2006.

28. C. A. Zapffe and C. E. Sims, 'Hydrogen embrittlement, internal stress and defects in steel', Transactions AIME, Vol. 145, 1941; pp. 225–261.

29. S. Charca, O. N. C. Uwakweh and V. A. Agarwala 'Hydrogen Transport in Cathodically Polarized AF1410 Steel: Hydrogen Transport Conditions and Effects' NACE: Tri-Service Corrosion Conference, Session on Corrosion Mechanisms and Kinetics', Orlando Florida, November 2005.

30. A. R. Troiano, 'Metals; Hydrogen embrittlement; Congresses; Stress corrosion; Cracking', American Society for Metals, Metals Park, Ohio, 1984.

31. D. J. Unger. 'Analytical Fracture Mechanics', Dover Publications Inc. 1995, New York.

32. H. L. Ewalds and R.J.H. Wanhill. 'Fracture Mechanics', Edward Arnold edition-

DUM edition, 1984; pp.174-179.

33. N.E. Frost, K.J. Marsh and L. P. Pook. 'Metal Fatigue', Dover Publications Inc. 1999.

34. N. Perez. 'Fracture Mechanics (Mathematics & Its Applications)', Springer, First Edition, November 7, 2006.

35. H. Ishii, S. Jong Choi, K. Tohgo. 'AFM Fractography of Fatigued Aluminum Alloy', ICM8 1999; Vol.12: 73-78.

36. J. Goldstein, D. Newbury, P. Echlin, D. Joy, A. Romig, C. Lyman, C. Fiori, and Lifshin Eric. 'Scanning Electron Microscopy and X-Ray Analysis', Plenum Press, Second edition, 1992.

37. Nondestructive Testing Handbook, 2nd edition, American Society for Nondestructive Testing 5, 1987.

38. D. Harris and H. Dunegan. 'Continuous Monitoring of Fatigue Crack Growth by Acoustic Emission Technique', Third SESA International Congress on Experimental Mechanics, Los Angeles, California, 1974.

39. Hartmut Vallen. 'AE Testing Fundamentals, Equipment, Applications', NDT.net, Vol. 7 No. 9, September 2002.

40. A. Saxena and S. Hudak. 'Review and extension of compliance information for common crack growth specimens', International Journal of Fracture, Vol. 14, No. 5, 1978; pp. 453-468.

41. H. Tada, P. Paris, and G. Irwin. 'Stress Analysis of Cracks Handbook', Del Research Corporation, 1973.

42. S. Yi. 'The rate of creep deformation', PhD Dissertation, University of Cambridge, Cambridge, UK, August 2003.

43. T. Nicholas and T. Weerasooriya. 'Hold-Time Effects in Elevated Temperatures Fatigue Crack Propagation', Fracture Mechanics: Seventeenth Volume, ASTM STP 905, American Society for Testing and Materials, Philadelphia, 1986; pp. 155-168.

44. H. En-Hou and K. Wei. 'Chemical and Electrochemical Conditions within Corrosion Fatigue Cracks', Corrosion Science, Vol. 35, No. 1-4, 1973; pp. 599-610.

45. F. P. Ford. 'Corrosion Fatigue Crack Propagation in Aluminum-7% Magnesium Alloy' Corrosion, Vol. 35, No. 7, 1979, pp. 281-287.

46. B. Shafiq, A. Quispitupa, O. N. C. Uwakweh. 'Hydrogen Assisted Fatigue Lifetime Characteristic of AF1410 Steel', Submitted to International Journal of Fatigue, 2006.

47. D. Li, R. P. Gangloff and J.R. Scully. 'Hydrogen Trap States In Ultrahigh Strength Aermet 100 Steel', Metallurgical and Materials Transactions, Vol. 35A, 2004; pp 849-864.

48. R. Wei and M. Gao. 'Hydrogen Embrittlement and Environmentally Assisted Crack Growth.', Proceedings of the NACE Conference, NACE/Houston, 1990; pp. 789-816.

49. R. L.S. Thomas, J. R. Scully and R. P. Gangloff. 'Internal Hydrogen Embrittlement of Ultrahigh Strength Aermet 100 Steel', Metallurgical and

Materials Transactions A, Vol. 34A, No. 2, 2003; pp 327-344.

50. Y. Nakai and R. P. Wei. 'Effects of Frequency and Temperature on Short Fatigue Crack Growth in Aqueous Environments', Metallurgical Transactions, Vol. 19A, No. 3, 1988; pp. 543-548.

51. Y. Nakai, T. Kusukawa, N. Hayashi. 'Scanning Atomic Force Microscopy on Initiation and Growth Behavior of Fatigue Slip-Bands in a-Brass', Fatigue and Fracture Mechanics, Vol. 32, ASTM STP 1406, R. Chona Ed., 2001; pp. 122-135.

52. Fractography, ASM International Handbook, Vol. 12, 1999; pp. 41-42.

53. Santosh S. Hosmani. 'Development of Ultra High Strength Steel', Master Thesis, Dept. of Metallurgical Eng. and Materials Science Indian Institute of Technology, Bombay, India, March 2002.

54. R. A Oriani. 'The Diffusion and Trapping of Hydrogen in Steel' Acta Metallurgica Vol. 18, January 1970; pp. 147-157.

55. S. Yuyama, T. Kishi, and Y. Hisamatsu. 'Fundamental Aspects of AE Monitoring on Corrosion Fatigue Process in Austenitic Stainless Steel', Journal of Materials for Energy Systems, Vol. 5 No. 4, March 1984; pp 212-221.